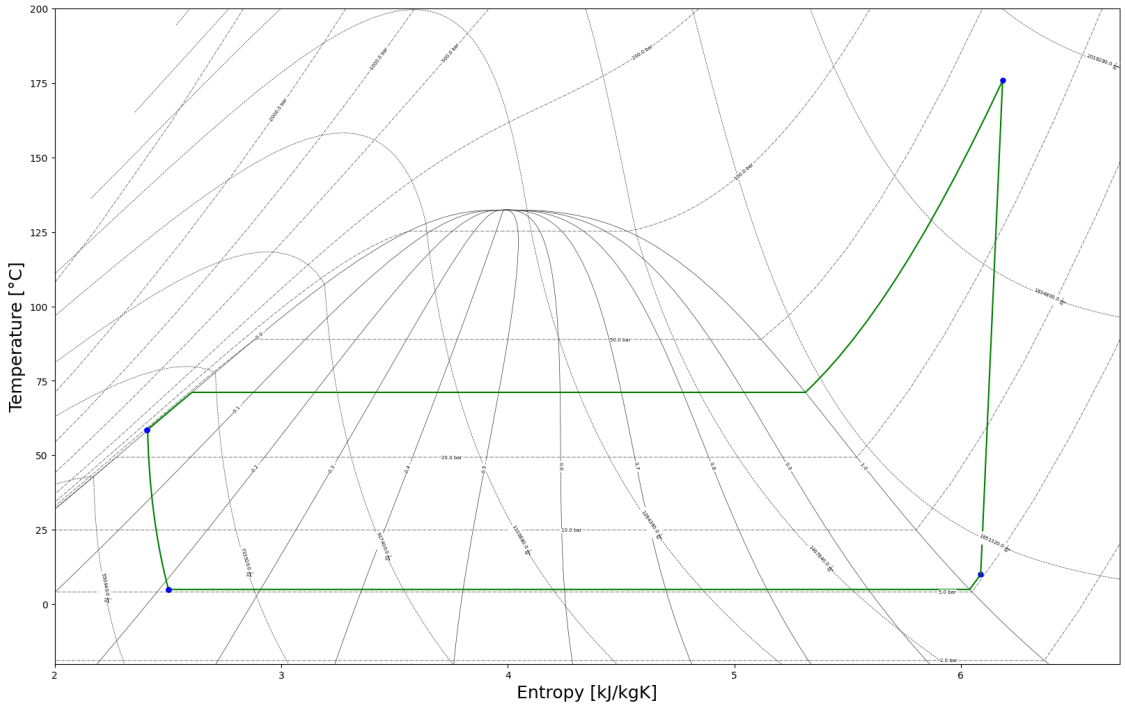


# Heat pumps for drying applications

## Thermodynamic cycles, design and techno-economic evaluation

Master's thesis in Sustainable Energy Systems

Erik Augustsson, Erik Hedström

DEPARTMENT OF SPACE, EARTH AND ENVIRONMENT

CHALMERS UNIVERSITY OF TECHNOLOGY
Gothenburg, Sweden 2024
www.chalmers.se

Master's thesis 2024

# Heat pumps for drying applications

Thermodynamic cycles, design and techno-economic evaluation

Erik Augustsson
Erik Hedström


CHALMERS
UNIVERSITY OF TECHNOLOGY

Department of Space, Earth and Environment
*Division of Energy Technology*
Chalmers University of Technology
Gothenburg, Sweden 2024

Heat pumps for drying applications
Thermodynamic cycles, design and techno-economic evaluation
ERIK AUGUSTSSON
ERIK HEDSTRÖM



Supervisor: Roger Nordman, CIT Renergy AB
Examiner: Simon Harvey, Department of Space, Earth and Environment

Master's thesis 2024
Department of Space, Earth and Environment
Division of Energy Technology
Chalmers University of Technology
SE-412 96 Gothenburg
Sweden
Telephone +46 31 772 1000

Cover: T-s diagram of a simple vapor-compression heat pump using the refrigerant R717. For further details, see Section 4.3 of this report.

Typeset in LaTeX
Printed by Chalmers Reproservice
Gothenburg, Sweden 2024

Heat pumps for drying applications
Thermodynamic cycles, design and techno-economic evaluation
Erik Augustsson, Erik Hedström
Department of Space, Earth and Environment
Chalmers University of Technology

# Abstract

Due to the imminent challenge of escalating global warming caused by the release of greenhouse gases (GHGs) such as carbon dioxide ($CO_2$) from human activities, actions throughout our society must be taken to reduce harmful emissions. One approach to mitigate greenhouse gas emissions is to optimize resource utilization, such as recovering low-grade excess heat using heat pumps. Therefore, this thesis investigates the techno-economic feasibility of implementing heat pumps in two low- to medium-temperature drying processes: the drying of municipal sewage sludge and concrete during construction.

In both cases, low-GWP (<4) 100-year time horizon global warming potential ($GWP_{100}$) and non-Per- and polyfluoroalkyl substances (PFAS) refrigerants have been used in cycle simulations using the simulation tool Aspen Plus, to investigate cycle performance, with the objective of finding viable solutions for integration into the aforementioned drying applications. The study analyzed how the performance of vapor compression heat pumps (VCHPs) differs when using R290, R717, R744, R1270, R600a and RE170 as working fluids.

The heat pump solutions have been evaluated with respect to coefficient of performance (COP), payback-period (PBP), net present value (NPV), and $CO_2$-equivalent emission reduction, compared to reference systems. From this, conclusions are drawn regarding the feasibility of the proposed heat pump-integrated drying systems. The findings of this study indicate that the integration of a water-to-water VCHP in the sludge drying case would be economically viable. Moreover, it would result in an annual reduction of 70% in $CO_2$-equivalent emissions compared to using district heating as heat srouce for sludge drying. The results are similar for the air-to-water VCHP in the concrete drying study. Additionally, it was found that the air-to-air heat pumps (HPs) in the concrete case study had difficulties to achieve the desired delivery temperature when the ambient air temperature was low.

In conclusion, it is recommended to further investigate the water-to-water VCHP cycle using R717 for medium-temperature drying applications such as sludge drying. Additionally, the air-to-water VCHP using RE170 is an interesting candidate for low-medium temperature drying applications that should be further investigated in future work.

Keywords: VCHP, Refrigerants, Drying, Process Integration, Sludge, Concrete, COP, Energy Efficiency.

# Acknowledgements

We would like to extend our gratitude to our supervisor, Roger Nordman at CIT Renergy AB, for his invaluable guidance throughout this project. Your insightful feedback and valuable contacts have greatly contributed to the success of our work. We also wish to thank our examiner, Simon Harvey at the Department of Space, Earth and Environment, for his guidance and constructive feedback, which have been instrumental in shaping this project.

Secondly, we want express our gratitude to Karl Malm at Hydropress Huber AB, Kent Bergström at Polygon Group, and Bardh Limnai at Gryaab for providing us with crucial information that has significantly contributed to this project.

Erik Augustsson & Erik Hedström, Gothenburg, May 2024

# List of Acronyms

Below is the list of acronyms that have been used throughout this thesis listed in alphabetical order:

| | |
|---|---|
| AHP | Absorption heat pump |
| CAA | Concrete study with air-to-air heat pump |
| $CaCO_3$ | Calcium carbonate |
| CaO | Calcium oxide |
| $CO_2$ | Carbon dioxide |
| CAW | Concrete study with air-to-water heat pump |
| CF | Cash flow |
| COP | Coefficient of performance |
| CRF | Capital recovery factor |
| CS | Case specific |
| DH | District heating |
| DM | Dry matter |
| DME | Dimethyl ether |
| F-gases | Fluorinated greenhouse gases |
| GHG | Greenhouse gases |
| $GWP_{100}$ | 100-year time horizon global warming potential |
| HACHP | Hybrid absorption-compression heat pump |
| HCFCs | Hydrochlorofluorocarbons |
| HFCs | Hydrofluorocarbons |
| HFOs | Hydrofluoro-olefins |
| HP | Heat pump |
| $H_2O$ | Water |
| IEA | International Energy Agency |
| IHP | Industrial heat pump |
| IHX | Internal regenerative heat exchanger |
| KPI | Key performance indicator |
| LCOH | Levelized cost of heat |
| MVR | Mechanical vapor recompression |
| NBP | Normal boiling point |
| NPV | Net present value |
| $N_2$ | Nitrogen |
| ODP | Ozone depletion potential |

| | |
|---|---|
| O&M | Operation and maintenance |
| $O_2$ | Oxygen |
| PBP | Payback period |
| PFAS | Per– and polyfluoroalkyl substance |
| PPA | Pinch point analysis |
| R1270 | Polypropylene |
| R290 | Propane |
| R600a | Iso-Butane |
| R717 | Ammonia |
| R744 | Carbon dioxide |
| RBK | Rådet för ByggKompetens |
| RE170 | Dimethyl ether |
| RH | Relative humidity |
| SH | Supplementary heating |
| SWW | Sludge: Water-to-water |
| TBE | Tight building envelope |
| TCI | Total capital investment cost |
| TFA | Trifluoroacetic acid |
| TVR | Thermal vapor recompression |
| VCHP | Vapor compression heat pump |
| WF | Working fluid |
| WWTP | Wastewater treatment plant |

# Nomenclature

Below is the nomenclature of indices, parameters, and variables that have been used throughout this thesis.

## Indices

| | |
|---|---|
| 1 | Inlet of a stream |
| 2 | Outlet of a stream |
| $CAA$ | The CAA case |
| $CAW$ | The CAW case |
| $CO_2$-eq | $CO_2$-equivalents |
| $CS$ | Case specific data |
| $Carnot$ | Carnot cycle |
| $Cond$ | Condenser |
| $Evap$ | Evaporator |
| $Fixed, OM$ | Fixed O&M costs |
| $HP$ | Heat pump |
| $H_{Sink}$ | Heat sink stream |
| $H_{Source}$ | Heat source stream |
| $SH$ | Supplementary heating |
| $Supply$ | Heat supply |
| $Variable, OM$ | Variable O&M costs |
| $air$ | Air |
| $amb$ | Ambient air |
| $diesel$ | Diesel |
| $dryer$ | Dryer |
| $dryer, continuous$ | Continuous dryer |
| $el$ | Electricity |
| $exh$ | Exhaust air |
| $gas$ | Natural gas |
| $h$ | Hourly value |
| $hot$ | Hot side of a heat exchanger |
| $init$ | Initial value |
| $lift$ | Temperature lift |
| $losses$ | Pressure or heat loss |
| $min$ | Minimum value |

| | |
|---|---|
| $ref$ | Refrigerant |
| $sink$ | Heat sink |
| $sludge$ | Mass flow of sludge |
| $source$ | Heat source |
| $sub$ | Substance in air |
| $subcooling$ | Subcooling |
| $suction$ | Suction side of compressor |
| $superheating$ | Superheating |
| $t$ | Annual value |
| $water$ | Mass flow of water |
| $water, evaporated$ | Mass flow of evaporated water |

# Parameters

| | |
|---|---|
| $\alpha$ | Scaling factor |
| $C_{DH}$ | Specific cost of DH |
| $C_{diesel}$ | Specific cost of diesel |
| $C_{el}$ | Specific cost of electricity |
| $C_{gas}$ | Specific cost of gas |
| $Conv$ | SEK to EUR conversion |
| $\Delta P_{losses}$ | Pressure loss in VCHP |
| $\Delta Q_{losses}$ | Heat loss in VCHP |
| $\Delta T_{SWW,source}$ | Heat source temperature difference in the SWW case |
| $\Delta T_{min}$ | Minimum temperature difference |
| $\Delta T_{subcooling}$ | Subcooling temperature difference |
| $\Delta T_{superheating}$ | Superheating temperature difference |
| $\dot{E}_{dryer}$ | Sludge dryer's specific heat demand |
| $\eta_{is}$ | Isentropic efficiency |
| $K$ | Annual percentage price increase |
| $\gamma$ | Fixed O&M percentage of TCI |
| $U$ | Overall heat transfer coefficient |

# Variables

| | |
|---|---|
| $CF_{Fixed,OM}$ | CF related to fixed O&M |
| $CF_{Supply}$ | CF related to heat transferred to heat sink |
| $CF_{Variable,OM}$ | CF related to variable O&M |
| $CF_{Utility}$ | CF related to reference utility or cost of heat source |
| $\Delta T_{lift}$ | Temperature lift |
| $\dot{m}_{CAW,air}$ | Mass flow of air cycle in case CAW |
| $\dot{m}_{CAW,water}$ | Mass flow of water cycle in case CAW |
| $\dot{m}_{ref}$ | Mass flow of refrigerant |
| $\dot{m}_{sink}$ | Mass flow of heat sink |

| | |
|---|---|
| $\dot{m}_{sludge,1}$ | Amount of incoming sludge |
| $\dot{m}_{sludge,2}$ | Amount of outgoing sludge |
| $\dot{m}_{source}$ | Mass flow of heat source |
| $\dot{m}_{water,1}$ | Amount of incoming water |
| $\dot{m}_{water,2}$ | Amount of outgoing water |
| $\dot{m}_{water,evaporated}$ | Amount of evaporated water |
| $\dot{V}_{CAA,air}$ | Volume flow of air in the case CAA |
| $Em_{HP}$ | $CO_2$-eq emission associated with the HP |
| $Em_{utility}$ | $CO_2$-eq emission of reference utility |
| $h_{concrete}$ | Operating hours of VCHP in cases CAW & CAA |
| $h_{sludge}$ | Operating hours of VCHP in case SWW |
| $Q_{CAA}$ | Heat associated with heat sink in case CAA |
| $Q_{CAW}$ | Heat associated with heat sink in case CAW |
| $Q_{SH}$ | Heat delivered by SH |
| $Q_{SWW}$ | Heat associated with heat sink in case SWW |
| $RH_{amb,air}$ | RH of ambient air |
| $RH_{exh,air}$ | RH of exhaust air |
| $T_{CAW_{H_{sink},1}}$ | Temperature of heat sink inlet in case CAW |
| $T_{CAW_{H_{sink},2}}$ | Temperature of heat sink outlet in case CAW |
| $T_{CAW_{H_{source},1}}$ | Temperature of heat source inlet in case CAW |
| $T_{CAA_{H_{sink},1}}$ | Temperature of heat sink inlet in case CAA |
| $T_{CAA_{H_{sink},2}}$ | Temperature of heat sink outlet in case CAA |
| $T_{CAA_{H_{source},1}}$ | Temperature of heat source inlet in case CAA |
| $T_{SH,1}$ | Temperature before SH in case CAA |
| $T_{SH,2}$ | Temperature after SH in case CAA |
| $T_{sink}$ | Heat sink temperature |
| $T_{source}$ | Heat source temperature |
| $T_{SWW_{H_{sink},1}}$ | Temperature of heat sink inlet in case SWW |
| $T_{SWW_{H_{sink},2}}$ | Temperature of heat sink outlet in case SWW |
| $T_{SWW_{H_{source},1}}$ | Temperature of heat source inlet in case SWW |
| $W_{comp}$ | Compressor work |
| $X_{sub,amb,air}$ | Mass fraction of substance in ambient air |
| $X_{sub,exh,air}$ | Mass fraction of substance in exhaust air |

# Contents

**List of Acronyms** **ix**

**Nomenclature** **xiv**

**List of Figures** **xxi**

**List of Tables** **xxv**

**1 Introduction** **1**
1.1 Background . . . 1
1.2 Aim and objectives . . . 2
1.3 Limitations / Demarcations . . . 3

**2 Process backgrounds** **5**
2.1 Sludge . . . 5
2.1.1 The waste hierarchy . . . 6
2.1.2 Wastewater Management . . . 6
2.1.3 Disposal Strategies . . . 7
2.1.4 Moisture Distribution in sludge . . . 9
2.1.5 Characteristics of sludge drying . . . 9
2.2 Concrete . . . 10
2.2.1 Concrete production . . . 11
2.2.2 Concrete emission reduction . . . 11
2.2.3 Concrete hydration and curing . . . 12
2.2.4 Climate control and drying criteria for concrete during construction . . . 14
2.2.5 Concrete humidity measurement and requirements . . . 16
2.3 Dryers . . . 17
2.3.1 Sludge dryers . . . 17
2.3.2 Concrete dryers . . . 18

**3 Theory** **21**
3.1 Heat pump technology and working principles . . . 21
3.1.1 Vapor compression heat pumps . . . 21
3.1.2 Absorption heat pumps . . . 22
3.1.3 Mechanical vapor recompression heat pumps . . . 23
3.1.4 Hybrid heat pumps . . . 23
3.2 Refrigerants . . . 24

3.2.1 Environmental indicators . . . 24
3.2.2 Refrigerant types and history . . . 25
3.2.3 Refrigerants studied . . . 26
3.3 Thermodynamics and heat pump optimization . . . 27
3.3.1 The Antoine equation . . . 27
3.3.2 Thermodynamic expressions . . . 28
3.3.3 Pinch point-based analysis and cycle visualization . . . 29
3.3.4 Heat pump improvement measures . . . 32
3.3.5 Mass flow correlations . . . 35
3.4 Performance indicators . . . 36
3.4.1 Thermodynamic performance . . . 36
3.4.2 Economic indicators . . . 38
3.4.3 Greenhouse gas emissions related indicators . . . 40

**4 Methodology** **41**
4.1 Refrigerant screening . . . 41
4.2 Simulation and modeling . . . 42
4.3 The Python script . . . 45
4.4 Cases . . . 47
4.4.1 Sludge: Water-to-water . . . 48
4.4.2 Concrete: Air-to-water . . . 49
4.4.3 Concrete: Air-to-air . . . 50
4.5 Case description . . . 52
4.5.1 Sludge: Water-to-water . . . 52
4.5.2 Concrete: Air-to-water . . . 54
4.5.3 Concrete: Air-to-air . . . 54
4.6 Economic Evaluation . . . 56
4.7 Sensitivity analysis . . . 57
4.7.1 Economic sensitivity analysis . . . 58

**5 Results and Analysis** **59**
5.1 Refrigerant screening . . . 59
5.2 Thermodynamic evaluation . . . 61
5.2.1 Sludge: Water-to-water . . . 62
5.2.2 Concrete: Air-to-water . . . 63
5.2.3 Concrete: Air-to-air . . . 63
5.3 Economic evaluation . . . 64
5.3.1 Sludge: Water-to-water . . . 64
5.3.2 Concrete: Air-to-water . . . 66
5.3.3 Concrete: Air-to-air . . . 68
5.4 Greenhouse gas emission evaluation . . . 70
5.4.1 Sludge: Water-to-water . . . 70
5.4.2 Concrete: Air-to-water . . . 71
5.4.3 Concrete: Air-to-air . . . 72
5.5 Sensitivity analyses . . . 73
5.5.1 Thermodynamic sensitivity analyses . . . 73
5.5.2 Economic sensitivity analyses . . . 75

5.6 Comparative economic evaluation . . . . . 86

**6 Discussion and Conclusion** **89**
6.1 Future work . . . . . 93

**Bibliography** **97**

**A Appendix A** **I**
A.1 Approximation of district heating price . . . . . I

**B Appendix B** **III**
B.1 Python script code . . . . . III

**C Appendix C** **XIII**
C.1 Sensitivity analysis results . . . . . XIII
C.2 Sludge: Water-to-water . . . . . XIII
C.3 Concrete: Air-to-water . . . . . XV
C.4 Concrete: Air-to-air . . . . . XVII

**D Appendix D** **XIX**
D.1 Total capital cost estimations . . . . . XIX

**E Appendix E** **XXI**
E.1 Mechanical vapour reheat study . . . . . XXI

**F Appendix F** **XXIII**
F.1 System variation - Concrete: Air-to-air . . . . . XXIII

# List of Figures


2.1 The EU waste hierarchy. . . . . 6
2.2 Sludge end destinations in EU and Sweden. . . . . 7
2.3 Water distribution in sludge. . . . . 9
2.4 General sludge drying curve [39, 41]. . . . . 9
2.5 Temperature profile in concrete during hydration [64]. . . . . 13
2.6 Complications from concrete related moisture evaporation. . . . . 15
2.7 Mounted Altiflex TBE [76]. . . . . 16
2.8 A simplified representation of a sludge belt-dryer . . . . . 18
2.9 El-Björn heating fan [82]. . . . . 19
2.10 El-Björn condensation dehumidifier [83]. . . . . 19

3.1 Schematic representation of a generic VCHP. . . . . 22
3.2 Schematic representation of an AHP type I. . . . . 22
3.3 Schematic representation of a generic MVR. . . . . 23
3.4 Schematic representation of a hybrid water-ammonia HACHP [92]. . 24
3.5 Schematic VCHP cycle and a general T-s diagram. . . . . 29
3.6 Representation of a generic VCHP cycle in a T-s diagram. . . . . 30
3.7 Comparison of two heat exchangers: one where the hot stream temperature is always higher than the cold stream (left), and one where the stream temperatures have a crossover (right). . . . . 31
3.8 Flowsheet diagram of a VCHP cycle with an IHX. . . . . 33
3.9 Flowsheet diagrams of two multi-stage compression cycles: one featuring intercooling (left) and the other employing a cascaded system with two distinct pressure levels (right). . . . . 34
3.10 Visual representation of HP working principle. . . . . 37
3.11 Generalized representation of temperature levels in an air-to-air HP system, showing two distinct ambient temperatures, $T_{1a}$ and $T_{1b}$. . . . 38

4.1 Tree structure of the refrigerant screening. . . . . 42
4.2 Flowsheet diagram of a VCHP cycle using one compressor. . . . . 42
4.3 Iterative Aspen-Python methodology for determination of HP cycle performance for varying refrigerants and case studies. . . . . 43
4.4 Diagram of temperature profiles over transferred heat. . . . . 44
4.5 Python script output for a VCHP in the SWW case using R717. . . 46
4.6 Proposed design of a water-to-water HP-integrated sludge dryer. . . . 48
4.7 Proposed design of a water-to-air HP integrated concrete drying system 49
4.8 Proposed design of a air-to-air HP integrated concrete drying system 50

5.1 Refrigerant limits in the sludge drying case using a water-to-water HP. 60

5.2 Refrigerant limits in the concrete drying case using an air-to-water HP. 60
5.3 Refrigerant limits in the concrete drying case using an air-to-air HP. . 61
5.4 COP of VCHP cycles in the sludge drying using a water-to-water HP case using selected refrigerants. . . . . 62
5.5 COP and estimated TCI of VCHP cycles in the concrete drying case using an air-to-water HP using selected refrigerants. . . . . 63
5.6 COP and COSP of VCHP cycles in the concrete drying case using an air-to-air HP using selected refrigerants. . . . . 63
5.7 NPV of VCHPs using selected refrigerants in relation to the reference utility assumed to be replaced in the sludge drying case. . . . . 65
5.8 PBP of VCHPs using selected refrigerants in relation to the reference utility assumed to be replaced in the sludge drying case. . . . . 65
5.9 NPV of VCHPs using selected refrigerants in relation to the reference utility assumed to be replaced in the concrete drying case using an air-to-water HP. . . . . 66
5.10 PBP of VCHPs using selected refrigerants in relation to the reference utility assumed to be replaced in the concrete drying case using an air-to-water HP. . . . . 67
5.11 NPV of VCHPs using selected refrigerants in relation to the reference utility assumed to be replaced in the concrete drying case using an air-to-air HP. . . . . 68
5.12 PBP of VCHPs using selected refrigerants in relation to the reference utility assumed to be replaced in the concrete drying case using an air-to-air HP. . . . . 69
5.13 $CO_2$-equivalent emission of VCHP cycles using the selected refrigerants compared to the emissions of the reference utilities in the sludge drying case using a water-to-water HP. . . . . 70
5.14 $CO_2$-equivalent emissions of VCHP cycles using the selected refrigerants compared to the emissions of the reference utilities in the concrete drying case using an air-to-water HP. . . . . 71
5.15 $CO_2$-equivalent emission of VCHP cycles using the selected refrigerants compared to the emissions of the reference utilities in the concrete drying case using an air-to-air HP. . . . . 72
5.16 Effect of heat source inlet temperature on VCHP cycle performance in the sludge drying case using a water-to-water HP. . . . . 73
5.17 Effect of heat source inlet temperature on VCHP cycle performance in the concrete drying case using an air-to-water HP. . . . . 74
5.18 Effect of heat sink inlet temperature on VCHP cycle performance in the concrete drying case using an air-to-air HP. . . . . 75
5.19 Effect of heat source inlet temperature on the NPV of VCHP cycles in the sludge drying case using a water-to-water HP. . . . . 76
5.20 Effect of heat source inlet temperature on the PBP of VCHP cycles in the sludge drying case using a water-to-water HP. . . . . 76
5.21 Effect of heat source inlet temperature on the LCOH of VCHP cycles in the sludge drying case using a water-to-water HP. . . . . 77

5.22 Break-even electricity price yielding NPV=0 as a function of TCI for the sludge drying case using a water-to-water HP with R717 (left) and R744 (right) as refrigerants. . . . . 78
5.23 Effect of heat source inlet temperature on the NPV of VCHP cycles in the concrete drying case using an air-to-water HP. . . . . 79
5.24 Effect of heat source inlet temperature on the PBP of VCHP cycles in the concrete drying case using an air-to-water HP. . . . . 80
5.25 Effect of heat source inlet temperature on the LCOH of VCHP cycles in the concrete drying case using an air-to-water HP. . . . . 80
5.26 Break-even electricity price yielding NPV=0 as a function of TCI for the concrete drying case using a air-to-water HP with RE170 (left) and R744 (right) as refrigerants. . . . . 82
5.27 Effect of heat sink inlet temperature on the NPV of VCHP cycles in the concrete drying case using an air-to-air HP. . . . . 83
5.28 Effect of heat sink inlet temperature on the PBP of VCHP cycles in the concrete drying case using an air-to-air HP. . . . . 83
5.29 Effect of heat sink inlet temperature on the LCOH of VCHP cycles in the concrete drying case using an air-to-air HP. . . . . 84
5.30 Break-even electricity price yielding NPV=0 as a function of TCI for the concrete drying case using a air-to-air HP with R717 (left) and (right) as refrigerants. . . . . 85

# List of Tables


2.1 Average levels of metals and nutrients in sludge spread on farmland in Sweden 2022 as well as the maximum allowed levels [36]. . . . . 8

3.1 List of potential WFs, with their characteristic properties [106, 107, 108]. . . . . 26
3.2 Antoine equation coefficients for water [109]. . . . . 27

4.1 Python script input parameters . . . . . 45
4.2 Variables used in the evaluation of the sludge case using water-to-water HP. . . . . 49
4.3 Variables used in the evaluation of the concrete case using air-to-water HPs. . . . . 50
4.4 Variables used in the evaluation of the concrete case using air-to-air HPs. . . . . 51
4.5 HP associated assumptions applied in all simulations. . . . . 52
4.6 Input values used in sludge drying system evaluation. . . . . 53
4.7 Input values used in the evaluation of the concrete case using air-to-water HPs. . . . . 54
4.8 Input values used in the evaluation of the concrete case using air-to-air HPs. . . . . 55
4.9 Summary of assumptions made for the economic evaluation of the three HP solutions. . . . . 56

5.1 Potential refrigerant candidates studied in the thermodynamic screening. 59
5.2 Estimated TCI values for all cases investigated. . . . . 64
5.3 Estimated LCOH values of the VCHP solutions in the sludge drying using a water-to-water HP using selected refrigerants. . . . . 66
5.4 Estimated LCOH values in the concrete drying case using an air-to-water HP using selected refrigerants. . . . . 68
5.5 Estimated LCOH values in the concrete drying case using an air-to-air HP using selected refrigerants. . . . . 69
5.6 Change in NPV of VCHPs using R717 and R744 for the sludge drying using a water-to-water HP. . . . . 77
5.7 Change in NPV of VCHPs using RE-170 and R744 for the concrete drying case using an air-to-water HP. . . . . 81
5.8 Change in NPV of VCHPs using R717 and R744 for the concrete drying case using an air-to-air HP. . . . . 84

5.9 Estimated drying cost per metric ton of sludge using an R717 heat pump and reference utilities. For the reference utilities, only variable operation expenditures are considered. . . . . 86
5.10 Estimated drying cost per square meter using an RE170 heat pump in the concrete air-to-water case and reference utilities. For the reference utilities, only variable operation expenditures are considered. The drying costs are estimated assuming a demand of (a) 47 or (b) 116 kWh/m$^2$. . . . . 87
5.11 Estimated drying cost per square meter using an R717 heat pump in the concrete air-to-air case and reference utilities. For the reference utilities, only variable operation expenditures are considered. The drying costs are estimated assuming a demand of (a) 47 or (b) 116 kWh/m$^2$. . . . . 87

# 1

# Introduction

## 1.1 Background

Due to the imminent challenge of escalating global warming arising through the release of greenhouse gases (GHG) such as $CO_2$ from human activities, actions throughout our society must be taken to reduce harmful emissions [1]. Both high emission industries and current practices during production must swiftly and effectively change the ongoing mode of operation to align themselves with current emission reduction targets [2].

However, to limit global warming to 1.5°C above pre-industrial levels, as outlined in the Paris Agreement [3], significant efforts are required [2, 4]. In the most recent Emission Gap Report published by the UN Environment Programme, it is stated that the current national policy commitments made under the Paris Agreement would result in a 2.9°C temperature increase above pre-industrial levels [5]. Therefore, achieving the 1.5°C goal necessitates a radical transformation of energy consumption to reduce GHG emissions. The International Energy Agency (IEA) has published an updated version of their *Net Zero Roadmap* in 2023, where they conclude, amongst other things, that fossil fuel consumption must be decreased, and energy efficiency improved to reach net-zero GHG emissions by 2025 [4, 6, 7].

In 2022, fossil fuels accounted for 65% of industry's energy consumption [8]. One possible way to to shift from this fossil fuel dependency is to utilize heat pumps (HPs) in areas where a feasible substitution can be made. This aligns with the Net-Zero Industry Act, where HPs are listed as one of eight key technologies [9]. With these HPs, the goal is to take advantage of waste heat in process streams and use HPs to increase the overall energy efficiency of the process [10]. The possibility to recover low-grade excess heat by utilizing a HP enables a more energy-efficient process. This, together with the ongoing ramp-up of the renewable share in the energy mix [11], makes HPs a sustainable option where implementation is possible. There are many different types of HPs, which excel in different areas, depending on the process. Some of these different types of HP technologies are closed vapour compression cycle, mechanical vapour recompression, sorption cycle and absorption–compression cycle among others [12].

Research has underscored the potential benefits of integrating HPs in various ap-

plications. While concepts such as drying of sludge before incineration or drying of concrete on construction sites are neither new nor groundbreaking ideas, there is however a renewed interest driven by a political push towards enhanced efficiency and reduced GHG emissions [4, 6]. It is important to note that historically, one major barrier to implementing HPs in an industrial setting has been the absence of established technologies capable of upgrading heat to high temperatures, i.e. in excess of 100°C, as required by a substantial number of industrial processes [13]. This limitation warrants further research to contextualize the exploration of HP integration within industrial settings. However, the two investigated drying applications do not need high temperatures.

## 1.2 Aim and objectives

This Master's thesis project seeks to explore the potential application of HPs in two distinct contexts: drying sewage sludge and regulating climate conditions at construction sites to facilitate concrete drying. The study will include detailed case studies of both concrete and sludge drying processes, each subjected to modeling with the aim of assessing feasibility and potential benefits of the HP deployment. Various solutions will be proposed and analyzed for each case, aiming to provide insights into the feasibility of employing primarily vapor compression heat pumps (VCHP) but also investigating other HP technologies such as an mechanical vapor reheat (MVR) HP. This will be achieved using refrigerants with low 100-year time horizon global warming potential ($GWP_{100}$).

The HP solutions and models developed during the project's methodology will be thoroughly evaluated. The findings will be discussed in terms of relevant key performance indicators (KPIs) and potential future implementations, ultimately presenting the most promising solution for each application studied.

The following questions will guide the project in the investigation of the application of HPs for drying applications:

Q.1: What is the potential improvement in thermodynamic efficiency using heat pumps in drying processes compared to traditional methods used in concrete and sludge drying applications?

Q.2: What is the techno-economic potential of adopting heat pumps for concrete and sludge drying applications?

Q.3: What are the specific challenges of applying heat pumps in concrete and sludge drying processes?

Q.4: What kind of refrigerants are most likely to be used in the future, considering current and expected regulations restricting the use of refrigerants?

## 1.3 Limitations / Demarcations

The study is geographically confined to Sweden, and its findings may not directly apply to regions with significantly different climatic, industrial, or energy landscapes. The primary focus is on concrete and sludge drying applications within Sweden. Findings may have limitations in generalizability to other industrial sectors, and different applications might exhibit distinct challenges and opportunities. The study will assume an energy mix that is prevalent in Sweden, and a different energy mix may impact the techno-economic evaluation. Different energy mixes in other regions could yield different outcomes, but there will be a brief discussion of the results relating to this topic.

Additionally, the study focuses on theoretical HP cycle simulations using only refrigerants with low $GWP_{100}$-values. The study does not investigate heat exchanger area nor compressor availability, but rather investigate how the cycle performance is affected by choice of refrigerant. The regulatory framework considered is based on Sweden and EU during the research period. Changes in regulations or policies, both on national and international level, may influence the feasibility and implementation of HP solutions for industrial drying. There will be some consideration taken to ongoing policy work regarding working fluids.

Consideration will not be taken to the general drying profile of sludge and concrete, instead of using a simplified relation of these curves, i.e., to create a model that is adequately simplified only the heat demand will be considered. This is because the focus of the thesis report is not on the drying phenomena, but on the HP integration and the thermodynamic properties of the streams affecting the HP as well as its techno-economic feasibility. Furthermore, the study will not consider the drying technology itself, i.e. a belt-dryer will be modeled as the heat sink being a water stream that will heat a dry air influx that is drying the sludge. Since it is not the drying itself but an alternative source of heat to this drying that is to be investigated.

For concrete drying, the focus is on drying and indoor climate temperature based on optimal conditions, with adjustments made to meet quality requirements. For the specific case study of sludge drying, the discussion of end uses of dried sludge is beyond the scope of this project.

# 2

# Process backgrounds

## 2.1 Sludge

Sludge, in the context of sewage treatment, is defined by Britannica as "a solid matter that has settled out of suspension in sewage undergoing sedimentation in tanks or basins" [14]. And more generally, sludge describes a mass of particulates suspended in a fluid [15]. This section begins with a broader approach before narrowing down to more fundamental characteristics, such as moisture distribution and its relation to the rate of drying. In the case study of sludge drying the WWTP Ryaverket in Gothenburg is used as a reference. On average the WWTP has a load of approximately 966 thousand population equivalents, which refers to the amount of biodegradable organic material over seven days [16]. In 2022, the sludge generation at the WWTP was approximately 15 thousand metric tonnes of dry matter (DM) [17].

The drying mediums temperature naturally differs depending on each application but for the specific case of sludge it is expected to be in the range of 70-150°C [18]. The lower part of this interval coincides with the sink temperatures commonly used with HPs today, thus indicating great promise for potential integration. Ongoing research is being conducted on HPs capable of delivering high temperatures (>100°C) [19], with expectations that some will enter the market in the near future.

A majority of the industrial energy consumption is currently being met with fossil fuels which emit greenhouse gases, consisting primarily of $CO_2$, and therefore alternative ways to provide energy to the industrial sector is researched throughout the world [20]. Drying processes stand for 10-20% of the energy used in industrial processes in developed countries, showcasing that drying is an energy intensive process. This encompasses a wide spectrum depending on the scale of the specific drying process at hand [21].

Apart from industrial sludge, such as residues from pulp-and paper mills and the mining sector, wastewater treatment plants (WWTPs) in Sweden generate approximately 200 thousand metric tonnes of dry matter (DM) per annum [22]. In the EU, the overall annual sludge generation reaches around 8.7 million metric tonnes DM [23]. The two most commonly employed methods for the final disposal of sewage wastewater sludge, hereafter referred to as "sludge", are agricultural usage

and incineration [23]. The latter is considered a method with fewer associated risks compared to land spreading, given that sludge may contain various potentially harmful substances, including organic pathogens, heavy metals, microplastics, and pharmaceutical residuals, among others, which could pose significant threats to the land it is applied to [24, 25]. To combust sludge, a moisture content below 33% is needed, while sludge typically has an initial moisture content of around 98% [26]. Naturally, the sludge has to be both mechanically processed to remove the water content but also dried. HPs have been used for the thermal drying with good results [27, 28], and some manufacturers of dryers state HPs as a possible source of heat [18, 29].

### 2.1.1 The waste hierarchy

The waste hierarchy, an EU directive, serves as a guide on how waste management should be prioritised [30]. It provides a framework for optimizing the use of existing resources. In both Sweden and the EU, the most common method for sludge disposal is land spreading, leveraging its nutritional contents. This practice aligns with the waste hierarchy, which prioritizes different methods of waste treatment. An illustrative representation of the EU waste hierarchy is presented in Figure 2.1.

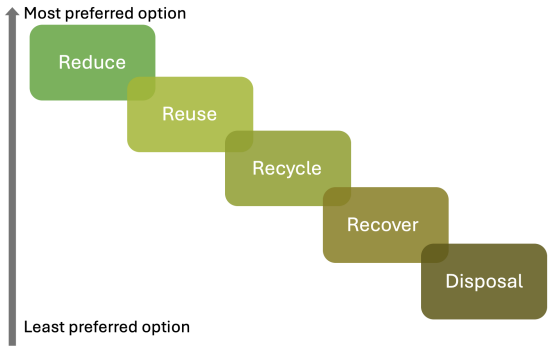


**Figure 2.1:** The EU waste hierarchy.

In the hierarchy in Figure 2.1, Reduce is the most preferred method of waste treatment, aiming to prevent waste from being created. Following Reduce is Reuse, Recycle, Recover, and Disposal as the least desired option [30].

However, concerning sludge management, the waste hierarchy in Figure 2.1 has been modified. The concept of Reuse has been interpreted by the Swedish EPA as Preparation for Recycling [31]. This involves various sludge treatment techniques depending on the sludge's intended end destination, as discussed in section 2.1.2.

### 2.1.2 Wastewater Management

In Sweden, it is common for WWTPs to combine different treatment techniques, with some form of mechanical treatment typically being the first step [32]. According to the Swedish Environmental Protection Agency, the most common combination is

mechanical-biological-chemical treatment processes [32]. It is during some of these treatment methods, especially mechanical and physical treatments, that sludge is generated.

At Ryaverket, the treatment of sludge is done in three steps; thickening, mesophillic digestion, and dewatering [17]. Thickening produces primary sludge with 4-8% DM, followed by mesophilic digestion, an anaerobic process. During mesophillic digestion, organic materials are converted into biogas containing methane (60-65%) and carbon dioxide (35-40%) [17]. This breakdown of organic materials removes most odors. Additionally, the temperature in the first digestion chamber at Ryaverket is maintained at 35°C by heat exchangers using hot water, sourced partly from compressor cooling in the WWTP and district heating (DH) [17].

The biogas produced from digestion is delivered via a pressurised gas delivery system to Göteborg Energi for further upgrading, while the digested sludge is mechanically dewatered to 25-35% DM by screw presses [17]. This digestate is transported from Ryaverket for long-term storage and eventually be used in agriculture. However, for sludge to be allowed for use on farmland in Sweden, it needs to be Revaq-certified [33]. This certification, implemented by Svenskt Vatten, involves upstream efforts to reduce hazardous contaminants from entering the sludge [33]. The certification provides transparent information on sludge composition and promotes active efforts to reduce contaminants upstream of WWTPs, ensuring safe end-use of sludge in agriculture [33]. Furthermore, Revaq-certified sludge must be sanitized, which can be achieved using various technologies to reduce pathogens in the sludge [34].

### 2.1.3 Disposal Strategies

In this section, the most common sludge management strategies will be examined to shed light on the challenges but also highlight areas for improvement. To begin, an overview of where the sludge ends up in both Sweden and EU is presented in Figure 2.2a and 2.2b.

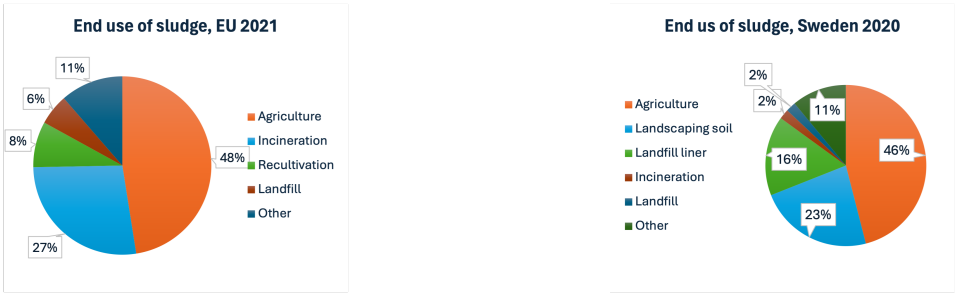


**(a)** Sludge end use EU [23]. **(b)** Sludge end use Sweden [22].

**Figure 2.2:** Sludge end destinations in EU and Sweden.

Out of the 200 thousand metric tonnes of DM, approximately 70% of the sludge generated in Sweden is subjected to digestion [35]. Of this, 46% of the digested sludge is used on farmland, and 16% is used as landfill liner [22]. In the EU, agricultural

usage accounts for 48%, while landfills account for 6%. A notable difference is the higher degree of incineration, 27% in the EU compared to 2% in Sweden [22, 23], where 'recultivation' and 'landfill liner' are different terms for the same process. The share of sludge used for recultivation is 8% in the EU and around 20% in Sweden.

In Table 2.1 the average levels of metals and nutrients in sludge spread on farmland is presented together with their regulated maximum level.

**Table 2.1:** Average levels of metals and nutrients in sludge spread on farmland in Sweden 2022 as well as the maximum allowed levels [36].

| **Substance** | **Average amount [mg/kg DM]** | **Maximum amount[1] [mg/kg DM]** |
|---|---|---|
| Cadmium | 0.606 | 2 |
| Copper | 334 | 600 |
| Nickel | 16.8 | 50 |
| Lead | 13.72 | 25 |
| Mercury | 0.341 | 2.5 |
| Chromium | 19.78 | 100 |
| Zink | 470 | 800 |
| Total Nitrogen | 49 510 | - |
| Total Phosphorus | 28 672 | - |

[1] Maximum level of substance in sludge spread on farmland in Sweden, according SFS 1998:944 [37].

From Table 2.1 it is evident that there is much nitrogen and phosphorus in the sludge, thus the primary objective of the spreading is to recover these nutrients. Moreover, there is commonly a presence various potentially harmful substances, including heavy metals as shown in the table, but also pathogen, microplastics, and pharmaceutical residuals [24, 25, 35].

For sewage sludge to be permissible for spreading on agricultural land, there are sanitation requirements, which can be achieved, among other methods, through long-term storage of the sludge for a period of up to 6 months [34].

Drying the sludge reduces biological activity, and at a DM content of 70%, microbial growth essentially ceases [34]. Whether this is due to the removal of moisture or the relatively high temperature used for the drying is still unclear [34]. Sludge is often dried to around 85-90% DM to further reduce the risk of biological growth during storage. However, highly dried sludge increases the risk of self-ignition and dust explosions [38]. Drying sludge is not without challenges, as during the 40-60% moisture range, it undergoes a sticky phase examined further in section 2.1.5 and tends to adhere to heat transfer surfaces, complicating the drying process [39].

### 2.1.4 Moisture Distribution in sludge

The initial moisture content of sludge can be very high, up to 99% [15], and the moisture distribution in sludge can be divided into four forms of water; free, interstitial, surface and intercellular water [40]. The different forms of water is conceptually depicted in Figure 2.3.

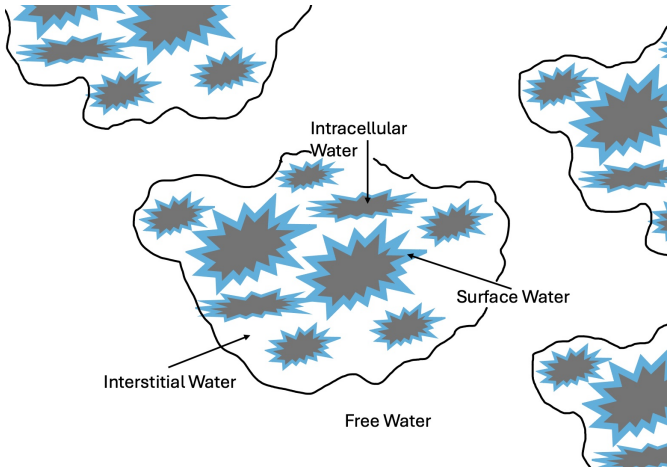


**Figure 2.3:** Water distribution in sludge.

In Figure 2.3 it can be seen that the free water is not attached to the sludge, and can hence be removed easily. Whereas interstitial water is bonded by capillary forces within the flocs, larger groups of particles [15, 40]. The surface water is interacting with the particle surface, and the intercellular water contained within the particles structure.

### 2.1.5 Characteristics of sludge drying

In section 2.1.4, the different forms of moisture in sludge were presented. Due to the various ways the water interacts with the sludge particles, the drying rate of sludge varies. A simplified representation of the mass flux of evaporating water as a function of the water content of sludge is illustrated in Figure 2.4.

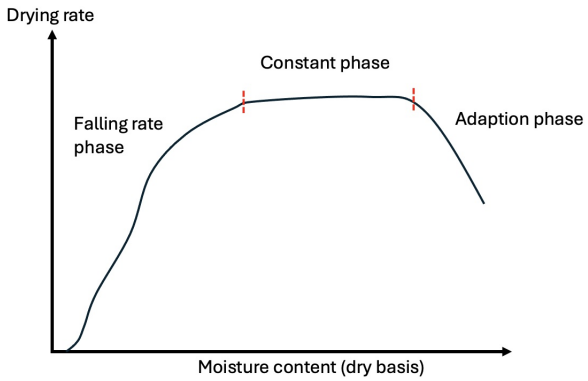


**Figure 2.4:** General sludge drying curve [39, 41].

In Figure 2.4, the different drying rate phases can be attributed to the moisture categories that are evaporating. When the sludge enters the dryer, its temperature increases rapidly, and so does the drying rate, which is the adaption phase. It is mainly the free water that evaporates during this phase, and it continues through the constant phase. When most of the free water has evaporated, the drying rate starts to fall. This falling rate phase, can be divided into a first and second falling rate phase [41]. The first is connected to the evaporation of interstitial moisture, and the second occurs when surface water evaporates. Further drying involves the removal of intercellular moisture, which can be done by incineration [39].

During the different stages, the character of the sludge transforms. Initially, it is more of a paste. However, when the percentage of DM is in the interval of 40-50%, the sludge becomes sticky [39]. This sticky phase can lead to fouling inside the dryer, depending on the type of dryer used, but there are different measures to avoid this. Most commonly, dried sludge is blended with moist sludge to surpass the 60% DM threshold, facilitating the drying process [39].

## 2.2 Concrete

Recently, the focus of the construction and real estate industry in terms of reducing energy demand has been to improve the energy performance during operation. The energy expenditure during the construction phase as well as efforts to improve the related efficiency are still in the initial stages [42]. This can partly be attributed to the fact that only 14% of the developers asked during a survey on the matter required that the energy usage during the production were to be accounted for [42]. Among several energy demanding processes present when building properties, the drying, or the climate control needed to ensure the adequate drying of concrete is a significant process. Not only for the structural quality of the property but also for time-management reasons since it is not possible to continue with the the construction if the concrete does not fulfil an adequate moisture content [43, 44].

There are multiple different ways of drying concrete, where the optimal concrete drying temperature is between 10-27°C [45], with multiple drying solutions present on today's market. In a recent study, about 90% of all cases utilized heaters and 40% were combined with a dehumidifier. Floor heating was utilized in 13% of all cases [46]. However, the current most used technologies in use for drying are stand-alone systems such as heaters in different forms, which are often leased [46]. In the same study, it is mentioned that district heating is the most common type of energy source for the heaters (54%), followed by direct electricity (32%) and the rest being a mix of direct electricity, district heating, pellets and diesel-driven heaters.

### 2.2.1 Concrete production

The structural building material concrete, is defined in Britannica as "a hard, chemically inert particulate substance, known as aggregate (usually sand and gravel), that is bonded together by cement and water" [47]. As such, a cementing material and a mineral aggregate are mixed with water to cause the cement to set during a part of the cement curing phase called hydration, which will be discussed further in Section 2.2.3. Concrete-like materials have been used for centuries, with the bonding substances differing depending on available resources. Clay, limestone, gypsum, or a combination of similar materials were used by the ancient Babylonians as well the Egyptians [47]. In modern concrete, it is common to use about 10% cement, 20% water, 30% sand and 40% gravel [48].

When it comes to the most consumed materials in the world, concrete ranks second, with only water having a higher consumption per person [49]. Sweden produces around 2.5 million tons of cement for concrete, approximately 0.25 tonnes of cement per person per year [50]. Sweden also accounts for around 0.05% of the global production [50]. Twice as much concrete is being used as all other building materials combined [49, 51]. Due to its flexibility, low cost, and availability, concrete has wide applications in the construction of buildings, roads, bridges, tunnels, dams, power plants, ports, and airports to name a few [51]. Therefore, it is highly likely that concrete will continue to be extensively used in the future.

There are also problematic environmental aspects of concrete, specifically related to cement, which is impossible to circumvent as a modern cementing material. It is mainly the fact that generation of $CO_2$ as a by-product from the production of cement but also the combustion of fossil fuels in the cement manufacturing plant. In the cement manufacturing production, the raw feed is converted from limestone ($CaCO_3$) to lime (CaO) and carbon dioxide ($CO_2$) in the calciner according to the reaction shown in eq. (2.1).

$$CaCO_3 \rightarrow CaO + CO_2 \tag{2.1}$$

The calcination reaction is highly temperature dependent, and in general, an optimal calcination temperature is around a minimum of 900°C [52]. A rotary kiln facilitates chemical reactions such as the calcination but mainly the formation of clinker, which is the fine powder that cement is made out of. The rotary kiln, located in the last part of the cement production needs to heat the raw feed to temperatures of around 1400-1500°C [53]. Both the calciner and the rotary kiln typically utilize fossil fuels, adding to the environmental problems associated with cement production.

### 2.2.2 Concrete emission reduction

Although concrete is an immensely valuable asset in the construction of a vast number of buildings, it has a downside that cannot be ignored: the associated $CO_2$ emissions of the entire cement industry. The manufacturing of cement accounts for

4% of Sweden's total GHG emissions, while globally it stands for 8%, highlighting the severity of the GHG related to the cement industry [54, 55].

Multiple trajectories to reduce the overall emissions are available, where some of them are the following:

- **In-situ Carbon Capture and Storage (CCS)** - CCS captures $CO_2$ emissions at the point of emission using methods like postcombustion, precombustion and oxy-fuel combustion capture. As cement plants are major $CO_2$ emitters, CCS is crucial for reducing emissions and meeting future climate goals [56, 57].
- **In-situ combustion alteration** - Replacing fossil fuels in the calciner and rotary kiln with alternative fuels like municipal solid waste or biomass which can reduce the carbon footprint of the cement plant. Another option can be to use an electrically driven plasma cannon to replace traditional fossil fuel-driven thermal heat sources [58, 53].
- **Adjustment of concrete mixture** - The water-to-cement (w/c) ratio measures the amount of water compared to cement in the concrete mixture. If it is increased, the cement usage in the concrete is reduced, making it more environmentally friendly. This approach brings challenges in managing the extra water during the drying process, further discussed in 2.2.4.

This thesis focuses on the drying of concrete given that the adjustment of the concrete mixture is the main trajectory for more climate-friendly concrete. The potential to impact $CO_2$ emissions is therefore done by reducing the cement usage and hence the corresponding the $CO_2$ emissions.

### 2.2.3 Concrete hydration and curing

The process of casting concrete essentially involves five steps: preparing the formwork, mixing and placing the concrete in the formwork, curing the concrete, removing the formwork, and then adjusting the moisture, for example, by drying or climate controlling the environment surrounding the concrete.

One of the most common type of cement used in concrete production is Portland cement [59]. Portland cement is made by heating limestone, clay, and other minerals in the aforementioned rotary kiln that gets finely ground into a powder. Upon mixing with water, it undergoes a chemical reaction, forming a paste that binds the aggregates together. Some minerals react rapidly with water during the hydration, which is the chemical reaction between cement and water that results in the hardening and setting of concrete, while other minerals contributes more to the long-term strength of the concrete as they hydrates more slowly [60]. Naturally, additional minerals are used to build a specific final cement profile. The specific concentrations of each mineral and their proportion also varies depending on unique manufacturing processes and the desired properties of the cement [60].

In order to obtain the optimal strength and durability, concrete must undergo a

process called curing. Curing is defined as "action taken to maintain moisture and temperature conditions in a freshly placed cementitious mixture to allow hydraulic cement hydration and (if applicable) pozzolanic reactions to occur so that the potential properties of the mixture may develop" [61]. Essentially, curing aims to ensure specified strength, hardness, impermeability, and longevity in the concrete while avoiding flaws such as micro-cracks, shrinkage cracks, and a weak surface layer. This is achieved by regulating variables such as mixture proportions, size and shape of the concrete additives, while considering ambient weather conditions and future exposure conditions [61, 62].

The hydration of a cementitious material is when the mixture becomes a firm hardened mass as an effect of the added water, i.e., concrete. [63]. This process can be divided into five distinct stages, each with different implications. The general hydration processes of concrete is shown in Figure 2.5.

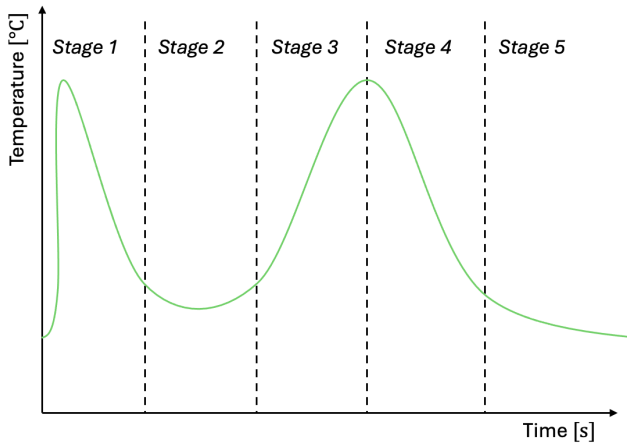


**Figure 2.5:** Temperature profile in concrete during hydration [64].

The five stages are the following: initial exothermic reactions with a temperature spike, dormancy with a reduction in reactivity with a setting of the mixture, strength acceleration with calcium silicate hydrate formation with another temperature peak, speed reduction as reactions slow down with strength solidification and steady development where the final strength is achieved [65, 66, 60].

In an ideal scenario, the concrete is maintained at a controlled and specified temperature and humidity during the curing period. There are various methods for achieving this, but typically, concrete slabs are sprayed with so called curing compounds. The primary objective of these compounds is to create a film on the surface of the freshly poured concrete that retains water inside [67]. Methods for ensuring adequate moisture on the surface and within the concrete slab, with or without the curing compounds, include utilizing continual spraying on the surface or ponding, where the concrete slabs are submerged under the curing compound [61]. Alternative methods may involve wrapping the concrete slab in plastic sheet coverings or similar materials to retain the moisture.

As the moisture evaporation from the concrete is driven by the difference in vapor

pressure on the concrete surface and the surrounding air, it is crucial to regulate both the temperature and the relative humidity (RH), as these are the main contributors to the vapor pressure on the concrete's surface [68]. Molecular speeds increase with temperature, leading to higher vapor pressure. The RH is related to the water vapor's partial pressure in the air; evaporation occurs when the vapor pressure is higher than the partial pressure, and condensation occurs vice versa [69]. At 100% humidity, the vapor pressure equals the partial pressure, meaning no more water can enter into the vapor phase. Since all thermodynamic systems strive to reach equilibrium, moisture will evaporate from the surface of the concrete into the air if the vapor pressure the air is higher. The evaporation of moisture from the concrete into the surrounding air is more related to the post-hydration drying of the concrete, which will be discussed in Section 2.2.4.

### 2.2.4 Climate control and drying criteria for concrete during construction

A final RH value ranging between 85 and 90% is traditionally considered the target for concrete, with a tendency to be closer to 85% [46]. This means that the air residing in the pores of the concrete has a moisture content which is equivalent to 85% of the maximum amount it could hold at the concrete's current temperature. As mentioned in Section 2.2.3, the drying, or rather climate control of the concrete post-hydration is highly dependent on the temperature and RH of the surrounding air. Therefore, it is crucial to control of the variables that affect the temperature and RH in order to efficiently reach the concretes RH-targets.

According to a review conducted by LÅGAN on energy use in climate control and dehumidification, it was observed that out of 72 construction projects, 90% of utilized radiant heaters and 40% utilized condensation dehumidifiers [46]. Additionally, in the same review, it was noted that climate control equipment was put in use before establishing a tight building envelope (TBE) in 36% of the cases.

An important reason for drying the concrete after the curing process is to ensure that the water enclosed in the concrete slabs does not cause problems for the surrounding constructions in the following years. As the water present in the slabs will exit through the top surface by evaporation, several unwanted consequences could appear. Apart from adhesive failures that can occur with any flooring due to the use of more environmentally friendly adhesives, which are more sensitive to moisture, other complications are illustrated in Figure 2.6 [44, 70].

**(a)** Mold, mildew or rot buildup on carpets and wooden structures [71].

**(b)** Warping or skewering wood-based flooring such as strip-wood or parquetry [72].

**(c)** Bubbling and delamination in low-permeability floors such as vinyl. [73].

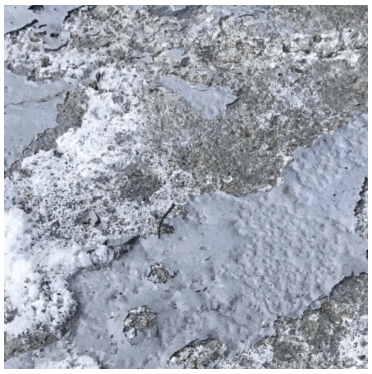

**(d)** Efflorescence in concrete, grout or tiles [74].

**Figure 2.6:** Complications from concrete related moisture evaporation.

A TBE is defined in this study analogously to the definition found in P. Brander's licentiate thesis, which states that "When a building achieves resistance against precipitation (snow, driving rain) and has such minimal air infiltration that a drying environment with acceptable moisture risks can be established throughout the building" [75].

If climate control has started or is in operation without a TBE, the energy efficiency of the heaters and dehumidifiers drastically decreases. When a construction is tightly sealed in with a TBE, it effectively lowers heat transfer between the interior and exterior environments. This added insulation property help mitigate heat loss to the surroundings, even when the exterior environments are fluctuating. It is essential to keep the climate control in check, as variations in the ambient temperatures and RH may lead to uneven and delayed drying. The energy efficiency of the drying and climate control equipment benefits greatly from a TBE, as the overall load and demand can be lower if heat losses are minimized. The ingress of external moisture is also minimized [75].

A provisional TBE from the Danish company Altiflex is shown in Figure 2.7. With the Altiflex modules, it is possible to enclose the construction in a flexible manner and thus ensure lower heat loss and moisture ingress [76].

**Figure 2.7:** Mounted Altiflex TBE [76].

Ideally, with the TBE in place, there are a plethora of methods for managing the climate control of the enclosure where there is cured concrete. The possible methods of evaporating and thus drying out the concrete are as follows:

- **Raising the temperature of the surrounding air** - By increasing the temperature of the surrounding air, the temperature of the concrete increases as a consequence, facilitating the evaporation of the moisture within the concrete. Additionally, as the temperature of the air increases, the capacity of the air to hold moisture increase.
- **Drying out the surrounding air** - By reducing the relative humidity of the air, more evaporated moisture can be absorbed by the air.
- **Direct heating of the concrete** - By applying heat directly to the surface of the concrete, its temperature increases, accelerating the evaporation of moisture within the concrete. By utilizing units like radiant floor heaters, the drying process can be sped up in cold areas where the natural evaporation rate is slow. This method is more commonly used when large quantities of moisture needs to be evaporated due to water damage or leaks [77].

Overheating, directly or by the surrounding air, or excessive dryness of the air can be detrimental by causing cracking or damage to the structure. Therefore, it is of great importance to not oversize the heating and drying techniques used [78].

### 2.2.5 Concrete humidity measurement and requirements

Rådet för ByggKompetens (RBK) is a Swedish center for competence development in the construction industry, aiming to ensure a high level of education and knowledge assessment for professionals in the field [79, 80]. RBK is responsible for administering a system that standardizes moisture measurement in concrete. The goal of RBK-

authorized measurements is to ensure the safety of constructions by preventing moisture-related damage. RBK-authorized moisture inspectors follow set regulations and provide a measurement of RH in the concrete, where the RH-values need to be taken with special constraints in mind [80]. According to moisture consultant K. Bergström (personal communication 2024-03-20), some of the conditions for an RBK-authorized measurement are as follows:

- A concrete temperature during measurement should be withing the range of 15 and 25°C.
- Only small temperature fluctuations are allowed, with no more than 2°C variation in the surrounding air and 1°C in the concrete during the measurement.
- A TBE should be established [80].

The key takeaway lies in maintaining a stringent temperature range with minimal fluctuations. Therefore, it is of paramount importance to establish an effective climate control system in conjunction with a TBE before proceeding with any concrete moisture level measurements.

## 2.3 Dryers

Numerous drying technologies exists, each with various industrial usages. Dryers can be classified by whether drying operation is done in batch or continuous mode.

Batch operation is generally associated by lower production rates of dried goods whereas for higher production rates a continuous dryer is preferred [81]. The batch dryer will provide heat to a smaller batch of goods until the desired amount of water is evaporated, a new batch of wet goods is then fed to the dryer and the batch drying cycle starts anew.

In continuous operation, there is a flow of wet goods in and dry goods out at any instant in time. The continuous cycle does not have distinct start and stop, rather it has an ongoing production of dried goods from a continuous feed of wet goods. Apart from just classifying the dryer by drying operation, it is common to classify dryers by the mechanism of heat transfer [81]. The two major alternatives are convective or conductive driers, also known as direct and indirect driers [34]. During convective drying, fluids such as hot air, steam, or combustion gases have direct contact with the wet goods, causing the evaporation of water. During conductive drying, fluids such as steam, hot water or thermal oil is kept separate using e.g. metal surfaces or pipes as an heat exchanger [34].

### 2.3.1 Sludge dryers

There are many different companies providing dryers developed for the specific application of drying sludge with solutions such as belt-dryers and solar dryers. The majority being continuous dryers, utilizing different ways of heating the sludge to

evaporate the water contents. In this section a sludge belt-dryer is presented more in detail.

In this project, a sludge dryer like the conductive belt-dryer manufactured by Hydropress Huber AB is investigated. It is designed specifically for drying organic materials such as sewage sludge and digestion residues. Huber's feeding system presses strands of sludge, which are then slowly conveyed through the machine. This feeding method can enhance the sludge's permeability, while also reducing the amount of dust generated [18]. The sludge is transported gently through the dryer, further minimizing dust formation while the low operating temperature eliminates the risk of dust explosions [18]. According to Huber's technical sales coordinator K. Malm (personal communication 2024-03-14), the potentially problematic nature of the sludge, such as the sticky-phase, is handled by using back-mixing where a fraction of dried sludge is blended with the incoming wet sludge.

The belt-dryer produces a granulated sludge product that is easy to handle with small volumes of exhaust air, thanks to its proprietary recirculation system [18]. The exhaust needs to be treated before release into the environment. A simplified drawing of the process is presented in Figure 2.8.

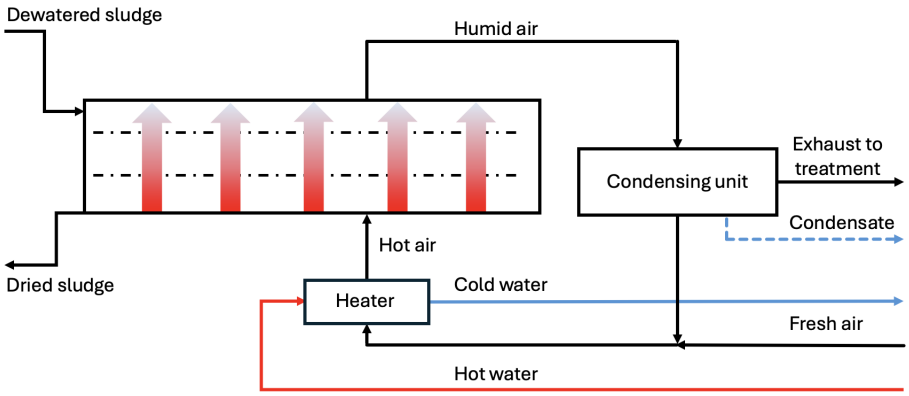


**Figure 2.8:** A simplified representation of a sludge belt-dryer

In the schematic of the dryer depicted in Figure 2.8, a heater, specifically an air-water heat exchanger, is utilized to supply hot air to the wet sludge. As the air transfers heat to evaporate the moisture, it cools down, and the resulting colder, now more humid air, is directed to a condensing unit to remove moisture. A portion of the air is then sent for treatment as exhaust, while the remainder is recirculated and mixed with fresh air.

### 2.3.2 Concrete dryers

In Sweden, the dominant equipment used for drying and climate control on construction sites are heating fans and condensation dehumidifiers [46]. These devices are commonly used individually as well as in combination with each other [46]. A common type of heating fan in Sweden is illustrated in Figure 2.9.


**Figure 2.9:** El-Björn heating fan [82].

This type of heating fan, which can be driven by both hot water and electricity, works by way of convection. The electric heating fans converts electrical energy into heat to the surrounding air while the hot water heating fans utilize a hot water supply system where hot water is circulated and supplies heat to the surrounding air. In both cases, fans are circulating air which gets heated along its path into the surroundings which in turn increases the temperature of the air in the heating fans vicinity [82]. By doing this, the temperature of the air in a room increases and thus the evaporation of moisture from adjacent materials is promoted. A controlled and directed source of heat is provided which is essential for the drying and climate control. In order to adequately affect the humidity of the air, a condensation dehumidifier can be used, shown in Figure 2.10.

**Figure 2.10:** El-Björn condensation dehumidifier [83].

The condensation dehumidifier works by removing the moisture from the air by condensation where a refrigeration cycle is utilized. A fan circulates air which passes through a set of cold coils with a temperature below the dew point of the air, which in turn causes the condensation. The condensed water is drained while the air is reheated and discharged back into the surroundings, but now with a lower humidity [83]. Dehumidifiers complements the heating provided from devices such as heating fans well for the aforementioned reasons.

# 3

# Theory

The following chapter presents an overview of common HP technologies and their working principles, followed by a literature review on refrigerant regulations. Furthermore, thermodynamic expressions, HP improvement measures, and the key performance indicators selected are presented.

## 3.1 Heat pump technology and working principles

A HP draws heat from various sources such as the surrounding air, geothermal energy stored underground, or nearby water bodies, as well as waste heat from industrial processes [84]. The temperature of this extracted heat is then amplified, making it useful. Due to the focus on heat transfer rather than generation, HPs boast significantly higher efficiency compared to traditional heating systems like boilers or electric heaters. Typically, the heat output is several times greater than the energy input required to power the HP, usually in the form of electricity [84].

There are many different kinds of HPs, and they can be classified in various ways. One classification is based on whether the cycle is open or closed. In a closed cycle, the working fluid (WF) is circulated, whereas in an open or semi-open, the WF flows through the system [85, 86]. Another classification is based on the heat sink and source [87]. For example, if the heat source is ambient air and the heat sink is water, it would be an air-to-water HP. A selection of these classifications will be presented in the following subsections.

### 3.1.1 Vapor compression heat pumps

The vapor compression heat pump (VCHP) operates by utilizing the pressure-related boiling temperature properties of the working fluid (WF) [88]. By adjusting the pressure in the expansion valve the WF boiling point is altered, causing it to evaporate at a desired temperature and absorb heat from the heat source [88]. Subsequently, compression to a higher pressure follows, where heat exchanging to the colder heat sink leads to condensation. A schematic representation of a VCHP is presented in Figure 3.1.

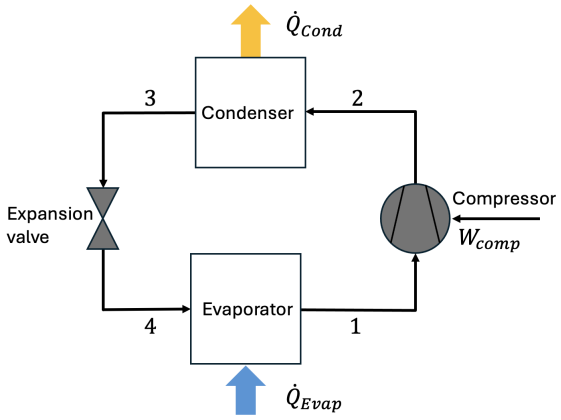


**Figure 3.1:** Schematic representation of a generic VCHP.

The WF undergoes vaporisation, in the evaporator, at a lower pressure utilizing a heat source ($\dot{Q}_{Evap}$), resulting in refrigerant vapor stream in point 1. The vapor stream is compressed, resulting in a temperature and pressure increase. To make use of this temperature increase, the refrigerant is condensed at the higher pressure, releasing its latent heat of vaporisation. This heat is delivered to a processes stream ($\dot{Q}_{Cond}$). The refrigerant is then expanded in an expansion valve back to the initial state of the cycle.

### 3.1.2 Absorption heat pumps

Absorption heat pumps (AHP) are divided into type I and II [89]. Both utilize a two-component mixture as WF in order to have an increased boiling point of the solution compared to the boiling point of the pure substance [10]. Furthermore, the components in the two types of AHPs are the same but the applications differ, where type I generally for cooling and type II is used for temperature increasing purposes [90]. In Figure 3.2 a schematic representation of an AHP type I is presented.

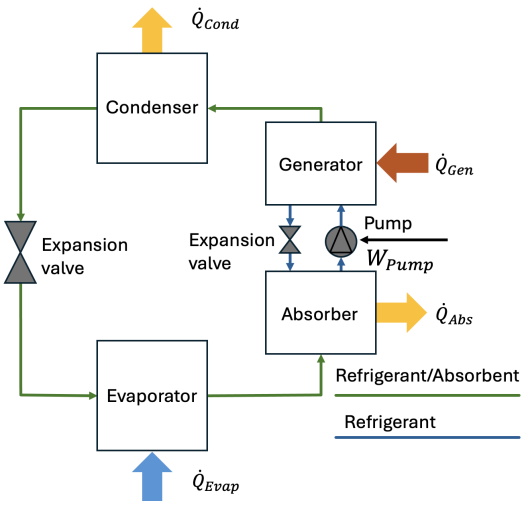


**Figure 3.2:** Schematic representation of an AHP type I.

The general AHP consists of four components: an evaporator, condenser, generator, and absorber, as depicted in Figure 3.2. The generator receives high-temperature heat ($\dot{Q}_{Gen}$), such as steam, causing vapor to be released from the WF at elevated pressure. The condensed high-pressure vapor undergoes heat recovery in the condenser, releasing heat to process stream ($\dot{Q}_{Cond}$). Subsequently, the high-pressure condensate is depressurized in the evaporator, utilizing waste heat to vaporize the low-pressure condensate ($\dot{Q}_{Evap}$). In the absorber, concentrated WF from the generator interacts with low-pressure vapor from the evaporator, releasing heat, ($\dot{Q}_{Abs}$). The WF completes the cycle by returning to the generator [28].

### 3.1.3 Mechanical vapor recompression heat pumps

The mechanical vapor recompression (MVR) HPs, are an open cycle HP where a schematic representation is shown in Figure 3.3.

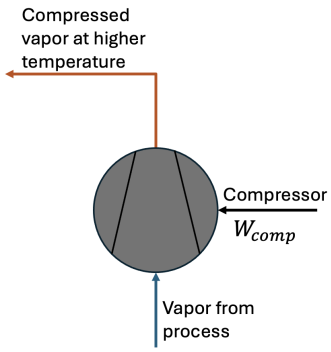


**Figure 3.3:** Schematic representation of a generic MVR.

Similarly to the VCHP, the MVR utilizes compression work to lift the temperature of a gaseous stream, thus providing more useful heat to a process. As seen in Figure 3.3 a gaseous stream is compressed, this compression results in a temperature increase. This compressed and hot vapor can be utilized in for example heat exchanging, making use of the available heat.

### 3.1.4 Hybrid heat pumps

This category include different hybrid setups, the one presented here is one of many and consists of a combination of an AHP an a VCHP. The ammonia-water hybrid absorption-compression heat pump (HACHP) is using a $NH_3/H_2O$ mixture and is considered as a promising high-temperature technology [91], and its functionality has already been proven in industry [92]. The schematic of the HACHP is shown in Figure 3.4.

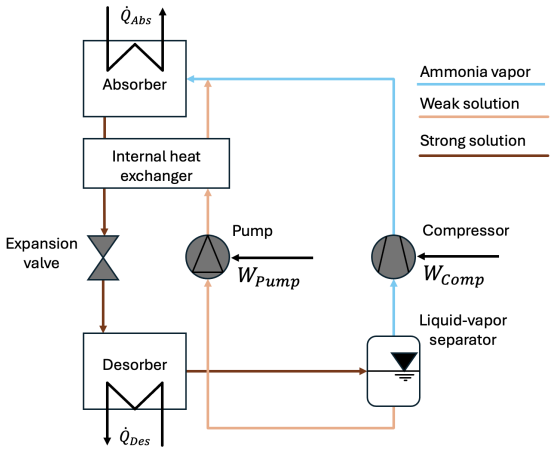


**Figure 3.4:** Schematic representation of a hybrid water-ammonia HACHP [92].

The desorber receives low-grade heat ($\dot{Q}_{Des}$), such as waste heat stream as an example, causing vaporisation of part of the $NH_3$ in the strong $NH_3/H_2O$ solution. The stream is lead to a liquid-vapor separator, where the ammonia vapor is directed to a compressor, which constitutes the VCHP part of the system. The weak solution, $NH_3/H_2O$ mixture with a lower $NH_3$ fraction, is pumped through an internal heat exchanger (IHX), where the return stream from the absorber serves as heat source. The heated weak solution is mixed with the compressed hot ammonia vapor and delivers heat ($\dot{Q}_{Abs}$) to a process stream [91, 92].

## 3.2 Refrigerants

In this section, environmental indicators, types of refrigerants, and a combination of history and regulations on refrigerants are discussed.

### 3.2.1 Environmental indicators

Two metrics are commonly used when evaluating WFs for the effects on the environment are [93]:

- 100-year time horizon global warming potential ($GWP_{100}$)
- Ozone depletion potential (ODP)

$GWP_{100}$ is a widely used environmental metric. It compares the warming effect of greenhouse gas emissions to that of CO2 emissions over a specific time frame, typically 100 years. $GWP_{100}$ is easy to understand: the lower the $GWP_{100}$, the less a substance contributes to global warming [93].

The ODP is a measure to compare to what extent a given chemical can harm the ozone layer relative to trichlorofluoromethane (CFC-11), which has an ODP of 1.0 [94]. This serves as the benchmark for comparison. A higher ODP indicates greater harm to the ozone layer.

### 3.2.2 Refrigerant types and history

Refrigerants are chemical substances, typically categorized as natural or synthetic, each possessing unique qualities and properties that influence their application and environmental impact. In the following section, both natural and synthetic refrigerants will be introduced in a historical context.

Almost 200 years ago, in 1834, the vapor compression cycle using refrigerants was invented [95]. During the 19th and early 20th centuries, natural refrigerants were widely used. However, some of the refrigerants were associated with safety issues, such as flammability and toxicity, which prompted the creation and use of refrigerants like chlorofluorocarbons (CFC) and hydrochlorofluorocarbons (HCFCs) [96].

In 1974, it was revealed that CFCs could be a major contributor to the presence of inorganic chlorine in the stratosphere, due to their photolytic decomposition [96]. This presence of chlorine in the stratosphere had been linked to the depletion of ozone [97], and in 1984 a group of British researchers described ozone holes [96]. In response, a global environmental treaty, the Montreal protocol, an agreement to decrease the use and manufacturing of ozone-depleting refrigerants, was signed in 1987. The industry developed two substitutes: the HCFCs and the hydrofluorocarbons (HFCs) [96]. However, the HCFCs still contained chlorine, and in the Copenhagen amendment of the Montreal protocol called for their production to be eliminated by the year 2030 [96]. Instead, the HFCs were considered one of the best substitutes for reducing stratospheric ozone loss because of their short lifetime and lack of chlorine, and refrigerants such as R134a became the go-to option [96].

Even if HFCs are ozone-friendly alternatives with widespread usage, they have become regulated with the Kigali amendment, due to their high $GWP_{100}$ [98]. Their projected emissions being 7-19% of global $CO_2$ by 2050, thus challenging the efforts keeping the global warming well below 2°C stated in the Paris agreement [3]. In 2016, it was agreed to add HFCs to the list of controlled substances and approved a timeline for their gradual reduction by 80-85% by the late 2040s.

The European Union published the F-gas regulation (EU 842/2006) in 2006, which started to place some restrictions on use and control of F-gases in a number of applications. In 2014, the F-gas regulation was updated with (EU 517/2014), imposing larger reductions in the use of HFCs in the EU [99]. The regulation was further revised in 2024, with the new F-gas regulation (EU 2024/573). This revised version states that by early 2036, the production of F-gases with high $GWP_{100}$-values should be decreased to 15%, measured in $CO_2$-equivalents, compared to the average level in 2011-2013 [100]. By the year 2050, the total amount of F-gases allowed to be released on the market measured in $CO_2$-equivalents should be zero [100]. The EU Commission does, however, state that the yearly quota can be adjusted for the HP-sector if deemed necessary [100]. Not all F-gases are being targeted; the focus of the regulation is those with higher $GWP_{100}$-values. Furthermore, the regulation introduces different phase-out dates of F-gases in certain applications and updates regulations governing best practices, leak inspections, record-keeping, training, waste disposal, and sanctions.

Finding replacements for the HFCs is ongoing, and the most recent development of F-gases have focused on hydrofluoro-olefins (HFOs), which are being introduced to the market as a zero ODP and low $GWP_{100}$ replacement of the HFCs [101]. Although HFOs are fluorinated, they are not currently undergoing phase-down regulations, due to their low $GWP_{100}$. However, most of the HFOs are classified as per- and polyfluoroalkyl substances (PFAS), making them susceptible for phase-out. This relates to the proposal on restriction on PFAS published in 2023 by the European Chemicals Agency [102]. In nature, many HFOs are decomposed into trifluoroacetic acid (TFA), a very persistent chemical compound [103, 102]. Both HFCs and HFOs are classified as PFAS chemicals and if they are included in the Registration, Evaluation, Authorisation and Restriction of Chemicals regulation they might be regulated further or potentially be prohibited [104].

### 3.2.3 Refrigerants studied

A selection of refrigerants with low $GWP_{100}$ and not classified as PFAS has been included in the list as potential WFs. All of the presented WFs have zero ODP and are listed in Table 3.1. The table includes the $GWP_{100}$ value, normal boiling point (NBP), critical pressure and temperature of each WF, as well as their safety classification. The ASHRAE Standard 34 [105], allocates refrigerants based on toxicity and flammability. The toxicity is determined between a lower toxicity (A) and a higher toxicity (B). The flammability is determined between no flame propagation (1), lower flammability (2) and higher flammability (3). The flammability subclass 2L is classified as mildly flammable with a low burning velocity.

**Table 3.1:** List of potential WFs, with their characteristic properties [106, 107, 108].

| **Refrigerant** | **Ref. No.** | **$GWP_{100}$** | **NBP (°C)** | **Critical Pressure (bar)** | **Critical Temp. (°C)** | **Safety Class** |
|---|---|---|---|---|---|---|
| Ammonia | R717 | 0 | -33 | 112.8 | 132.4 | B2L |
| Carbon dioxide | R744 | 1 | -79 | 73.8 | 31.0 | A1 |
| DME | RE170 | 1 | -24 | 53.4 | 127.3 | A3 |
| Ethane | R170 | 6 | -88.6 | 48.7 | 32.2 | A3 |
| Ethylene | R1150 | 4 | -103.8 | 50.4 | 9.2 | A3 |
| Iso-Butane | R600a | 3 | -11.7 | 36.3 | 134.7 | A3 |
| Iso-Pentane | R601a | 4 | 27.8 | 33.8 | 187.3 | A3 |
| n-Butane | R600 | 4 | -0.5 | 152.0 | 38.0 | A3 |
| Propane | R290 | 3.3 | -42 | 42.6 | 96.7 | A3 |
| Propylene | R1270 | 1.8 | -48 | 46.3 | 92.4 | A3 |
| Water | R718 | 0 | 100 | 220.6 | 373.9 | A1 |

## 3.3 Thermodynamics and heat pump optimization

In this section, general thermodynamic expressions used for evaluating VCHP cycles are presented, along with the Antoine equation, which can be used to determine the moisture content in ambient air.

### 3.3.1 The Antoine equation

The Antoine equation is a mathematical model that correlates the vapor pressure and temperature of pure substances and is shown in eq. (3.1).

$$\log_{10}(P_{\text{sat}}) = A - \frac{B}{T + C} \qquad [mmHg] \tag{3.1}$$

In the Antoine equation, $P_{sat}$ is the vapor pressure of the substance, T is the temperature in Kelvins and A, B and C are substance specific coefficients which are determined by experimental data [109].

**Table 3.2:** Antoine equation coefficients for water [109].

| Substance | A | B | C |
|---|---|---|---|
| Water | 8.07131 | 1730.63 | 233.426 |

In order to adequately model the air streams mass flow composition used for the simulations in Chapter 4, eq. (3.1) can be used where the constants for water are shown in Table 3.2.

$$P_{\text{H}_2\text{O}} = \frac{RH}{100} \cdot P_{\text{sat}} \cdot 133.322 \qquad [Pa] \tag{3.2}$$

By specifying the temperature and relative humidity of an air stream, it is possible to determine the mass fractions of the air stream by inserting a temperature, $T$ in eq. (3.1) and a relative humidity, $RH$ in eq. (3.2). The partial pressure of the water vapor can be calculated and since $P_{sat}$ is expressed in mmHg the conversion factor 133.322 from mmHg to Pascals is included in eq. (3.2).

$$P_{\text{dry-air}} = P_{\text{atm}} - P_{\text{H}_2\text{O}} \qquad [Pa] \tag{3.3}$$

The partial pressure of the dry air stream can be determined with eq. (3.3) under the assumption that the total pressure is 1 atmosphere.

$$n_{\text{sub}} = \frac{P_{\text{sub}}}{R \cdot T} \cdot Y_{\text{sub}} \qquad [mol] \tag{3.4}$$

In eq. (3.4), the subscript *sub* refers to the substances present in the air. With the partial pressure of both the water vapor and the dry air known, the moles, $n_{sub}$ of each substance can be determined with eq. (3.4). By assuming the molar fractions $Y_{\text{sub}}$, i.e., assuming that the water vapor consists entirely of water and that the dry air consists of 21% oxygen and 79% nitrogen, the ideal gas law can be utilized to determine the amount of moles corresponding to the vapor pressure $P_{\text{sub}}$, temperature T and the universal gas constant R. Water has a vapor pressure $P_{\text{sub}}$ denoted as $P_{\text{H}_2\text{O}}$ and a molar fraction $Y_{\text{sub}}$ equal to 1. Oxygen and nitrogen have a vapor pressure $P_{\text{sub}}$ denoted as $P_{\text{dry-air}}$ with molar fractions $Y_{\text{sub}}$ equal to 0.21 and 0.79, respectively.

$$X_{\text{sub}} = \frac{n_{\text{sub}} \cdot \text{M}_{\text{sub}}}{\sum_i n_i \cdot \text{M}_i} \qquad [-] \tag{3.5}$$

With the moles of water vapor, oxygen, and nitrogen known, the mass fractions of each component in the air stream can be calculated using eq. (3.5), where $X_{\text{sub}}$ represents the mass fraction and $M_{\text{sub}}$ is the molar mass of the substance. The denominator of the equation, $\sum_i n_i \cdot M_i$, is the sum of the products of the number of moles and the molar masses of all components present in the air stream, which are assumed to be water, nitrogen and oxygen.

### 3.3.2 Thermodynamic expressions

In the following section the relevant equations used for mass and energy balances are presented.

Equation (3.6) is used to determine the heat transfer in the condenser and eq. (3.7) in the evaporator.

$$\dot{Q}_{sink} = \dot{m}_{sink} \cdot c_p \cdot \Delta T_{sink} = \dot{m}_{ref} \cdot \Delta h_{Cond} = \dot{Q}_{Cond} \qquad [W] \tag{3.6}$$

Where $\dot{m}_{sink}$ denotes the heat sink mass flow, $c_p$ is the specific heat of this stream and $\Delta T_{sink}$ denotes the temperature change of the heat sink. $\dot{m}_{ref}$ is the mass flow of refrigerant and $\Delta h_{Cond}$ is the enthalpy change of the refrigerant in the condenser. In this project the condenser is simulated as one unit, where gas cooling, condensation, and subcooling is taking place.

$$\dot{Q}_{source} = \dot{m}_{source} \cdot c_p \cdot \Delta T_{source} = \dot{m}_{ref} \cdot \Delta h_{Evap} = \dot{Q}_{Evap} \qquad [W] \tag{3.7}$$

Where $\dot{m}_{source}$ denotes the heat source mass flow and $\Delta T_{source}$ denotes the temperature change of the heat source. $\Delta h_{Evap}$ is the enthalpy change of the refrigerant in the evaporator. In this project the evaporator is simulated as one unit, where both evaporation and superheating is taking place.

A VCHP cycle and its T-s diagram, where T-s diagrams are further discussed in Section 3.3.3.1, are shown in Figure 3.5a and Figure 3.5b, respectively.

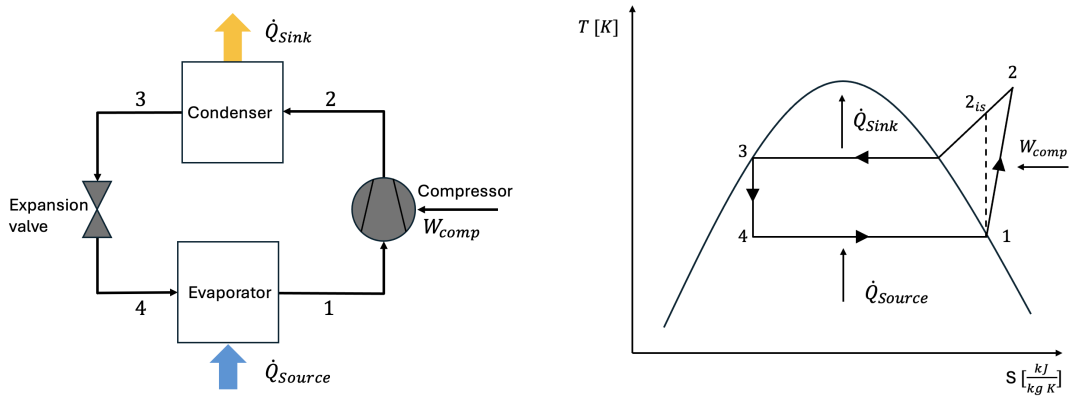


**(a)** Schematic VCHP cycle.

**(b)** T-s diagram of a VCHP cycle.

**Figure 3.5:** Schematic VCHP cycle and a general T-s diagram.

For the compressor, the isentropic efficiency is defined according to eq. (3.8):

$$\eta_{is} = \frac{h_{2,is} - h_1}{h_2 - h_1} \qquad [-] \tag{3.8}$$

where $h_{2,is}$ is the isentropic enthalpy value at point 2, $h_2$ is the actual enthalpy value at point 2, and $h_1$ is the enthalpy value of the refrigerant at point 1, as shown in Figure 3.5b.

By assuming that the throttling is adiabatic the enthalpy in point four is given by eq. (3.9).

$$h_4 = h_3 \qquad [\frac{kJ}{kg}] \tag{3.9}$$

### 3.3.3 Pinch point-based analysis and cycle visualization

In this section, the theory regarding a Pinch Point-based Analysis (PPA) by utilizing T-s diagrams will be introduced as a methodology for optimizing the integration of heat exchange between adjacent stream within the the VCHP system.

#### 3.3.3.1 T-s diagrams

T-s diagrams are diagrams that plot the temperature against the entropy for a fluid which are particularly useful for analysing processes that involve work and heat transfer. Process points and cycles such as an VCHP or Rankine Cycle can easily be visualised where key data and performance can be identified. In the T-s diagram, saturation lines are plotted which delineates the states at which a substance

exists as either a liquid, a vapor or a mixture of vapor and liquid in thermodynamic equilibrium. A generic T-s diagram for a VCHP is shown in Figure 3.6.

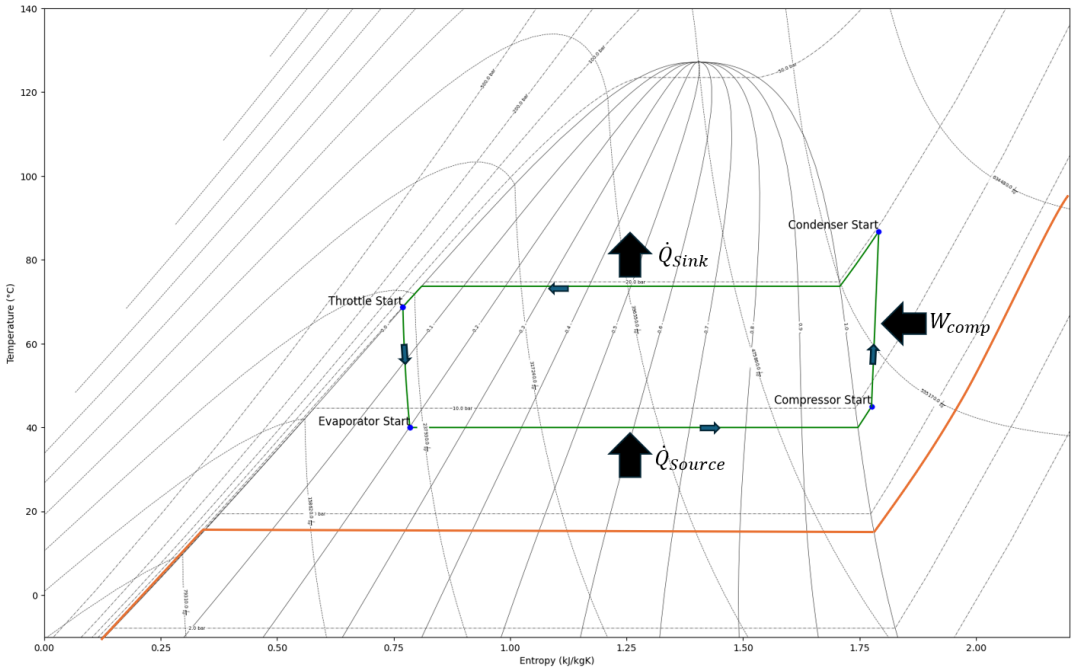


**Figure 3.6:** Representation of a generic VCHP cycle in a T-s diagram.

In Figure 3.6, the generic VCHP cycle with a strong resemblance to Figure 3.5b, is shown with each starting point indicated as well as the direction of the cycle. The orange line shown is an isobar, i.e., a line which follows a constant pressure throughout the entire T-s diagram from subcooled liquid to superheated vapor. The isobars are fundamental for the VCHP cycle as the VCHP works between two pressure levels where the entire cycle is made up of two isobars combined with adiabatic throttling and non-isentropic compression, shown in Figure 3.6.

The evaporation is shown starting at the lower isobar as a mixture of liquid and vapor and ending as a superheated vapor, where the concept of superheating will be discussed further in Section 3.3.4.1. The compression is shown starting as a superheated vapor at the lower pressure and ending as a superheated vapor at a higher pressure. The condensation is shown starting at the higher isobar as a superheated vapor and ending as a subcooled liquid. The throttle is shown starting at the higher pressure as a subcooled liquid and ending as a mixture of liquid and vapor at the lower pressure where the cycle is now closed.

The heat loads for the condenser and the evaporator are visualized by the two arrows. The heat load in the condenser, $\dot{Q}_{\text{sink}}$, signifies the released heat from the WF to the heat sink adjacent streams as it undergoes a phase change from vapor to liquid. As this process takes place at higher pressures, and thus temperatures, it facilitates the potential for heat sink adjacent streams to exchange heat at higher temperatures. In a similar manner, the heat load in the evaporator, $\dot{Q}_{\text{source}}$, signifies the absorbed heat

by the WF from the heat source adjacent streams as it undergoes a phase change from liquid to vapor. This process enables the WF to extract heat from adjacent streams, thereby facilitating the requisite heat exchange to power the VCHP. As the evaporator operates at lower pressure, and thus lower temperature, the potential integration of lower temperature heat sources is enabled. Additionally, the power input at the compressor, $W_{\text{comp}}$, represents the work required to compress the WF between the pressure levels. This increase in pressure also causes an increase in temperature.

#### 3.3.3.2 Heat exchange and the Pinch Point

PPA is a systematic methodology used to optimize the design and operation of heat exchanger networks [110]. A grassroots PPA can be utilized in conjunction with the T-s diagram to both graphically and mathematically determine if a heat exchanger matching is thermodynamically feasible. There are several scenarios in which a heat exchanger matching is not feasible, one of which is presented in Figure 3.7b, where the inlet hot stream temperature is lower than the desired outlet temperature of the cold stream. In other words, a stream match is feasible when the hot stream has a higher temperature than the cold stream everywhere in the heat exchanger, as shown in Figure 3.7a.

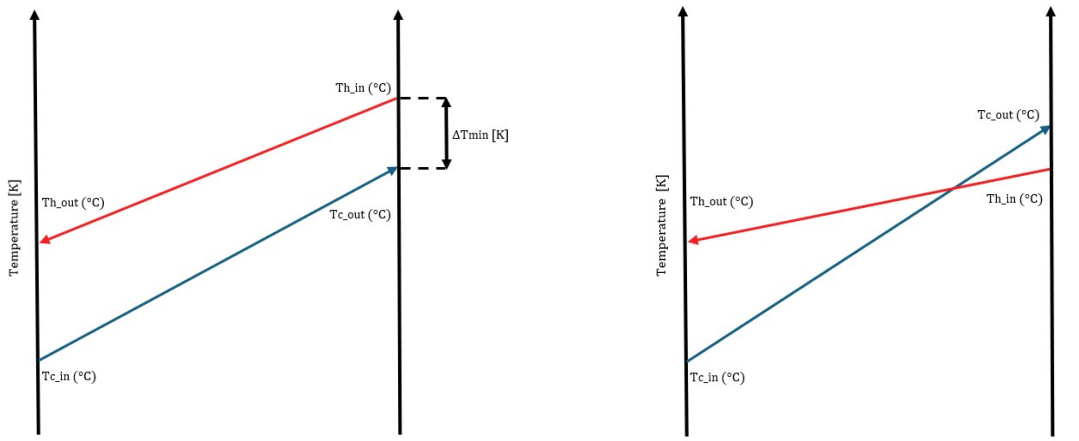


**(a)** Feasible heat exchanger. **(b)** Infeasible heat exchanger.

**Figure 3.7:** Comparison of two heat exchangers: one where the hot stream temperature is always higher than the cold stream (left), and one where the stream temperatures have a crossover (right).

It can be noted that in Figure 3.7a that the heat exchanger is feasible with a minimum temperature difference ($\Delta T_{\text{min}}$) located at the outlet of the cold stream and the inlet of the hot stream. In Figure 3.7b, as the cold stream crosses the hot stream it is not thermodynamically possible for the cold streams temperature to increase. The pinch point is defined as the point where the temperature profiles of the hot and cold streams intersect. This intersection represents the minimum temperature approach seen in Figure 3.7 which underscores the importance of maintaining a specified $\Delta T_{\text{min}}$ in heat exchanger design.

When the two streams are matched in a heat exchanger, it is then possible to determine the $\Delta T_{\min}$ criterion by checking the pinch point mathematically, graphically or with a combination of both. By analyzing the temperature profiles of the two streams, it is possible to validate if the absolute value of the temperature difference is equal or within a specified threshold. In a mathematical method, the generation of a vast amounts of temperature points between the two temperature profiles and utilization of a loop which calculates the temperature difference at every point in the temperature interval can be done. If the actual temperature difference exceeds the threshold, the mathematical method will either confirm compliance with the $\Delta T_{\min}$ criterion or flag a violation, prompting an adjustment in one of the streams. The graphical method involves plotting the temperature profiles of two streams and visually determining if the $\Delta T_{\min}$ criterion is met.

The required surface area $A$ needed for heat exchange is determined by eq. (3.10) [111].

$$A = \frac{\dot{Q}}{U \cdot \Delta T_{\mathrm{LM}}} \qquad [m^2] \tag{3.10}$$

The surface area, $A$, is dependant on the transferred heat, $\dot{Q}$, the overall heat transfer coefficient, $U$ and the logarithmic mean temperature difference, $\Delta T_{\mathrm{LM}}$, where the $\Delta T_{\mathrm{LM}}$ is shown in eq. (3.11) [111].

$$\Delta T_{\mathrm{LM}} = \frac{\Delta T_{\mathrm{hot}} - \Delta T_{\mathrm{cold}}}{\ln\left(\frac{\Delta T_{\mathrm{hot}}}{\Delta T_{\mathrm{cold}}}\right)} = \frac{(T_{\mathrm{hot,in}} - T_{\mathrm{cold,out}}) - (T_{\mathrm{hot,out}} - T_{\mathrm{cold,in}})}{\ln\left(\frac{T_{\mathrm{hot,in}} - T_{\mathrm{cold,out}}}{T_{\mathrm{hot,out}} - T_{\mathrm{cold,in}}}\right)} \quad [\mathrm{K}] \tag{3.11}$$

In order to maximize the energy efficiency, a $\Delta T_{\min}$ that is as low as possible is wanted, but it can be observed in eq. (3.10) that if $\Delta T_{\mathrm{LM}}$ becomes smaller, $A$ needs to increase to maintain the same $\dot{Q}$ [111]. A larger surface area means larger and thus more costly heat exchangers. Due to the nature of the $\Delta T_{\mathrm{LM}}$, it does not have a large impact if either one of $\Delta T_{\mathrm{hot}}$ or $\Delta T_{\mathrm{cold}}$ is larger than the other as the smaller temperature difference will dominate [111]. To achieve both an efficient energy transfer and a cost effective solution for a heat exchanger, a trade off between the investment and running costs is needed [112].

### 3.3.4 Heat pump improvement measures

In this section, the theoretical effects of intercooling, subcooling, superheating, and compression ratios on the VCHP cycle will be introduced. The goal is to explore various improvement measures that could be implemented, but in the project only subcooling and superheating are used.

#### 3.3.4.1 Subcooling and superheating

In a basic VCHP cycle, the refrigerant vapor is assumed to leave the evaporator as saturated vapor [113]. However, in the actual cycle, superheating is most often preferred before the refrigerant is compressed. This superheating is commonly achieved by extending the heat transfer area in the evaporator, allowing the refrigerant to become superheated. One of the benefits of superheating is that it ensures that the refrigerant is fully vaporized before entering the compressor [113], thereby minimising the risk of liquid droplets forming which may cause damage to the compressor. However, a potential drawback is that the compression work increases. In conclusion, the overall effect on the cycle performance can be either positive or negative [114].

Subcooling occurs when the refrigerant at the higher pressure level, in the condenser, is cooled below its boiling point. This ensures that all of the refrigerant is liquefied before reaching the expansion valve [113]. A more subcooled refrigerant will, when expanded, undergo less evaporation, allowing it to absorb more latent heat in the evaporator [113]. In other words, the heat transfer in the condenser increases with more subcooling, while simultaneously increasing the potential heat transfer in the evaporator. By transferring more heat in the condenser without requiring additional compression work, the cycle efficiency is increased. However, achieving subcooling requires increasing the heat transfer area.

Both superheating and subcooling can increase cycle performance; however, both measures require additional heat exchanger area, which can be costly. To determine the optimal level of superheating and subcooling, the trade-off between investment cost of additional heat exchanger area and the increase in cycle performance must be investigated.

#### 3.3.4.2 Internal regenerative heat exchanger

In addition to the previously mentioned methods of improving cycle performance, it is also possible to include an internal regenerative heat exchanger (IHX) [115], visualized in Figure 3.8.

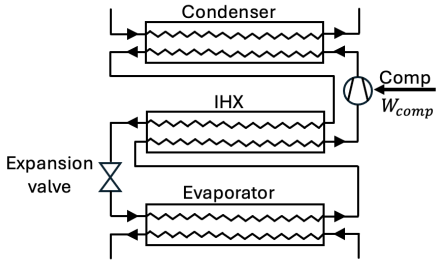


**Figure 3.8:** Flowsheet diagram of a VCHP cycle with an IHX.

The IHX facilitates heat exchange between the hot condenser outlet and the evaporator outlet in Figure 3.8. Thus, it makes it possible to avoid gas expansion after throttling while also ensuring that no liquid droplets enter the compressor. In other

words, the IHX enables subcooling of the high-pressure side by superheating the low-pressure side [115].

#### 3.3.4.3 Multi-stage compression

Multi-stage compression is another measure that can improve the COP of a VCHP. One benefit is that by dividing the compression into multiple stages, the compression ratio, discussed in section 3.3.4.4, can be limited. The intercooler cools the refrigerant after the first compressor stage. By lowering the suction temperature of the second compressor, the compressor work is reduced [116]. Furthermore, the discharge temperature can be lowered, ensuring it remains within recommended levels. A flowsheet diagram of a VCHP cycle with an intercooler is shown in Figure 3.9a.

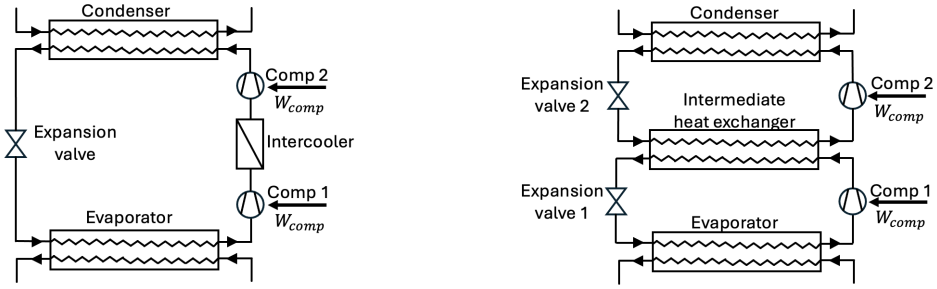


**(a)** Multi-stage compression with intercooling.

**(b)** Cascaded system, with two distinct pressure levels.

**Figure 3.9:** Flowsheet diagrams of two multi-stage compression cycles: one featuring intercooling (left) and the other employing a cascaded system with two distinct pressure levels (right).

Another approach to address high compression ratios and discharge temperatures is to use two separate refrigerant loops operating as a cascade system [117], one with a lower and one with a higher pressure level [118]. A flowsheet diagram of this system is shown in Figure 3.9b. An intermediate heat exchanger serves as the evaporator in the high-pressure loop and as a condenser in the low-pressure loop. This set-up can allow low temperature heat sources to be utilized for relatively high temperature temperature condenser levels [118].

#### 3.3.4.4 Compression ratio

Understanding the compression ratio is crucial for optimizing the performance and longevity of compressors in various systems. The compression ratio, defined in eq. (3.12), indicates the relationship between the condenser pressure level, $p_{discharge}$, and the evaporator pressure level, $p_{suction}$, i.e., the two pressure levels illustrated in Figure 3.6.

$$\beta = \frac{p_{discharge}}{p_{suction}} \qquad [-] \tag{3.12}$$

Different compressor types, such as reciprocating and rotary screw compressors, handle varying compression ratios differently. Operating at higher compression ratios often accelerates compressor wear and reduces its lifespan [119]. Consequently, high compression ratios can lead to elevated discharge temperatures, as discussed by Stewart [120], posing risks for component degradation. To mitigate this issue, dividing the compression process into multiple stages presents a viable solution. This approach allows for intercooling, facilitating a reduction in discharge temperatures by lowering the suction temperature, as discussed in detail in section 3.3.4.3.

### 3.3.5 Mass flow correlations

This section presents the fundamental equations used to determine the necessary mass flows required to ensure the drying processes. It begins with relations used to calculate the heat demand of the continuous sludge dryer, followed by a discussion on concrete drying.

#### 3.3.5.1 Continuous drying

To determine the desired dryer size in order to dry the sludge, the amount of evaporated water must be estimated. The amount of water into the dryer, $\dot{m}_{water,1}$, is defined by eq. (3.13)

$$\dot{m}_{water,1} = \dot{m}_{sludge,1} \cdot (1 - DM_1) \qquad [\frac{kg}{s}] \tag{3.13}$$

where $\dot{m}_{sludge,1}$ is the mass of incoming wet sludge to be dried, and $DM_1$ is the fraction of DM in the sludge before drying. The amount of water that remains in the sludge after drying is defined by eq. (3.14)

$$\dot{m}_{water,2} = \dot{m}_{sludge,2} \cdot (1 - DM_2) \qquad [\frac{kg}{s}] \tag{3.14}$$

where $DM_2$ is the desired DM fraction of the sludge at the outlet of the dryer, and $\dot{m}_{sludge,2}$ is the total amount of sludge leaving the dryer, defined by eq. (3.15)

$$\dot{m}_{sludge,2} = \dot{m}_{sludge,1} \cdot \frac{DM_1}{DM_2} \qquad [\frac{kg}{s}] \tag{3.15}$$

The amount of evaporated water, $\dot{m}_{water,evaporated}$, is calculated by eq. (3.16)

$$\dot{m}_{water,evaporated} = \dot{m}_{water,1} - \dot{m}_{water,2} \qquad [\frac{kg}{s}] \tag{3.16}$$

The dryer's heat demand, $\dot{Q}_{dryer,continuous}$, is calculated according to eq. (3.17)

$$\dot{Q}_{dryer,continuous} = \dot{m}_{water,evaporated} \cdot \dot{E}_{dryer} \qquad [W] \tag{3.17}$$

where the $\dot{E}_{dryer}$ is the sludge dryer's specific heat demand per kg of evaporated water.

#### 3.3.5.2 Batch drying

In batch drying, the heat demand varies over time, being higher at the beginning and declining as time passes. The climate control required to dry out concrete on a construction site resembles this profile. Initially, the concrete and its surrounding air are cold, resulting in a high heat demand. Once a stable indoor climate and concrete temperature are achieved, the heat demand stabilizes at a lower level. Once the specified dryness is confirmed in an RBK measurement, there is no need for further drying.

In the context of this work, the heat load $\dot{Q}_{dryer,batch}$ is of interest, as it is closely tied to the HP's condenser load. $\dot{Q}_{dryer,batch}$ is determined as a consequence of the choice of heating fans and their specified heat demand.

## 3.4 Performance indicators

The approach adopted in this work focuses on defining possible layouts and comparing HP cycles. To make fair comparisons, suitable criteria for evaluation and corresponding reasonable assumptions were identified.

### 3.4.1 Thermodynamic performance

The thermodynamic performance is measured by the coefficient of performance (COP), which is the ratio between useful heat supplied to the heat sink and the compression work, as described in eq. (3.18).

$$COP = \frac{\text{Useful Heat}}{\text{Compression work}} \qquad [-] \tag{3.18}$$

Understanding and using the COP for comparisons necessitates having consistent inlet and outlet temperatures for both the heat source and heat sink in all situations. The working principle of a HP is presented in Figure 3.10.

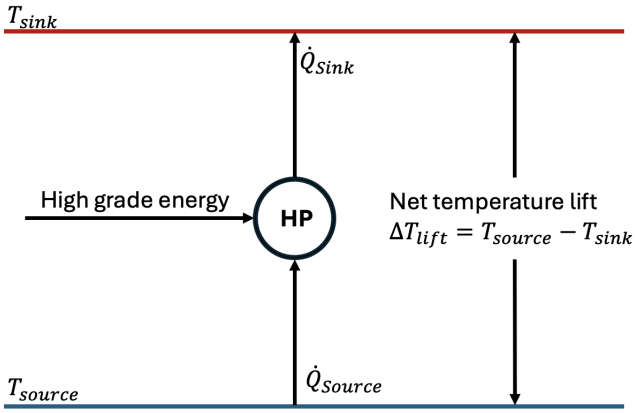


**Figure 3.10:** Visual representation of HP working principle.

From Figure 3.10 it can be seen that the $\Delta T_{lift}$ can be defined as eq. (3.19).

$$\Delta T_{lift} = T_{sink} - T_{source} \qquad [^{\circ}C] \tag{3.19}$$

The ideal HP cycle COP is often called $\text{COP}_{Carnot}$ and is defined in a number of ways relating to sink and source temperatures in eq. (3.20) where the temperatures are in Kelvin.

$$COP_{Carnot} = \frac{T_{sink}}{T_{sink} - T_{source}} = \frac{1}{1 - \frac{T_{source}}{T_{sink}}} \qquad [-] \tag{3.20}$$

The actual COP is calculated by dividing the condenser heat load by the compression work, and can be expressed as:

$$COP = \frac{\dot{Q}_{Sink}}{W_{comp}} \qquad [-] \tag{3.21}$$

where $W_{comp}$ is the compression work. The deviation from the $COP_{Carnot}$ is mainly due to reversibility of the compression in the ideal cycle, which cannot be achieved in a real system [121].

For a HP, the required $\Delta T_{lift}$ can be higher than the capacity of the HP, meaning that the target temperature cannot be delivered. This is exemplified in Figure 3.11.

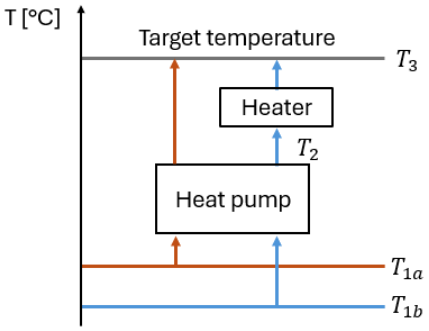


**Figure 3.11:** Generalized representation of temperature levels in an air-to-air HP system, showing two distinct ambient temperatures, $T_{1a}$ and $T_{1b}$.

In the figure, two distinct ambient temperatures, $T_{1a}$ and $T_{1b}$, are presented. At $T_{1a}$, the HP capacity allows the HP to deliver the target temperature $T_3$. However, if the ambient temperature is at $T_{1b}$, the $\Delta T_{lift}$ is larger than the HP's capacity. The temperature leaves at the temperature $T_2$. To ensure that the target temperature $T_3$ is reached, an additional electric heating coil is added to heat the air.

To evaluate this system configuration, a second performance indicator is introduced: the coefficient of system performance (COSP), as defined in eq. (3.22).

$$COSP = \frac{\dot{Q}_{Sink} + \dot{Q}_{SH}}{W_{comp} + \dot{Q}_{SH}} \qquad [-] \tag{3.22}$$

Where $\dot{Q}_{SH}$ is the supplementary heating required by the heater to ensure that the target temperature is reached. The heater is only operated when the ambient temperature, in this example, is lower than what the HP can lift to the target temperature.

### 3.4.2 Economic indicators

The economic performance can be assessed using various parameters, taking into account both the yearly cash flows and one-time investments. The one-time investments can be included in the absolute value of the total capital investment cost (TCI). The TCI can be obtained from suppliers or by the use of suitable cost functions.

To compare annual cash flows with one-time expenses, it is necessary to calculate the present values of future expenses. This was achieved using the capital recovery factor (CRF), assuming an effective interest rate, $i$, and a plant lifetime of $n$ years.

$$CRF = \frac{i \cdot (1+i)^n}{[(1+i)^n] - 1} \qquad [\frac{1}{year}] \tag{3.23}$$

The operational cost is defined by the annual cash flows (CF) involving both incomes

and expenses. For a HP, expenses include the cost for consumed electricity ($CF_{El}$). The income ($CF_{Utility}$) is generated through the supply of heat transferred to the heat sink. If the HP replaces, for example, a natural gas boiler, the income is viewed as the savings from not operating the boiler. The cash flow related to the heat source ($CF_{Source}$) can be negative, representing an expense if payment is required for the heat, or positive, indicating additional income, such as offering a cooling service.

By using the CRF, it is possible to determine the net present value (NPV), which describes the total value of the investment at the time of the investment. This involves aggregating the TCI and the present value of annual cash flows. In eq. (3.24) the TCI is assumed to be paid fully year 0 (overnight construction cost).

$$NPV = -TCI + \frac{CF_{Utility} - CF_{El} + CF_{Source} - CF_{Fixed,OM}}{CRF} \qquad [€] \tag{3.24}$$

Where the term, $CF_{Fixed,OM}$, denotes the expenses related to fixed operation and maintenance and can be estimated as a percentage, $\gamma$ of the TCI as shown in eq. (3.25).

$$CF_{Fixed,OM} = \gamma \cdot TCI \qquad [€] \tag{3.25}$$

When calculating the NPV there are two potential outcomes [122]:

NPV $> 0$: Indicates that the investment will be profitable.

NPV $< 0$: Indicates that the investment will be associated with a net loss.

The simple payback period (PBP) indicates the number of years needed to recover the initial investment, serving as an additional measure to evaluate the potential investment [123].

$$PBP = \frac{TCI}{CF_{Utility} - CF_{El} + CF_{Source} - CF_{Fixed,OM}} \qquad [years] \tag{3.26}$$

The PBP is commonly used in expensive projects as an indicator of financial risk [124], before calculating other economic indicators. Often, management has defined a cutoff PBP above which the project is deemed too risky. However when performing economic evaluations it is necessary to consider how assumptions regarding, e.g., price development may affect the outcome, this is true for both the NPV and PBP.

Another metric for comparing alternative technologies is the levelized cost of heat or specific heat (LCOH) which can be determined using eq. (3.27) [125].

$$LCOH = \frac{TCI + \frac{\sum_{t=0}^{n} CF_{OM,t}}{(1+i)^t}}{\sum_{t=0}^{n} \frac{\dot{Q}_t}{(1+i)^t}} \qquad [\frac{€}{MWh}] \tag{3.27}$$

Where $CF_{OM,t}$ represents the cash flow related to operation and maintenance in year $t$, considering both fixed and variable cash flows, and $\dot{Q}_t$ is the heat generated in year $t$. The value of $CF_{OM,t}$ can be estimated using eq. (3.28)

$$CF_{OM,t} = CF_{Fixed,OM} + CF_{Variable,OM} \qquad [€] \tag{3.28}$$

Here $CF_{Variable,OM}$ denotes the variable cash flows for the HPs, which can be estimated using eq. (3.29) [125].

$$CF_{Variable,OM} = \sum_{t=1}^{h} [\frac{C_{el} \cdot \dot{Q}_{sink,h}}{COP_h}] \qquad [€] \tag{3.29}$$

Where $h$ denotes hours of operation per year, $COP_h$ is the hourly COP of the HP, $\dot{Q}_{sink,h}$ denotes the hourly $\dot{Q}_{sink}$, and $C_{el}$ is the specific electricity price (€/MWh). This indicator can be used to compare different heat producing technologies, and see which has the lowest specific cost per MWh thermal energy.

### 3.4.3 Greenhouse gas emissions related indicators

The environmental performance of the HP system focuses on GHG emission related indicators, primarily the impact of annual GHG emissions related to adopting a HP compared to using a standard source of heat.

The reduction in GHG emissions per Wh can be estimated using eq. (3.30)

$$\Delta Em_{CO_{2-eq}} = Em_{utility} - Em_{HP} \qquad [\frac{tCO_{2-eq}}{Wh}] \tag{3.30}$$

where $Em_{utility}$ is the $CO_{2-eq}$ emissions of the reference system and $Em_{HP}$ the HP integrated system $CO_{2-eq}$ emissions.

# 4

# Methodology

This study consisted of three distinct stages: a literature review, interviews, and simulations. Where the literature did not provide enough information, interviews were conducted to better grasp e.g., the building construction processes and the specific problems with climate control in this environment. Furthermore, interviews were held to better understand the existing drying and climate control technologies.

The literature review focused on finding the drivers, such as policies, commitments, and regulations mainly regarding refrigerants. Thus, the major part of the refrigerant screening was based on the current legislation but ongoing national and international investigations on the topic. For example the exclusion of HFOs was based primarily on their uncertain future, with expected PFAS-regulations, as discussed in section 3.2.2.

For the simulations, this study used Aspen Plus® to perform heat pump system analysis. In addition, to support the PPA, a Python-code was developed in order to generate T-s diagrams, using open-source databases, to visualize the HP cycle working conditions. This enabled both a visual understanding of where in the VCHP cycle the $\Delta T_{min}$ in both condenser and evaporator occurs, while also enabling the minimum temperature difference to be quantified.

## 4.1 Refrigerant screening

The screening of the WFs was based on a literature review as well as a thermodynamic screening. The literature review identified potential natural refrigerants, see Table 3.1, primarily due to the F-gas regulation, discussed in section 3.2.2. The ideal choice of refrigerant would have zero ODP and low $GWP_{100}$. Since all natural refrigerants included in the screening had zero ODP, their $GWP_{100}$ value played a pivotal role in the selection. The thermodynamic screening considered NBP and critical temperature combined with operational conditions of the processes to be integrated with the proposed HP solutions. The screening process is summarized in Figure 4.1.

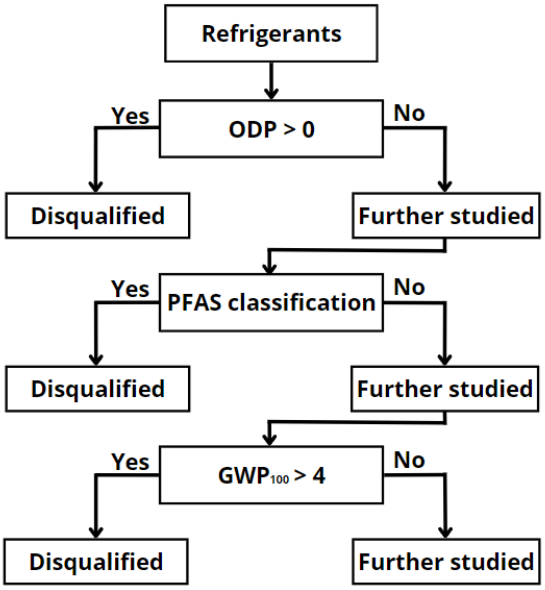


**Figure 4.1:** Tree structure of the refrigerant screening.

## 4.2 Simulation and modeling

In this section the simulation and modeling methodology used is presented in a general manner for all cases. A more detailed presentation of case specific (CS) assumptions and boundary conditions are presented in section 4.4. A flowsheet of the VCHP cycles is presented in Figure 4.2.

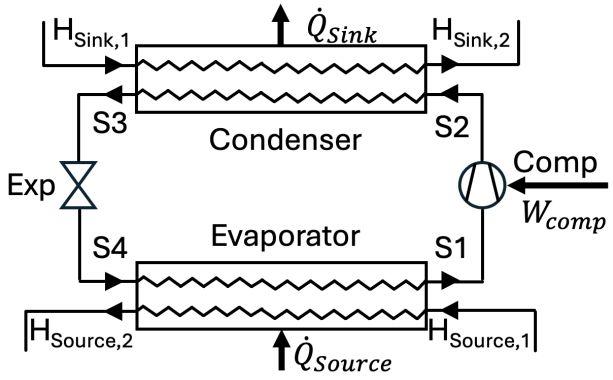


**Figure 4.2:** Flowsheet diagram of a VCHP cycle using one compressor.

In Figure 4.2 the streams indices $H_{Source,1}$ and $H_{Source,2}$ correlates to the heat source inlet and outlet, whereas $H_{Sink,1}$ and $H_{Sink,2}$ correlates to the heat sink inlet and outlet. The stream S1–S4 is the refrigerant loop.

The methodology for determining the HP cycle performance for varying refrigerants is presented in Figure 4.3. This methodology is applied to the cases further discussed in Section 4.4, with their unique CS target values.

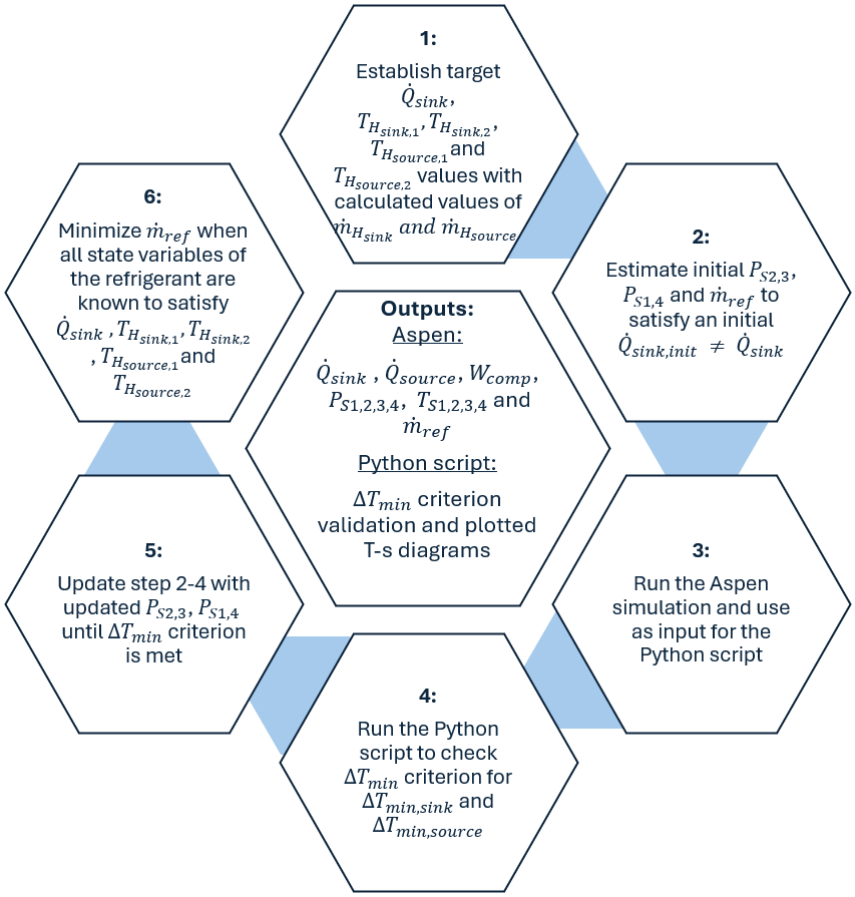


**Figure 4.3:** Iterative Aspen-Python methodology for determination of HP cycle performance for varying refrigerants and case studies.

The iterative methodology described in Figure 4.3, has the following steps:

1. The methodology starts by establishing the CS target values, from assumptions and specification from reference HPs and dryers further discussed in Section 4.4. The target values are the heat sink load, $\dot{Q}_{sink}$, temperatures of the heat sink and source streams $T_{H_{sink,1}}$, $T_{H_{sink,2}}$, $T_{H_{source,1}}$, $T_{H_{source,2}}$ as well as the heat sink and source streams mass flows $\dot{m}_{H_{sink}}$ and $\dot{m}_{H_{source}}$ respectively. The heat sink load and the temperatures are determined first, so that the mass flows can be calculated using eq. (3.6) and eq. (3.7). A generic representation of the temperature profiles of a VCHP-cycle is shown in Figure 4.4.

2. Initial pressure levels in the condenser and evaporator, $P_{S2,3}$ and $P_{S1,4}$ respectively, are estimated based on the heat sink and source streams temperatures, as well as tabulated values for the WF. The initial values were approximated to create a preliminary model of the VCHP-cycle, with the objective of enhancing its performance during the subsequent stages of the methodology. Generic iso-bars correlated to the pressure levels are shown in Figure 4.4. An initial mass flow of the refrigerant in the VCHP-cycle is also guessed. If wrong, the heat sink load, $\dot{Q}_{sink,init}$, calculated with eq. (3.6), is initially larger or smaller

than the target heat sink load, $\dot{Q}_{sink}$. The target temperatures of the heat sink and source streams are also affected for the same reasons. Analogously to the pressure levels, the mass flow of the refrigerant is adjusted in the later stages to enhance the cycles performance and reach the target values established in step 1.

3. With the pressure levels and refrigerant mass flow for the VCHP determined in step 2, the model can now be simulated in Aspen. The Aspen simulation output parameters used to determine the cycle performance is used as input parameters for the Python script, discussed further in Section 4.3, where the Aspen simulation output are shown in Table 4.1.

4. The simulation output parameters from Aspen in step 3 are used in the Python script, discussed further in Section 4.3, where the VCHP-cycle is plotted in a T-s diagram along with the heat sink and source temperature profiles. A PPA is done with the Python script, verifying that the $\Delta T_{min}$ criterion is fulfilled for both the condenser and heat sink as well as the evaporator and heat source. The Python scripts output is the T-s diagram and the two $\Delta T_{min}$ values.

5. If the $\Delta T_{min}$ criterion in step 4 is not fulfilled, the pressure levels in step 2 are updated, whilst maintaining the initially higher refrigerant mass flow. The Aspen simulation is run with the updated values and the Python script is run with the updated Aspen simulation output parameters to repeat the $\Delta T_{min}$ criterion check. The aim with adjusting the pressure levels is e.g. to lower the condensation iso-bar seen in Figure 4.4 closer to the red line of the heat sink if the $\Delta T_{min}$ value is too large and vice versa if the $\Delta T_{min}$ is too small. The same is done for the evaporation iso-bar and the blue line of the heat source. This process is repeated until the $\Delta T_{min}$ criterion is met in both cases.

6. With the working points of the VCHP determined in step 5, the initially higher refrigerant mass flow is minimized to satisfy the established target values in step 1 and the iterative Aspen-Python methodology is completed. The compressor work and state variables of the last iteration in Aspen, with acceptable $\Delta T_{min}$ values, is saved for further analysis in Section 5.

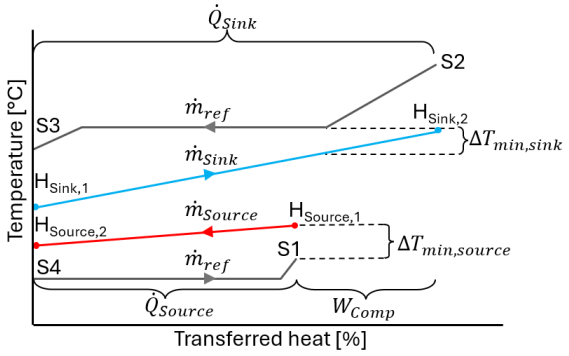


**Figure 4.4:** Diagram of temperature profiles over transferred heat.

## 4.3 The Python script

A Python script was developed to both visualize the VCHP cycles in a T-s diagram and perform a PPA, as discussed in Sections 3.3.3.1 and 3.3.3.2. The script was based on Fluprodia version 3.0, a Python package that enables users to create unique fluid property diagrams by utilizing the CoolProp database [126, 127]. The script was designed to account for general input parameters as well as the output from Aspen simulations and CS parameters, shown in Table 4.1.

**Table 4.1:** Python script input parameters

| **Input parameters type** | **Parameter** | **Unit** |
|---|---|---|
| **General:** | | |
| Compressor isentropic efficiency | $\eta_{is}$ | [-] |
| Minimum temperature difference | $\Delta T_{min}$ | [K] |
| Subcooling temperature difference | $\Delta T_{subcooling}$ | [K] |
| Superheating temperature difference | $\Delta T_{superheating}$ | [K] |
| **Aspen simulations output:** | | |
| Evaporator pressure | $P_{S4}$ | [bar] |
| Evaporator temperature | $T_{S4}$ | [°C] |
| Condenser pressure | $P_{S2}$ | [bar] |
| Condenser temperature | $T_{S2}$ | [°C] |
| Throttle temperature | $T_{S3}$ | [°C] |
| Throttle quality | $X_{S3}$ | [-] |
| **CS:** | | |
| Refrigerant used | $Ref$ | [-] |
| Refrigerant T-s diagram interval | $Ref_{\text{interval}}$ | [-] |
| Heat sink inlet temperature | $T_{H_{Sink,1}}$ | [°C] |
| Heat sink outlet temperature | $T_{H_{Sink,2}}$ | [°C] |
| Heat source inlet temperature | $T_{H_{Source,1}}$ | [°C] |
| Heat source outlet temperature | $T_{H_{Source,2}}$ | [°C] |

The general parameters in Table 4.1 were held constant for all simulations, presented in Table 4.5 later on. The Aspen simulation output values used to determine the cycle performance in Table 4.1 were derived using the general method described in Section 4.2 and the VCHP cycle shown Figure 4.2. $P_{S4}$=$P_{S1}$ and $T_{S4}$ correspond to the state variables of stream S1, $P_{S2}$ and $T_{S2}$ to the state variables of stream S2 and $T_{S3}$ and $X_{S3}$ to stream S3, respectively, in Figure 4.2. The CS values in Table 4.1 were derived from the unique target temperatures for each case as well as the refrigerants determined from Section 4.1, where the cases are further discussed in Section 4.4.

$T_{H_{H_{Sink,1}}}$ denotes to the heat sink inlet temperature, $T_{H_{H_{Sink,2}}}$ denotes to heat sink outlet temperature, $T_{H_{H_{Source,1}}}$ denotes to the heat source inlet temperature, and $T_{H_{H_{Source,2}}}$ denotes to the heat source outlet temperature, as shown in Figure 4.2. The main function of the script is to draw T-s diagrams in which saturation lines and iso-lines are clearly visible. Meaning that the script first draws the saturation

lines for a specified refrigerant, $Ref$, in a user-defined CS interval, $Ref_{\text{interval}}$.

An illustrative use of the script can be seen in Figure 4.5, with the code being presented in Appendix B for the concrete air-to-water case with R717 being used as the refrigerant.

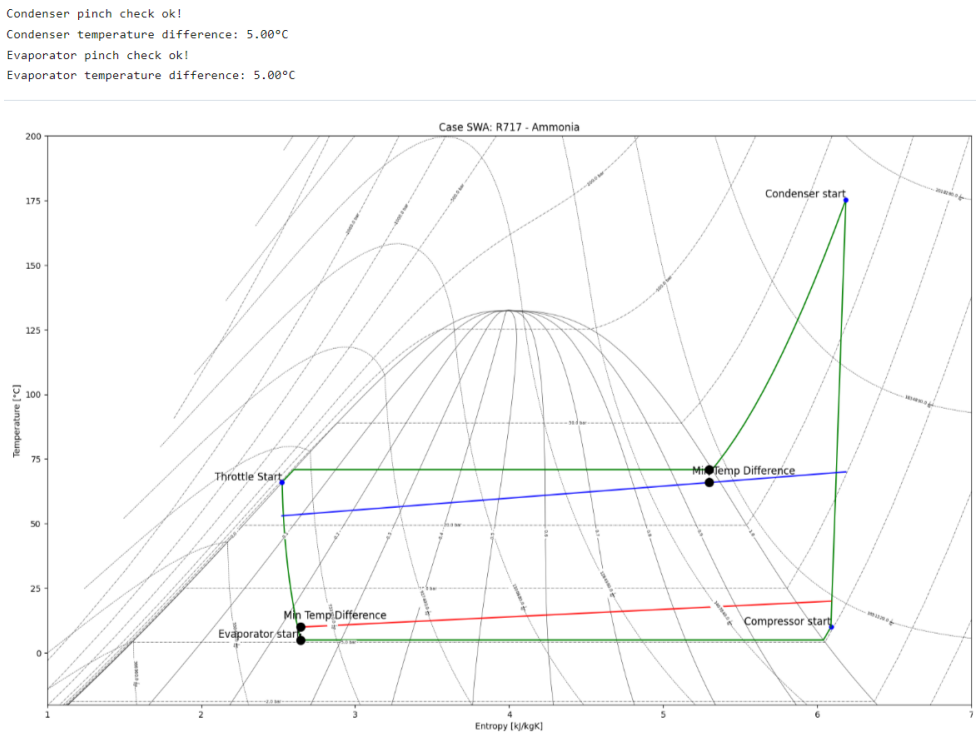


**Figure 4.5:** Python script output for a VCHP in the SWW case using R717.

With the background saturation lines, interval and scale of the T-s diagram done, the script then calculates four specific iso-lines corresponding to the VCHP-cycle shown in Figure 3.6:

- The first iso-line represents the iso-bar transition from the Evaporator start to the Compressor start, meaning that the script draws a line at a constant pressure $P_{\text{S4}}$=$P_{\text{S1}}$ from a start point determined by $P_{\text{S4}}$=$P_{\text{S1}}$, $T_{\text{S4}}$ and $X_{\text{S4}}$=$P_{\text{S1}}$ to the end point, determined by $P_{\text{S1}}$, saturated vapor line and the $\Delta \text{T}_{superheating}$.
- The second iso-line corresponding to the compression between the Compressor start and Condenser start, meaning that the script calculates the compression process while taking into account the isentropic efficiency of the compressor. The start point is the same as the end point for the first iso-line and the end point is determined by $P_{\text{S2}}$=$P_{\text{S3}}$ and $\eta_{is}$.
- The third iso-line represents the iso-bar transition from the Condenser start to the Throttle start, meaning that the script draws a line at a constant pressure $P_{\text{S2}}$=$P_{\text{S3}}$. The start point is the same as the end point for the second iso-line and the end point is determined by saturation liquid line and the $\Delta \text{T}_{subcooling}$.

- The fourth iso-line represents the isenthalpic expansion from Throttle start to Evaporator start, meaning that the script draws a line at a constant enthalpy, $h_{S3}$=$h_{S4}$. This enthalpy value is determined from the $T_{S3}$ and $P_{S3}$=$P_{S2}$ from the start point, which is the same as the end point of the third iso-line, to the end point, which is the start point of the first iso-line.

With the HP cycle drawn in the T-s diagram the script can perform the PPA. The temperature profiles of the heat sink and heat source are plotted in the T-s diagram based on the specified values of $T_{CS_{H_{Sink,1}}}$, $T_{CS_{H_{Sink,2}}}$, $T_{CS_{H_{Source,1}}}$ and $T_{CS_{H_{Source,2}}}$ respectively. The script then sequences the temperature profiles of the heat sink and heat source in evenly spaced intervals. The $\Delta T_{min}$ is calculated at every starting point of an interval between the first iso-line and the heat source temperature profile as well as the third iso-line and the heat sink temperature profile. The $\Delta T_{min}$-points are plotted for both the heat sink and heat source temperature profiles in the T-s diagram and the value of said points are printed. Further analysis in Aspen according to the method described in Section 4.2 is now possible if the $\Delta T_{min}$ criterion is not fulfilled.

## 4.4 Cases

To demonstrate and discuss the method, the procedure was applied to four case studies, one VCHP cycle and one MVR for the sludge case study and two different VCHP cycles for the concrete case study. These cases were determined, based on available reference technologies and products. A summary of the investigated HP integrated drying systems follows:

1. Sludge drying with an integrated water-to-water HP, using a process stream as heat source.

2. Concrete drying with an integrated air-to-water HP, using ambient air as heat source.

3. Concrete drying with an integrated air-to-air HP, using ambient air as heat sink, and room exhaust as heat source.

4. Sludge drying with an integrated MVR, using bio-gas from sludge pre-processing as the working fluid.

As shown in the list above, two different HP technologies were investigated. The MVR study was a preliminary study, where the produced raw biogas at a WWTP was considered as the WF. However, this alternative was disregarded after further investigation. See Appendix E for more information regarding this preliminary study. The potential heat sources for the VCHP include a process waste-heat stream, which can originate from a neighboring facility or the clean outlet stream from, for example, a WWTP. For simplicity, the three cases are hereafter referred to as follows: SWW (sludge drying using a water-to-water HP), CAW (concrete drying using an air-to-water HP), and CAA (concrete drying using an air-to-air HP).

In the SWW case, the reference utilities seen as potential heat supplies are an electric boiler, DH, or a gas boiler. In the CAW case, the reference heat supplies are either an electric-, DH-, or diesel-driven heating fan. These reference utilities were determined from the interviews with K. Bergström and K. Malm, but also from the literature review of the drying processes (personal communication 2024-03-20 and 2024-03-14 respectively).

### 4.4.1 Sludge: Water-to-water

In this section, the investigated HP-integrated sludge drying system is discussed, and the variables used in the simulations are presented. The proposed HP-integrated sludge dryer is depicted in Figure 4.6. The belt dryer used as a reference can be operated using, for example, district heating, a gas boiler, or an electric boiler as a heat source [18]. In this project, these three potential heat sources are to be replaced with a VCHP. The system recirculates a water stream between the heater and condenser, serving as the heat sink.

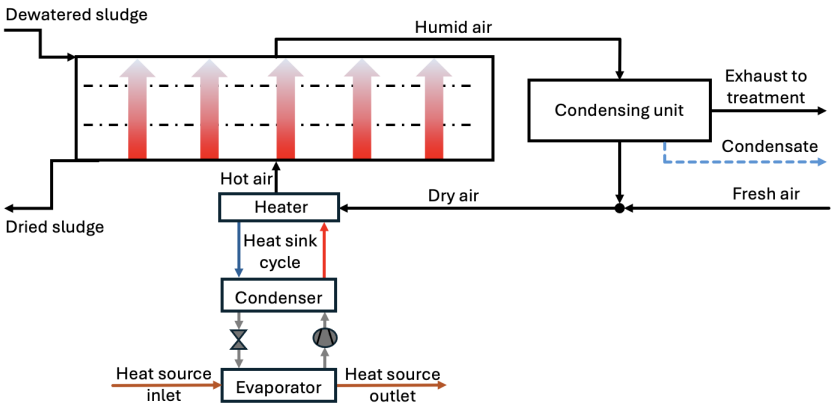


**Figure 4.6:** Proposed design of a water-to-water HP-integrated sludge dryer.

The depicted dryer system utilizes a water-to-water HP, which uses a waste heat stream as heat source. The system boundaries for evaluating the system were placed around the VCHP, as the dryer itself is outside the scope of this thesis project, but are depicted for clarity. The variables used for simulating the HP solutions used in the sludge case study are presented in Table 4.2. The variables include the heat source and sink temperatures used in the VCHP studies.

**Table 4.2:** Variables used in the evaluation of the sludge case using water-to-water HP.

| Case SWW | Variable |
|---|---|
| **HP design variables:** | |
| Heat sink inlet temperature | $T_{SWW_{H_{sink,1}}}$ |
| Heat sink outlet temperature | $T_{SWW_{H_{sink,2}}}$ |
| Heat source inlet temperature | $T_{SWW_{H_{source,1}}}$ |
| **Process variables:** | |
| Mass flow of digested sludge | $\dot{m}_{sludge,1}$ |
| Heat sink load | $\dot{Q}_{\mathrm{SWW}}$ |
| Percentage of DM before dryer | $DM_1$ |
| Percentage of DM after dryer | $DM_2$ |
| **Other assumptions:** | |
| Heat source temperature difference | $\Delta \mathrm{T}_{SWW,source}$ |

### 4.4.2 Concrete: Air-to-water

In this section, one of the investigated HP-integrated concrete drying systems is discussed, and the variables used in the simulations are presented. This system is illustrated in Figure 4.7, and it utilizes an air-to-water HP that provides hot water to a water-heated fan, as depicted in Figure 2.9.

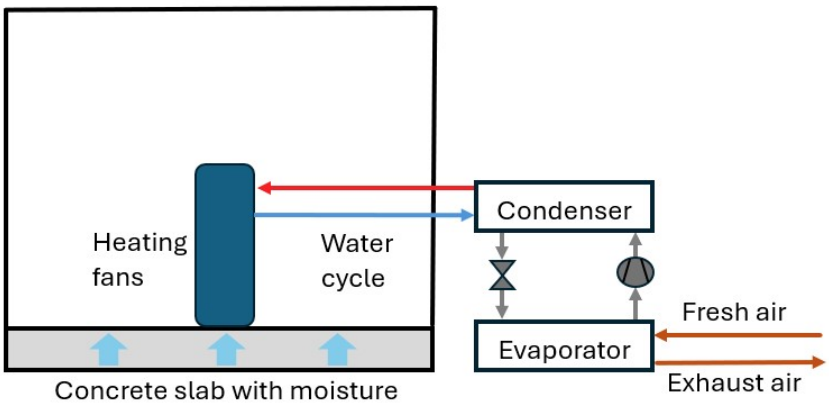


**Figure 4.7:** Proposed design of a water-to-air HP integrated concrete drying system

The proposed system uses ambient air as heat source, as depicted in Figure 4.7. A water loop is used to transfer heat between the heating fans and the condenser. The set-up of the thermoeconomic evaluation of the HP integrated CAW drying system, using ambient air as heat source, is presented in Table 4.3.

**Table 4.3:** Variables used in the evaluation of the concrete case using air-to-water HPs.

| Case CAW | Variable |
|---|---|
| **HP design variables:** | |
| Heat sink load | $\dot{Q}_{\text{CAW}}$ |
| Heat sink inlet temperature | $T_{CAW_{H_{sink,1}}}$ |
| Heat sink outlet temperature | $T_{CAW_{H_{sink,2}}}$ |
| Heat source inlet temperature | $T_{CAW_{H_{source,1}}}$ |
| **Process variables:** | |
| Relative humidity ambient air | $RH_{\text{amb,air}}$ |
| Mass fractions ambient air | $X_{\text{sub,amb,air}}$ |
| Fresh air mass flow | $\dot{m}_{\text{CAW,air}}$ |
| Water cycle mass flow | $\dot{m}_{\text{CAW,water}}$ |

### 4.4.3 Concrete: Air-to-air

In this section, the second concrete drying systems will be discussed, and the variables used in the simulations will be presented. This system is illustrated in Figure 4.8, and it utilizes an air-to-air HP.

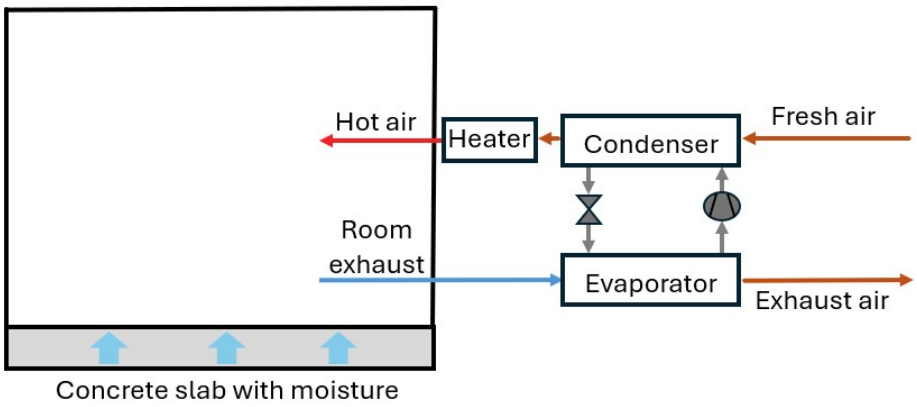


**Figure 4.8:** Proposed design of a air-to-air HP integrated concrete drying system

The condenser in this system heats ambient air, and if the capacity is too low, i.e., that the ambient air does not carry enough heat, an additional heater is used to ensure that the hot air entering the building reaches the specified temperature. The return air, or the room exhaust, is used as the heat source. It would be possible to recirculate this heat source, see Appendix F, where results from a preliminary study of this are presented.

The set-up of the thermoeconomic evaluation of the HP integrated CAA drying system, using ambient air as a heat source, is presented in Table 4.4.

**Table 4.4:** Variables used in the evaluation of the concrete case using air-to-air HPs.

| **Case CAA** | **Variable** |
|---|---|
| **HP design variables:** | |
| Heat sink load | $\dot{Q}_{\text{CAA}}$ |
| Supplementary heating load | $\dot{Q}_{\text{SH}}$ |
| Heat sink inlet temperature | $T_{CAA_{H_{sink},1}}$ |
| Heat sink outlet temperature | $T_{CAA_{H_{sink},2}}$ |
| Supplementary heating inlet temperature | $T_{\text{SH},1} = T_{CAA_{H_{sink},2}}$ |
| Supplementary heating outlet temperature | $T_{\text{SH},2}$ |
| Heat source inlet temperature | $T_{CAA_{H_{source},1}}$ |
| **Process variables:** | |
| Relative humidity exhaust air | $RH_{\text{exh,air}}$ |
| Mass fractions exhaust air | $X_{\text{sub,exh,air}}$ |
| Relative humidity ambient air | $RH_{\text{amb,air}}$ |
| Mass fractions ambient air | $X_{\text{sub,amb,air}}$ |
| Fresh air volume flow | $\dot{V}_{\text{CAA,air}}$ |
| Fresh air mass flow | $\dot{m}_{\text{CAA,air}}$ |

## 4.5 Case description

In the following section, all assumptions and data used in the VCHP cycle simulations are presented, beginning with general assumptions related to the HP.

Table 4.5 presents the general assumptions applicable to all VCHP cycle simulations.

**Table 4.5:** HP associated assumptions applied in all simulations.

| HP assumptions | Value | Unit |
|---|---|---|
| Expansion valve | Adiabatic | [-] |
| $\eta_{is}$ | 87.5 | [%] |
| $\Delta T_{min}$ | 5 | [K] |
| $\Delta T_{subcooling}$ | 5 | [K] |
| $\Delta T_{superheating}$ | 5 | [K] |
| $\Delta P_{losses}$ | 0 | [-] |
| $\Delta \dot{Q}_{\text{losses}}$ | 0 | [-] |
| $U$ | 0.0203019012 [a] | [kW/m$^2$,K] |

[a] Default value in Aspen Plus.

The expansion valve was assumed to be adiabatic, providing an isenthalpic expansion process. The compressor efficiency, $\eta_{is}$, was assumed to be 87.5%. Furthermore, the WFs were assumed to leave the evaporator superheated by 5 K and, for all WFs except $CO_2$, be subcooled by 5 K in the condenser. Another assumption made in the evaluation was to have a specified minimum temperature, $\Delta T_{min}$, of 5 K. To enable a fair comparison between the VCHP cycles, the operation conditions for each cycle was adjusted in an iterative manner to achieve the specified $\Delta T_{min}$. The working fluid properties were calculated by Aspen Plus using the REFPROP property method [128]. Moreover, pressure drops and heat losses in piping and heat exchangers were neglected. The heat transfer coefficient, $U$, in the condenser and evaporator were kept constant using a standard value provided by Aspen, presented in Table 4.5. Moreover, the condenser are modelled as one unit, instead of a separate gas cooler, condenser, and subcooler. Similarly, the evaporator and superheater are modelled as one unit.

### 4.5.1 Sludge: Water-to-water

For dimensioning the sludge drying system, the belt dryer from Hydropress Huber AB was used as a reference. This dryer has a stated thermal heat requirement of 0.85 kWh/kg of evaporated water [18]. Additionally, the annual generation of digested sludge uses Ryaverket in Gothenburg as reference, assuming that all generated sludge goes to incineration, thus this amount of digested sludge should be dried.

In Table 4.6 the values of all variables used in the sludge drying case study are presented.

**Table 4.6:** Input values used in sludge drying system evaluation.

| Case SWW | Value | Unit |
|---|---|---|
| **HP design values:** | | |
| $T_{SWW_{H_{sink,1}}}$ | 53 | [°C] |
| $T_{SWW_{H_{sink,2}}}$ | 70[a] | [°C] |
| $T_{SWW_{H_{source,1}}}$ | 20[b] | [°C] |
| **Process input values:** | | |
| $\dot{m}_{sludge,1}$ | 6725 | [kg/h] |
| $\dot{Q}_{SWW}$ | 3874.3 | [kW] |
| $DM_1$ | 0.29 | [-] |
| $DM_2$ | 0.90 | [] |
| **Other assumptions:** | | |
| $\Delta T_{SWW,source}$ | 10 | [K] |

[a] One of multiple possible operating temperatures according to Huber's technical sales coordinator K. Malm (personal communication 2024-03-14).
[b] Based on the cumulative waste heat in EU28 [129], where the amount available waste heat at 20°C is substantial.

The mass flow rate of wet digested sludge, $\dot{m}_{sludge,1}$, was calculated as the annual generation divided by the assumed number of operating hours. The value of $\dot{Q}_{SWW}$ was determined using eq. (3.17). The temperature related to the heat source, $T_{SWW_{H_{source,1}}}$, was assumed based on cumulative waste heat data at different temperatures in EU28 [129], rather than directly referencing a process stream. The cumulative amount of waste heat peaked at around 20°C [129], which was considered a feasible waste heat temperature likely to be found either at a WWTP or a power plant in sufficient quantities. To provide a more comprehensive understanding of how this assumption, regarding available waste heat temperature, affects the results, this value was varied in a sensitivity analysis discussed in Section 5.2.

As the heat source temperature involved uncertainties instead of assuming an outlet temperature, the temperature difference, $\Delta T_{SWW,source}$, between the heat source inlet and outlet was assumed to be 10 K.

The temperatures of the heat sink, $T_{SWW_{H_{sink,1}}}$ and $T_{SWW_{H_{sink,2}}}$, are based on possible operating temperature in Huber's belt-dryer according to Huber's technical sales coordinator K. Malm (personal communication 2024-03-14). The inlet DM fraction, $DM_1$, was based on data on digested sludge from Ryaverket [17], while the outlet DM fraction, $DM_2$, was assumed based on literature values presented in Section 2.1.3.

### 4.5.2 Concrete: Air-to-water

In the CAW case, ambient air acts as the heat source, its temperature, $T_{CAW_{H_{source,1}}}$, was assumed to be 7°C with a relative humidity, $RH_{\text{amb,air}}$, of 77%, based on average data in Gothenburg [130]. All of the variable values used in the simulations for the CAW case are presented in Table 4.7.

**Table 4.7:** Input values used in the evaluation of the concrete case using air-to-water HPs.

| Case CAW | Value | Unit |
|---|---|---|
| **HP design values:** | | |
| $\dot{Q}_{\text{CAW}}$ | 86.4 | [kW] |
| $T_{CAW_{H_{sink,1}}}$ | 40 | [°C] |
| $T_{CAW_{H_{sink,2}}}$ | 45 | [°C] |
| $T_{CAW_{H_{source,1}}}$ | 7 | [°C] |
| **Process input values:** | | |
| $RH_{\text{amb,air}}$ | 77 | [%] |
| $X_{\text{amb,air}}$ | $\sum X_{sub,i} = 1$ | [-] |
| $X_{\text{H}_2\text{O}}$ | 0.00474 | [$\text{kg}_{H_2O}/\text{kg}_{amb,air}$] |
| $X_{\text{O}_2}$ | 0.23181 | [$\text{kg}_{O_2}/\text{kg}_{amb,air}$] |
| $X_{\text{N}_2}$ | 0.76345 | [$\text{kg}_{N_2}/\text{kg}_{amb,air}$] |
| $\dot{m}_{\text{CAW,water}}$ | 4.135 | [kg/s] |

The heat sink in this system is a water stream that is heated in the condenser and directed to portable heating fans, where the heat is transferred to the room, as depicted in Figure 4.7. Moreover, based on an existing HP-integrated drying system [131], the operating conditions related to the heat sink were set to have a heating capacity, $\dot{Q}_{\text{CAW}}$, of 86.4 kW, an incoming temperature, $T_{CAW_{H_{sink,1}}}$, of 40°C and outgoing temperature, $T_{CAW_{H_{sink,2}}}$ of 45°C. Additional data presented in Table 4.8 include the estimated mass flow, $\dot{m}_{\text{CAW,water}}$, of the heat sink, and the mass fractions of oxygen, water vapor, and nitrogen in the ambient air, $X_{\text{O}_2,amb}$, $X_{\text{H}_2\text{O},amb}$, and $X_{\text{N}_2,amb}$. The mass fractions were calculated using eq. (3.1) through (3.5).

### 4.5.3 Concrete: Air-to-air

In the CAA case, ambient air acts as the heat sink. The inlet temperature, $T_{CAA_{H_{sink,1}}}$, was assumed to be 7°C with a relative humidity of $RH_{\text{amb,air}}$ of 77%, similar to the heat source in the CAW case. However, the HP system uses warm exhaust air from the construction site as its heat source, with an assumed relative humidity, $RH_{\text{exh,air}}$, of 60% and a temperature, $T_{CAA_{H_{source,1}}}$, of 15°C [132]. All of the variable values used in the simulations for the CAA case are presented in Table 4.8.

**Table 4.8:** Input values used in the evaluation of the concrete case using air-to-air HPs.

| **Case CAA** | **Value** | **Unit** |
|---|---|---|
| **HP target values:** | | |
| $\dot{Q}_{\text{CAA}}$ | 86 | [kW] |
| $\dot{Q}_{\text{SH}}$ | 30.2 | [kW] |
| $T_{CAA_{H_{sink},1}}$ | 7 | [°C] |
| $T_{CAA_{H_{sink},2}}$ | 20.3 | [°C] |
| $T_{\text{SH},1} = T_{CAA_{H_{sink},2}}$ | 20.3 | [°C] |
| $T_{\text{SH},2}$ | 25 | [°C] |
| $T_{CAA_{H_{source},1}}$ | 15 | [°C] |
| **Process input values:** | | |
| $RH_{\text{exh,air}}$ | 60 | [%] |
| $X_{\text{exh,air}}$ | $\sum \text{X}_{sub,exh,i}$=1 | [-] |
| $X_{\text{H}_2\text{O,exh}}$ | 0.0063 | [$\text{kg}_{H_2O}/\text{kg}_{exh,air}$] |
| $X_{\text{O}_2,exh}$ | 0.23145 | [$\text{kg}_{O_2}/\text{kg}_{exh,air}$] |
| $X_{\text{N}_2,exh}$ | 0.76225 | [$\text{kg}_{N_2}/\text{kg}_{exh,air}$] |
| $RH_{\text{amb,air}}$ | 77 | [%] |
| $X_{\text{amb,air}}$ | $\sum \text{X}_{sub,amb,i}$=1 | [-] |
| $X_{\text{H}_2\text{O,amb}}$ | 0.00474 | [$\text{kg}_{H_2O}/\text{kg}_{amb,air}$] |
| $X_{\text{O}_2,amb}$ | 0.23181 | [$\text{kg}_{O_2}/\text{kg}_{amb,air}$] |
| $X_{\text{N}_2,amb}$ | 0.76345 | [$\text{kg}_{N_2}/\text{kg}_{exh,air}$] |
| $\dot{V}_{\text{CAA,air}}$ | 18500 | [$\text{m}^3/h$] |
| $\dot{m}_{\text{CAA,air}}$ | 6.35 | [kg/s] |

The air flow, $\dot{m}_{\text{CAA,air}}$, was calculated using the assumed air conditions stated in Table 4.8 and volumetric air, $\dot{V}_{\text{CAA,air}}$, of 18,500 $\text{m}^3$/h flow based on an existing air-to-air HP [132]. Additionally, the heating capacity, $\dot{Q}_{\text{CAA}}$, was assumed to be 86 kW and the target temperature of the air entering the construction site, $T_{\text{SH},1}$, was assumed to be 25°C based on the same existing air-to-air HP [132]. With the given heating capacity, it was concluded that an additional electric heater was needed to ensure that 25°C was achieved. Using the ambient conditions stated in the table, the additional heating, $\dot{Q}_{\text{SH}}$, was determined to be 30.2 kW. In Table 4.8, $X_{\text{O}_2,exh}$, $X_{\text{H}_2\text{O},exh}$, $X_{\text{N}_2,exh}$, $X_{\text{O}_2,amb}$, $X_{\text{H}_2\text{O},amb}$, and $X_{\text{N}_2,amb}$ are the mass fractions of oxygen, water vapor, and nitrogen in the exhaust and ambient air respectively. The mass fractions was determined as functions of the relative humidity $RH_{\text{amb,air}}$ and the temperature $T_{CAA_{H_{source},1}}$ by utilizing eq. (3.1) through (3.5).

## 4.6 Economic Evaluation

The economic evaluation consisted of two parts, the first using constant reference costs of electricity, DH, and gas. The second, presented in Section 4.7.1 included sensitivity analyses in which the reference prices were varied, simulating price developments in order to determine their impact on NPV.

In Table 4.9 a summary of all assumed economical parameters used is presented. The methodology used for approximating the cost of DH and gas will be discussed briefly after the table.

**Table 4.9:** Summary of assumptions made for the economic evaluation of the three HP solutions.

| **Economic variables** | **Value** | **Unit** |
|---|---|---|
| Sludge-HP: Annual operating, $h_{sludge}$ | 7680 | [h/year] |
| Concrete-HP: Annual operating, $h_{concrete}$ | 3000 | [h/year] |
| Lifetime, $n$ | 20 | [years] |
| Interest rate, $i$ | 8 | [%] |
| Cash flow related to heat source, $CF_{Source}$ | 0 | [-] |
| $CF_{Fixed,OM}$ percentage of TCI, $\gamma$ | 5 | [%] |
| SEK to Euro conversion, $Conv$ | 11.6216[a] | [SEK/€] |
| Specific cost, electricity, $C_{el}$ | 47.55[b] | [€/MWh] |
| Specific cost, district heating, $C_{DH}$ | 50.95[c] | [€/MWh] |
| Specific cost, gas boiler, $C_{gas}$ | 90.55[d] | [€/MWh] |
| Specific cost, diesel, $C_{diesel}$ | 170.57[e] | [€/MWh] |
| Sludge-HP: Index markup | 1.2298[f] | [-] |
| Concrete-HP: Index markup | 1.2781[g] | [-] |

[a] Conversion rate on 18th of April 2024 09:43 (GMT+2).
[b] Average value of 2023s monthly electricity price on Nordpool, in SE3 [133].
[c] Based on 2024s prices, if bought from Göteborg Energi [134].
[d] Assumed boiler efficiency of 90% and average prices in Sweden 2023 [135].
[d] Assumed efficiency of 75% and Swedish diesel price on 13th of May 2024 excl. VAT [136].
[f] Inflation index markup applied used for TCI estimation in the SWW case [137].
[g] Inflation index markup applied used for TCI estimation in the CAW/CAA cases [138].

In Table 4.9, it can be seen that the economic lifetime of all VCHPs was assumed to be 20 years, with an assumed interest rate of 8%. The operation hours for the sludge case were assumed to be 7680 hrs, and for the concrete case, 3000 hrs. The $CF_{Fixed,OM}$ for each year was assumed to be 5% of the TCI, which was estimated using cost functions presented in Appendix D. Additionally, the cash flow related to the heat sources, $CF_{Source}$, ambient air or excess heat, used in the simulations have been neglected.

Since this study is confined in the Gothenburg region, the price of DH was estimated using price data from the local DH provider, Göteborg Energi. Their DH price consists of three parts, energy, power, and efficiency [134]. The energy relates to the energy consumption, the power is based on the average of the measured power

output and is calculated by multiplying the system's average power output by the variable power price, to this a fixed power price is added. For the efficiency Göteborg Energi uses the return temperature, from the consumer, compared to the DH systems' average temperature as a measure of efficiency [134]. In Appendix A, the assumptions and data used in this study to estimate the average specific cost of DH are presented.

The specific cost associated with natural gas was determined using the average price in Sweden in Q2, 2023, and assuming a boiler efficiency of 90% [135]. Given the drastic fluctuations in the price of natural gas in recent years, caution should be exercised when using this value. However, since natural gas was included to provide a broader perspective rather than being considered a reasonable reference utility in a Swedish context, this approach was deemed appropriate for determining the specific cost. In a similar manner the specific cost associated with diesel was conducted. The diesel conversion efficiency was assumed to be 75%, and the diesel price used was from the 13th of May 2024 excluding VAT [136].

## 4.7 Sensitivity analysis

In the following section, the methodology used to perform a sensitivity analysis on one of the assumed system boundary conditions is discussed. Starting with the procedure for the SWW solution for sludge drying, followed by CAW and CAA in the concrete case study.

In the SWW case, the heat source is the process parameter with the highest uncertainty. Thus, the heat source stream was varied between 20°C to 55°C assuming a constant $\Delta T_{SWW,source}$ of 10 K between inlet and outlet temperature to limit the number of unknown variables. An example of a suitable heat source stream is a stream in need of cooling in an industrial process. could as an example be water used in industrial processes which removes heat from machinery or equipment.

In the CAW case, the ambient air, acting as the heat source, was subject to a sensitivity analysis. The temperature was varied in three steps: -7°C, 7°C, and 21°C.

Similarly, for the CAA case, the ambient air was also subjected to a sensitivity analysis. In this case, the ambient air serves as the heat sink, and the analysis involved varying the temperature with the same three steps as in the CAW case: -7°C, 7°C, and 21°C.

The sensitivity analysis for all three cases followed the same methodology as that of the general cycle simulation presented in Section 4.2.

A final analysis was done for the CAA case, as it was of interest to see how the performance of the HP system varied if the exhaust air from the heat source was looped and used as a heat sink, specifically during operation with cold ambient temperatures. The system variation also followed the same methodology as that of the general cycle simulation presented in Section 4.2, but with adjustment to its input values. The CAA system variation is shown and discussed further in Appendix

F.

### 4.7.1 Economic sensitivity analysis

As mentioned in section 4.6, the economic sensitivities with respect to the cost development of the electricity and DH were investigated. Changes of the gas/diesel price were not studied. Furthermore, when estimating the TCI the cost function used was rather rough, thus it was concluded that the TCI should be varied. This to see how the economic potential is affected when the TCI is varied to achieve break-even (NPV = 0).

Another economic sensitivity analyses aimed to investigate the impact on NPV of introducing an annual price development, denoted by $K$, for electricity and DH. The two price development scenarios being an annual increase of 0, 2, or 4%. Multiple combinations of these price development scenarios were investigated, where the price development of electricity, for instance, was calculated using eq. (4.1):

$$C_{el}(y) = C_{el}(0) \cdot (1 + K)^y \qquad [€] \tag{4.1}$$

Here, $y$ represents the specific year, $K$ is the annual percentage price increase, $C_{el}(0)$ denotes the initial price, and $C_{el}(y)$ denotes the price in year $y$. Equation (4.1) was used for all reference costs, with the only difference being the initial value. However, an alternative formulation to eq. (3.24) was utilized to determine the NPV when prices varied between years:

$$NPV = -TCI + \sum_{y=1}^{n} \frac{CF_y}{(1+i)^y} \quad [€] \tag{4.2}$$

Here, $CF_n$ represents the annual cash flow in year $n$. The annual cash flows serve as the numerator in eq. (3.24), $(CF_{Source,y} - CF_{El,y} + CF_{Utility,y})$, where the annual value of each component is determined using eq. (4.1) and the annual consumption of the respective component.

For the investigation regarding the TCI estimation and its impact on the NPV, eq. (4.3) was used.

$$TCI_\alpha = TCI_{estimate} \cdot \alpha \qquad [€] \tag{4.3}$$

where $TCI_\alpha$ is the new value dependent on the scaling factor, $\alpha$, that was varied, and $TCI_{estimate}$ is the estimated TCI cost, calculated via eq. (D.1), (D.2), or (D.3) in Appendix D depending on the specific case.

# 5

# Results and Analysis

The results from the refrigerant screening, dryer dimensioning, thermodynamics and economical evaluation of the modelled HPs are presented in this chapter. The results from the two case studies will be presented individually, each time starting with the sludge case study followed by the concrete case study. The refrigerant screening is however presented for both sludge and concrete drying combined.

## 5.1 Refrigerant screening

The screening of refrigerants was based upon a literature review and a thermodynamic screening. The literature review resulted in a list consisting of potential natural refrigerants, primarily due to the F-gas regulation. The ideal refrigerant would have zero ODP and low $GWP_{100}$. Since all natural refrigerants included in the screening had zero ODP, the $GWP_{100}$ value played a pivotal role in the selection. The literature review resulted in a list of 11 potential candidates of which only 7 had a $GWP_{100}$-value $< 4$, which was set as a limit to ensure very low environmental impact if a leakage were to occur. These seven refrigerants are presented in Table 5.1, which are the refrigerants included in the thermodynamic screening.

**Table 5.1:** Potential refrigerant candidates studied in the thermodynamic screening.

| **Refrigerant** | **Refrigerant Number** |
|---|---|
| Ammonia | R717 |
| Carbon dioxide | R744 |
| DME | RE170 |
| Iso-Butane | R600a |
| Propane | R290 |
| Propylene | R1270 |
| Water | R718 |

Based on the thermodynamic data in Table 3.1, combined with case-specific process data, the thermodynamic screening results for the cases are presented in Figure 5.1, 5.2 and 5.3. In the figures, blue points indicate critical temperatures, while red points indicate the NBPs of each refrigerant. The NBP for R744 is located below the x-axes, at -79°C presented in Table 3.1.

The operational limits selected for the SWW case were set to operate between 10°C and 70°C, as indicated by the yellow area.

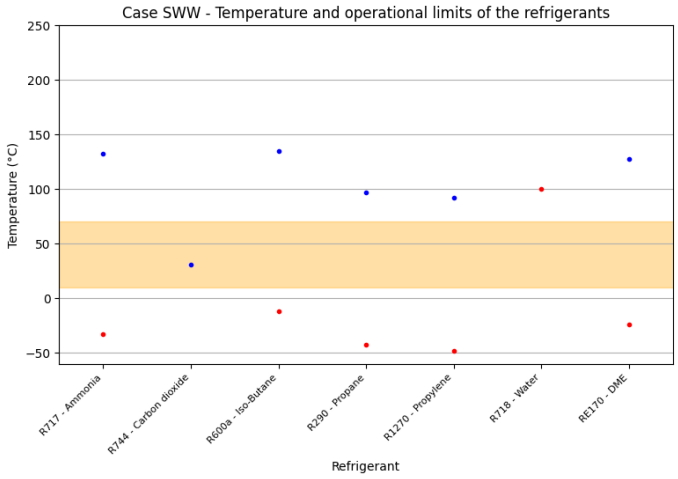


**Figure 5.1:** Refrigerant limits in the sludge drying case using a water-to-water HP.

Refrigerants with a boiling point lower than the operational limit, correlating to the incoming heat source temperature, will evaporate easily at moderate pressures. Notably, the boiling point of water is 100°C, thus requiring a pressure below 1 bar to evaporate within the process temperature interval. Moreover, refrigerants with a critical temperature below or within the colored area would necessitate a HP cycle operating with transcritical pressures, which is common for systems utilizing $CO_2$.

In Figure 5.2, the thermodynamic screening results for the CAW cycle, used in the concrete case study, are presented. The concrete drying systems were set to operate between 2°C and 45°C.

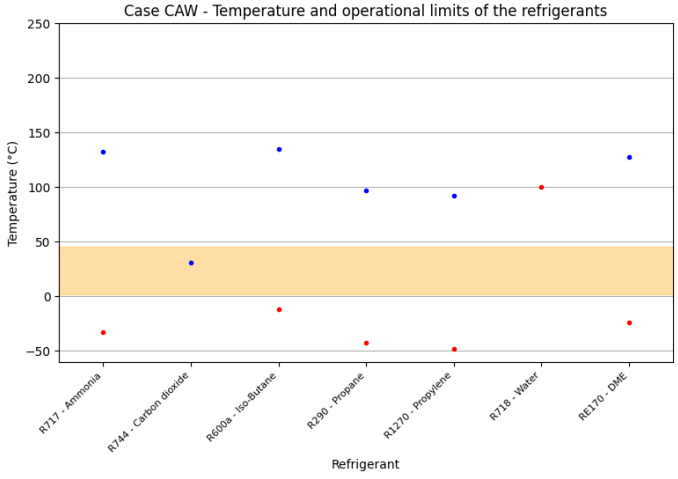


**Figure 5.2:** Refrigerant limits in the concrete drying case using an air-to-water HP.

Compared to the thermodynamic screening in the sludge case study, the results in Figure 5.2 show a similar outcome, where all refrigerants, except for water, can be

evaporated at pressures above 1 bar, given the temperature of operation. In Figure 5.3, the results from the thermodynamic screening for the CAA system are presented. This system was assumed to operate between 15°C and 25°C.

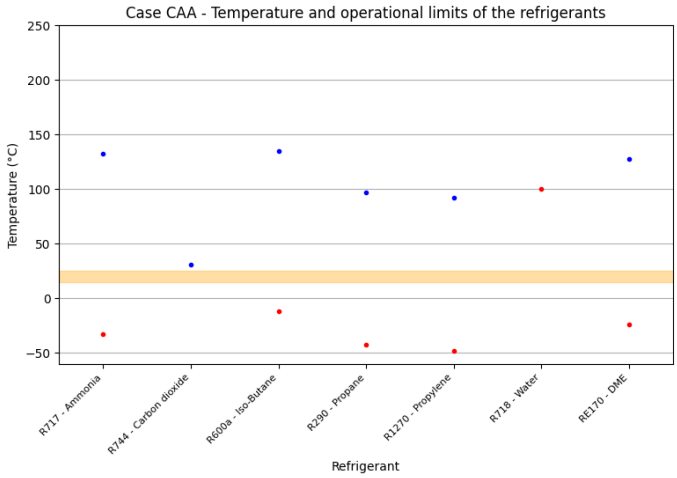


**Figure 5.3:** Refrigerant limits in the concrete drying case using an air-to-air HP.

The results shown in Figure 5.3 differ from both of the earlier presented thermodynamic screenings. In this system, using an air-to-air VCHP, the HP's temperature interval of operation is low enough to allow for a standard VCHP cycle for all refrigerants. This implies that there is no need for a transcritical cycle when using R744, since the critical temperature of R744 is higher than the upper operating temperature.

All VCHP simulations were performed with the refrigerants presented in Table 5.1, which are those deemed to have the most potential, while considering both environmental, primarily $GWP_{100}$, and thermodynamic properties. Notably, R718, although included in the table, was not utilized in the simulations as it was found unfavorable based on the thermodynamic screening, primarily because of its high boiling temperature. This would require sub-atmospheric pressure in the evaporator. Although this is possible, it was considered to be outside the scope of simple VCHP cycles.

## 5.2 Thermodynamic evaluation

This section presents the thermodynamic performance, measured as COP, of all VCHP cycle simulations conducted for both case studies. Additionally, it was found that the proposed air-to-air HP system in the CAA case required an additional electric heater to ensure the target air temperature was achieved when the ambient temperature was low (-7°C). Consequently, the performance indicator COSP will be used in the evaluation of the CAA case.

For the SWW case, the presented results were obtained using a waste heat stream with a temperature of 20°C as the heat source and a water loop return at 53°C as the

heat sink. In the CAW case, the presented results were obtained using ambient air with a temperature of 7°C as the heat sink and room exhaust air at 15°C as the heat source. In the CAA case, the presented results were obtained using ambient air with a temperature of 7°C as the heat sink and the room exhaust as heat source. This heat pump had a specified volume flow and temperature to deliver. When the heat sink was 7°C or lower, the specified temperature could not be delivered. Consequently, an additional electric heater was included in the system with a maximum capacity of 132 kW, of which 30.2 kW was used at 7°C.

### 5.2.1 Sludge: Water-to-water

In Figure 5.4, the COP results of the VCHP cycles in the SWW case are presented.

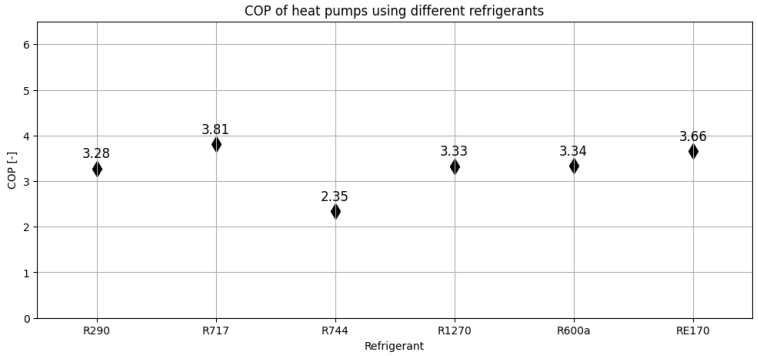


**Figure 5.4:** COP of VCHP cycles in the sludge drying using a water-to-water HP case using selected refrigerants.

It can be seen that the COP varied among the cycles, with the cycle using R717 achieving the highest thermodynamic performance, while the cycle using R744 showed the lowest performance. The VCHP cycles using either R290, R1270, and R600a showed small differences in their thermodynamic performance. Most of the cycles are seen having a COP around 3.5.

### 5.2.2 Concrete: Air-to-water

In Figure 5.5, the COP results of the VCHP cycles in the CAW case are presented.

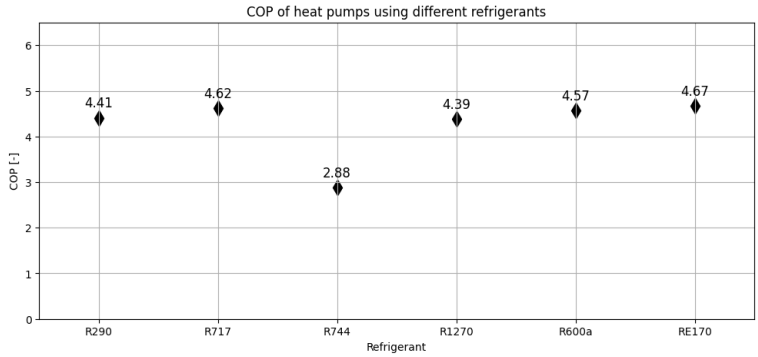


**Figure 5.5:** COP and estimated TCI of VCHP cycles in the concrete drying case using an air-to-water HP using selected refrigerants.

From the figure it can be seen that the cycle using RE170 is having the highest COP of 4.67, which is much higher than the worst cycle using R744 having 2.88. The VCHP cycles using either R717 and R600a showed small differences in their thermodynamic performance.

### 5.2.3 Concrete: Air-to-air

In Figure 5.6, the COP results of the VCHP cycles in the CAA case are presented.

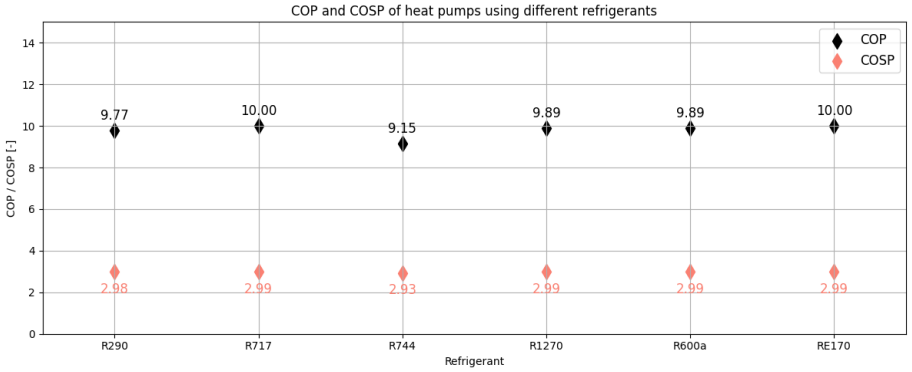


**Figure 5.6:** COP and COSP of VCHP cycles in the concrete drying case using an air-to-air HP using selected refrigerants.

It can be seen that the COP values are high for all cycles, with the cycles using R717 and RE170 showing the highest thermodynamic performance, while the cycle using R744 showed the lowest performance, but the difference being much smaller than in the previously presented cases.

Due to the design of the air-to-air heat pump, where both target temperature and volumetric flow were specified, the heating capacity of the VCHPs was exceeded

when the heat sink inlet temperature was lower. Thus, as previously mentioned, an additional heating coil was used to ensure the heat sink's specified target temperature of 25°C was achieved. Therefore, the COSP is also included in Figure 5.6. It can be seen that the COSP is much lower than the COP. The figure indicates that the overall system has a thermodynamic performance (COSP) of around 3.

## 5.3 Economic evaluation

In this section, the results related to the economic indicators, NPV and PBP, are presented for the VCHP cycles, beginning with the results of the sludge case study followed by those of the two concrete HPs. In the following results, the reference utilities, electricity, DH, and gas or diesel have been assumed to have no price development for simplicity. To ensure the economical evaluation provides a more diverse outlook, the price development of these have been studied in the economic sensitivity analyses, discussed in section 5.5.2.

In Table 5.2 the TCIs of all cases investigated are presented. The estimation of the TCI in all cases used cost functions that depend solely on the delivered heat. As a result, the TCI is equal for all solutions, since the delivered heat is identical for each case. Equation (D.1), (D.2) and (D.3) in Appendix D are being used for case SWW, CAW and CAA, respectively.

**Table 5.2:** Estimated TCI values for all cases investigated.

| **Case** | SWW | CAW | CAA |
|---|---|---|---|
| **TCI** | 3.42 M€ | 42.89 k€ | 26.75 k€ |

The TCI of all HPs in the SWW case was estimated to be 3.42 M€, as seen in Table 5.2. Furthermore, the TCI of all HPs in the CAW case was estimated to be 42.89 k€, and the TCI of all HPs in the CAW case was estimated to be 26.75 k€. However, it is not very likely that the different VCHP cycles would have the same TCI; thus, this value might differ among them in reality but should be considered as a rough estimate.

### 5.3.1 Sludge: Water-to-water

The NPV was estimated using either electricity, DH, or gas as the reference cost for the alternative source of drying heat. The NPV results from the simulations of each of the six VCHPs using the selected refrigerants are presented in Figure 5.7.

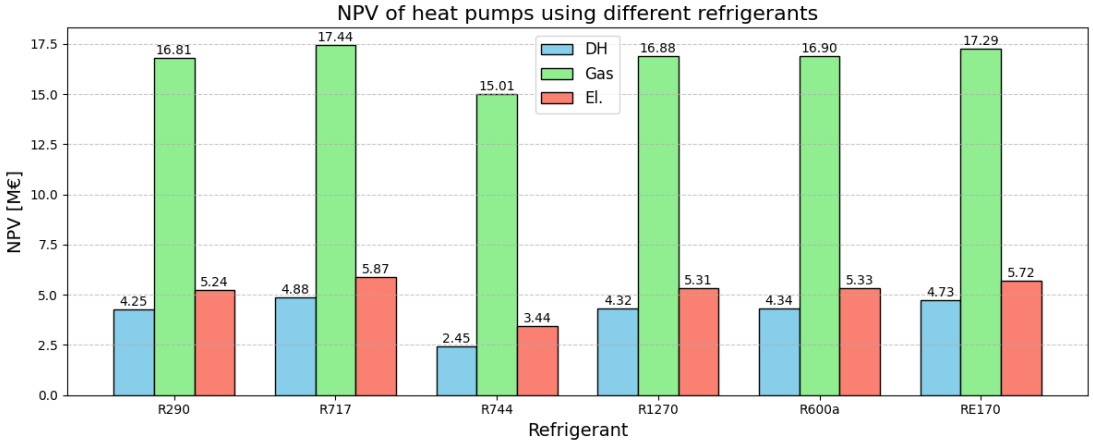


**Figure 5.7:** NPV of VCHPs using selected refrigerants in relation to the reference utility assumed to be replaced in the sludge drying case.

In Figure 5.7, the NPV values are in million euros (M€), with each VCHP system having three values: blue bars represent the reference cost with DH, green bars represent the cost with gas as the reference, and red bars represent the cost with an electric boiler as the reference. The values above each bar represent the NPV of the HP when the HP replaces the usage of the respective utility. It can be observed that the NPV is much higher if the HPs replace the usage of a gas boiler, which is attributed to the high specific cost of gas compared to both electricity and DH. Furthermore, the NPV is higher for all cycles when an electric boiler is replaced with any of the VCHP cycles compared to when DH is replaced. Additionally, comparing the NPVs of all solutions, it is clear that the VCHP cycle using R744 as the WF has the lowest NPV, while the cycle using R717 has the highest NPV, closely followed by RE170.

The PBP was estimated using either electricity, DH, or gas as reference utilities, the PBP results from the simulations are presented in Figure 5.8.

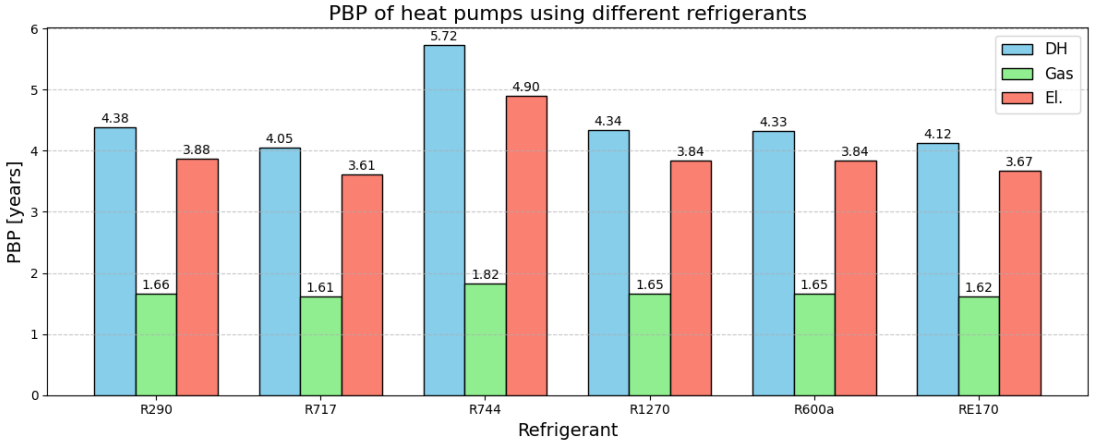


**Figure 5.8:** PBP of VCHPs using selected refrigerants in relation to the reference utility assumed to be replaced in the sludge drying case.

In Figure 5.8, the PBP is in years, with each VCHP system having three values: blue bars represent the reference cost with DH, green bars with gas as the reference, and red bars with an electric boiler as the reference. It can be seen that the VCHP using R744 has the longest payback period, whereas the VCHP using R717 has the shortest, similar to the results of the NPV. The values above each bar represent the PBP of the VCHP when it replaces the usage of the respective utility.

The LCOH of the HPs using selected refrigerants for the SWW case is presented in Table 5.3. These values were obtained using eq. (3.27), assuming that the fixed $CF_{Fixed,OM}$ is 5% of the TCI, and that the electricity price is constant.

**Table 5.3:** Estimated LCOH values of the VCHP solutions in the sludge drying using a water-to-water HP using selected refrigerants.

| **Refrigerant** | R290 | R717 | R744 | R1270 | R600a | RE170 |
|---|---|---|---|---|---|---|
| **LCOH [€/MWh]** | 33.0 | 30.8 | 39.2 | 32.8 | 32.7 | 31.4 |

The results in Table 5.3 show the same trends as those of the NPV and PBP, namely that the VCHP cycle using R717 has a more promising economic potential, whereas the cycle using R744 shows the least promising economic potential. The difference between in LCOH of the two cycles being close to 10 €/MWh

### 5.3.2 Concrete: Air-to-water

The NPV was estimated using either electricity, DH, or diesel as the reference cost in eq. (3.24). The NPV results from the simulations of each of the six VCHPs using the selected refrigerants are presented in Figure 5.9.

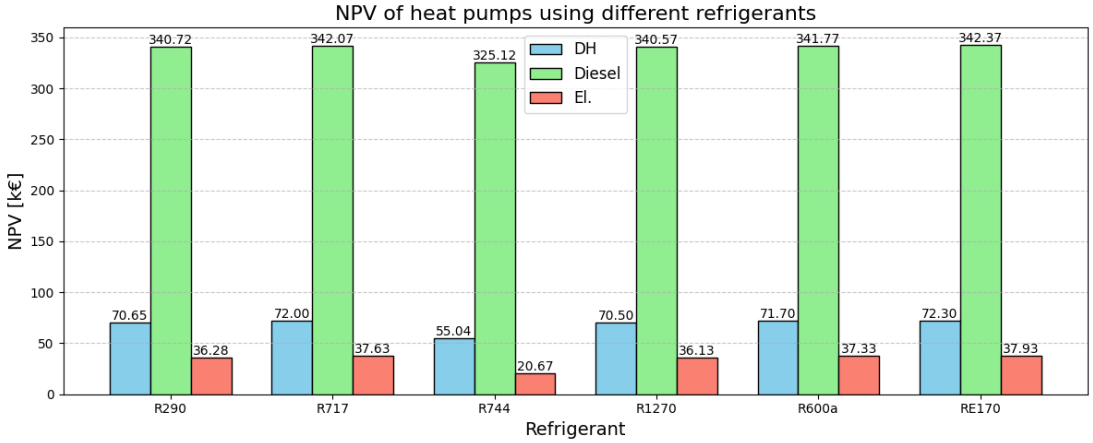


**Figure 5.9:** NPV of VCHPs using selected refrigerants in relation to the reference utility assumed to be replaced in the concrete drying case using an air-to-water HP.

In Figure 5.9 it can be observed that the NPV is much higher when the HPs replaces the use of a diesel boiler, which is attributed to the high specific cost of diesel

compared to both electricity and DH. Furthermore, the NPV is higher for all cycles when DH is replaced with any of the VCHP cycles compared to when an electric heating fan is replaced. Additionally, upon comparing the NPVs of all solutions, it is clear that the VCHP cycle using RE170 has a slightly higher NPV than the cycle using RE717, and the cycle using R744 has the lowest NPV. The values above each bar represent the NPV of the HP when the HP replaces the usage of the respective utility.

The results differ from those of the SWW case, where the NPV associated with the replacement of DH by any of the VCHPs was the lowest, whereas in the CAW case, the replacement of an electric heating fan is associated with the lowest NPV. This difference is associated with the somewhat higher fixed cost of DH when less capacity is used. Moreover, the difference between the most expensive reference utility and the other references are greater in this case, making the replacement of diesel boilers very favorable.

The PBP was estimated using the same method as in the SWW case, but using a diesel boiler instead of a gas boiler as one of the reference utilities, and the results of each VCHP simulation in the CAW case are presented in Figure 5.8.

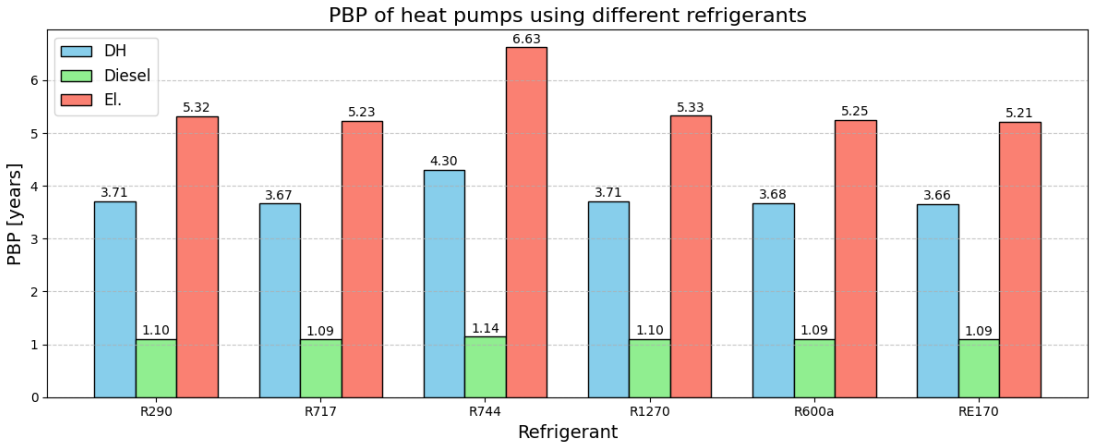


**Figure 5.10:** PBP of VCHPs using selected refrigerants in relation to the reference utility assumed to be replaced in the concrete drying case using an air-to-water HP.

The PBP of each solution in the CAW case in Figure 5.10 ranges from around 1 to 6.6 years for scenarios where the VCHPs replace the usage of an electric heating fan, DH, or a diesel boiler. It can be observed that the PBP would be around 3.7 years for all cycles when DH usage is replaced with the proposed HP system, and 5.3 years when an electric heating fan is replaced for all cycles except the one using R744. Overall, based on both the NPV and PBP, the application of HPs are having positive economic performance compared to the reference utilities. It is clear that if any of the VCHPs would replace the use of water-driven heating fans, the economic performance is better than if it replaces the use of electric heating fans. The reason being the higher cash flow savings in the scenario using district heating as reference, whereas in the scenario of when electricity is used. This relates to the need of the

supplementary heating coil, making the reduction in electricity consumption by implementing any of the VCHPs quite low compared to when using just electric heating fans.

The LCOH in the CAW case is presented in Table 5.4. These results were obtained using Eq. 3.27, using the same assumptions as in the SWW case.

**Table 5.4:** Estimated LCOH values in the concrete drying case using an air-to-water HP using selected refrigerants.

| **Refrigerant** | R290 | R717 | R744 | R1270 | R600a | RE170 |
|---|---|---|---|---|---|---|
| **LCOH [€/MWh]** | 36.69 | 36.16 | 42.81 | 36.75 | 36.27 | 36.04 |

The difference in LCOH among the VCHP cycles are relatively small, except for the cycle using R744 being approximately 6 €/MWh more expensive than the other LCOHs.

### 5.3.3 Concrete: Air-to-air

All results presented in this section are based on the system performance, taking into account the need of the supplementary heat provided by the heating coil.

The NPV was estimated using either electricity, DH, or diesel as the reference cost in eq. (3.24). The results of each of the six refrigerants used in the VCHP simulations in the CAA case are presented in Figure 5.11.

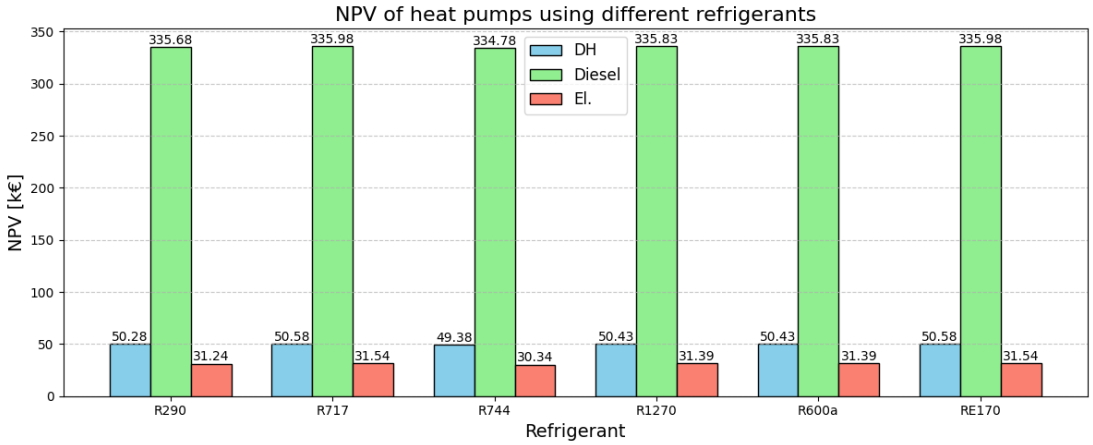


**Figure 5.11:** NPV of VCHPs using selected refrigerants in relation to the reference utility assumed to be replaced in the concrete drying case using an air-to-air HP.

In Figure 5.11, it can be observed similarly to in the CAW case that the NPV is much higher when the HPs replace the use of a diesel generator, which is attributed to the high specific cost of diesel compared to both electricity and DH. Furthermore, the NPV is higher for all cycles when DH is replaced with any of the VCHP cycles

compared to when an electric heating fan is replaced. Additionally, upon comparing the NPVs of all solutions, it is clear that the VCHP cycles using R717 and RE170 have slightly higher NPVs than the cycle using R1270, which was the best cycle in the CAW case. The cycle using R744 has approximately the same economic outlook as all the other cycles in this case, indicating that when the R744 cycle is not operating transcritical, it has similar performance to the cycles using the other refrigerants.

The results are similar to those in the CAW case, where the NPV associated with the replacement of electric heating fans by any of the VCHPs has the lowest NPV. All NPVs are lower in this case compared to in the CAW case, indicating that the air-to-air HP cycles studied have worse economic potential.

The PBP results of each VCHP simulation in the CAW case are presented in Figure 5.8. These results exhibit the same trend as those in the CAW case. However, all the payback periods are shorter than in the CAW case. This is most likely due to the lower estimated TCI for the air-to-air HPs.

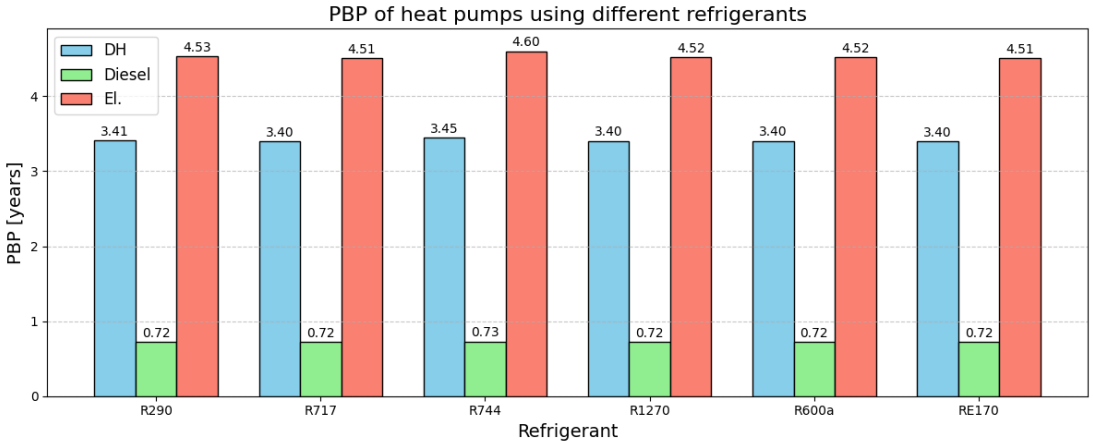


**Figure 5.12:** PBP of VCHPs using selected refrigerants in relation to the reference utility assumed to be replaced in the concrete drying case using an air-to-air HP.

As previously mentioned it can be seen from comparing Figure 5.12 with Figure 5.10, that the PBPs in the CAA case are shorter than in the CAW case. They are ranging between 0.7 to 4.6 years in the CAA case compared to 1.1 to 6.6 years in the CAW case.

In Table 5.5 the LCOH of each air-to-air VCHP cycle is presented. The LCOH of the cycles in the CAA case are all approximately 23 €/MWh.

**Table 5.5:** Estimated LCOH values in the concrete drying case using an air-to-air HP using selected refrigerants.

| **Refrigerant** | R290 | R717 | R744 | R1270 | R600a | RE170 |
|---|---|---|---|---|---|---|
| **LCOH [€/MWh]** | 32.85 | 32.76 | 33.1 | 32.80 | 32.80 | 32.76 |

The difference in LCOH between the CAW and CAA cases is marginal. The outcome in the CAW case is around 5 €/MWh higher than for the cycles in the CAA case, except for the cycle using R744, where the difference is around 10 €/MWh higher. This is due to the rather high LCOH value of the R744 VCHP cycle in the CAW case.

## 5.4 Greenhouse gas emission evaluation

In this section, the results related to the environmental indicator, emission reduction, are presented. As in previous sections, the results from the SWW case study are presented first, followed by the results from the concrete case study.

### 5.4.1 Sludge: Water-to-water

In Figure 5.13, the annual $CO_2$-equivalent emissions of both the reference utilities and the VCHPs are presented. The VCHP emissions only consider the electricity consumption of each compressor, thus the difference between the different cycles is directly related to the compressor work.

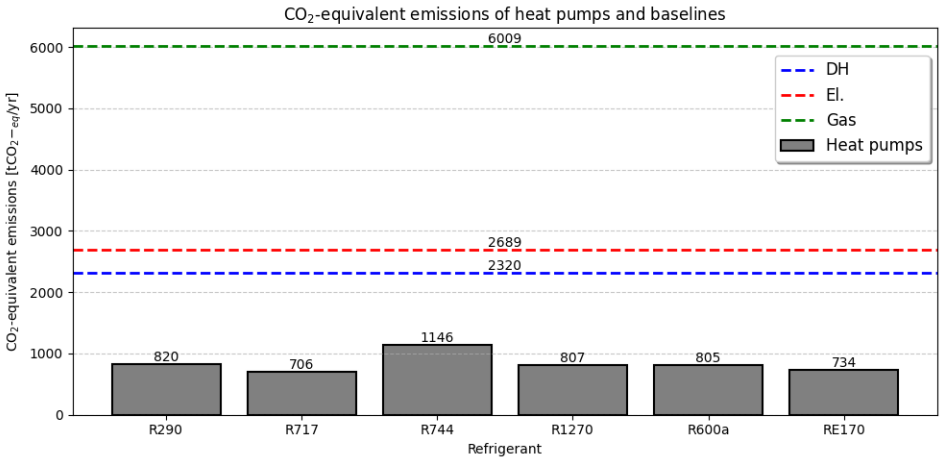


**Figure 5.13:** $CO_2$-equivalent emission of VCHP cycles using the selected refrigerants compared to the emissions of the reference utilities in the sludge drying case using a water-to-water HP.

The $CO_2$-equivalent emissions in Figure 5.13 have the unit of metric tonnes per year. It can be seen that all VCHP cycles have lower annual emissions than all reference utilities. The cycle using R717 has the lowest emissions, whereas the cycle using R744 has the highest emission level of the VCHP cycles. For example, if the VCHP using R717 would supply the sludge dryer with heat instead of an electric boiler it would achieve an annual emissions savings of approximately 2000 $tCO_2$-equivalents. The savings are somewhat lower if the comparison is conducted between the same VCHP cycle and DH.

If the VCHP cycle using R744 were implemented instead of the cycle using R717 the annual emissions would be approximately 40% higher. The difference is due to the lower compression work in the cycle using R717. Moreover, it can be seen that the cycles using R290, R1270, and R600a are having approximately the same level of $CO_2$-equivalent emissions.

### 5.4.2 Concrete: Air-to-water

In Figure 5.14, the annual $CO_2$-equivalent emissions of both the reference utilities and the VCHPs are presented. Similar to in the SWW case the emissions only consider the electricity consumption of each compressor.

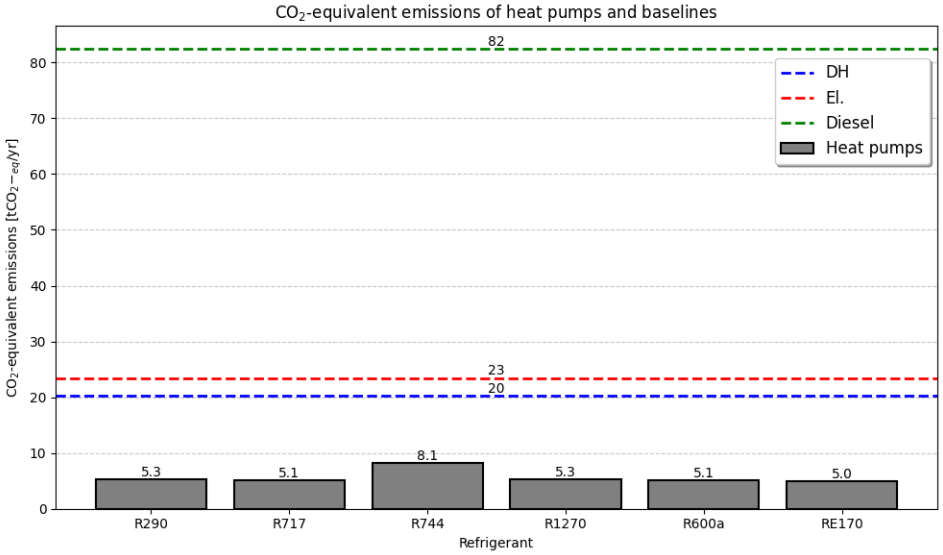


**Figure 5.14:** $CO_2$-equivalent emissions of VCHP cycles using the selected refrigerants compared to the emissions of the reference utilities in the concrete drying case using an air-to-water HP.

The $CO_2$-equivalent emissions in Figure 5.14 have the unit of metric tonnes per year. It can be seen that all VCHP cycles have lower annual emissions compared to all reference utilities. The cycle using RE170 has the lowest emissions, whereas the cycle using R744 has the highest emission level of the studied VCHP cycles in this case. For example, if the VCHP using RE170 would replace the use of electric fans it would result in an annual emissions reduction of approximately 15 $tCO_2$-equivalents. The reductions are somewhat lower if the comparison is conducted between the same VCHP cycle and water heated fans. The potential reduction by replacing the use of diesel generators with any of the VCHP would result is emission reduction of approximately 75 metric tonnes of $CO_2$-equivalents.

If the VCHP cycle using R744 were implemented instead of the cycle using RE170 the annual emissions would be approximately 60% higher. The difference is due to the lower compression work in the cycle using RE170. Moreover, it can be seen that

the cycles using R290, R717, R1270, and R600a are having approximately the same level of $CO_2$-equivalent emissions as the cycle using RE170.

### 5.4.3 Concrete: Air-to-air

In Figure 5.15, the annual $CO_2$-equivalent emissions of both the reference utilities and the VCHPs are presented. The VCHP emissions consider the electricity consumption of each compressor but also the electricity consumption of the additional heater, thus the difference between the different cycles is directly related to the compressor work and the heat load of the heater where both contributions are highlighted in Figure 5.15.

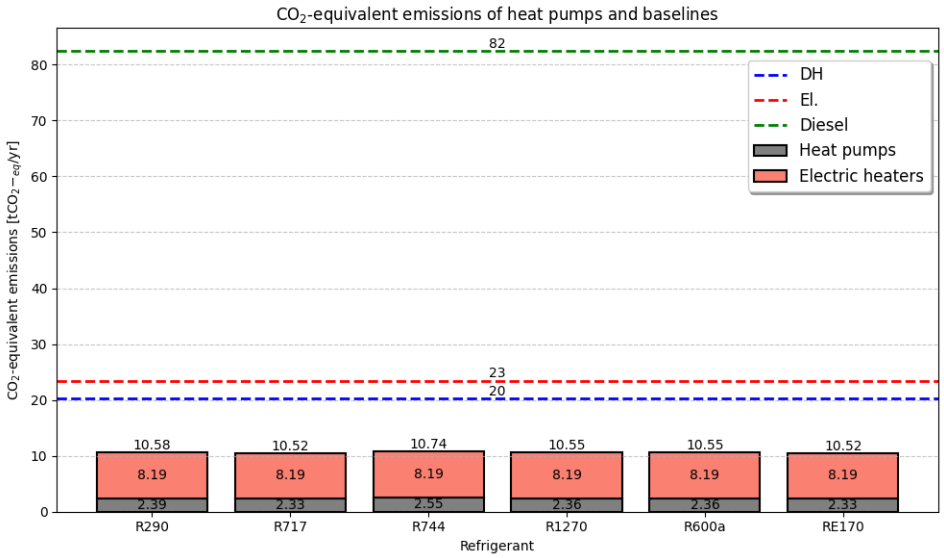


**Figure 5.15:** $CO_2$-equivalent emission of VCHP cycles using the selected refrigerants compared to the emissions of the reference utilities in the concrete drying case using an air-to-air HP.

It can be seen in Figure 5.15 that all VCHP cycles have lower annual emissions compared to all reference utilities. The cycles using either R717 or RE170 have the lowest emissions, whereas the cycle using R744 has the highest emission level of the studied VCHP cycles in this case. However, the difference between the studied cycles are very small. Furthermore, when comparing the the VCHP cycle related $CO_2$-equivalent emissions to those of the reference utilities the reduction is less than in the CAW case. This due to the need of the additional electric heating coil to ensure that the supply temperature can be delivered when the ambient temperature is low. It can be seen that the major contributor of each cycles $CO_2$-equivalent emission is the additional heater, making out almost 80% of the total annual emissions. The implementation of any of the VCHP cycles would still result in a reduction of $CO_2$-equivalent emissions. For example when any of the HPs would replace the use of electric heating fans the reduction would be 13 metric tonnes of $CO_2$-equivalents.

## 5.5 Sensitivity analyses

The HP cycle studies were based upon many simplifying assumptions. For the sludge drying case, these mostly concerned the available waste heat temperature for the heat source. Thus, the cycle studies were repeated for different heat source temperatures. Similarly, for the concrete case study, the available heat source for the CAW case and heat sink for the CAA case was assumed to be ambient air, and the temperature and relative humidity were varied to simulate operational scenarios during winter, summer and spring or fall in Gothenburg.

This section presents the results from all sensitivity analyses using district heating as a reference utility, starting with the sensitivity analysis related to the VCHP cycles' thermodynamic performance in section 5.5.1, followed by their economic performance in section 5.5.2. The sensitivity analysis results for gas/diesel and electricity are presented in Appendix C.

### 5.5.1 Thermodynamic sensitivity analyses

In the following section, the results of the thermodynamic sensitivity analyses are presented. These analyses focused on the heat source or heat sink stream with the greatest uncertainty in each case study.

#### 5.5.1.1 Sludge: Water-to-water

The first set of results concerns the sludge drying case study, as depicted in Figure 5.16. The inlet temperature of the heat source was varied between 20°C and 55°C while maintaining a constant temperature difference of 10 K between the heat source inlet and outlet in the sludge case study. Additionally, the VCHP cycle using R744 was not included in the last two simulations due to the nature of carbon dioxide, rendering the need of a fully transcritical cycle at these two temperatures, which was deemed outside the scope of this project.

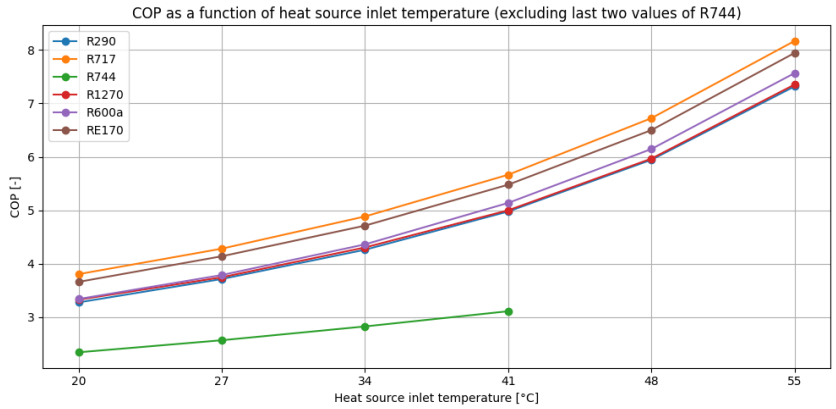


**Figure 5.16:** Effect of heat source inlet temperature on VCHP cycle performance in the sludge drying case using a water-to-water HP.

From the figure, it can be observed that increasing the heat source inlet temperature is beneficial for the cycle performance of all VCHP cycles. This is expected, as it leads to a lower temperature lift, resulting in a decrease in compression work. The difference between the overall COP improvement for the different cycles using the selected refrigerants is very small; no drastic changes are seen. Notably, the change in temperature has less impact on the COP for the R744 cycle compared to the cycles using the other refrigerants.

#### 5.5.1.2 Concrete: Air-to-water

The results presented in this section were obtained by varying the heat source inlet temperature between -7°C and 21°C simulating seasonal variations. The heat sink temperatures were fixed to the specified operating temperatures of 40°C to 45°C.

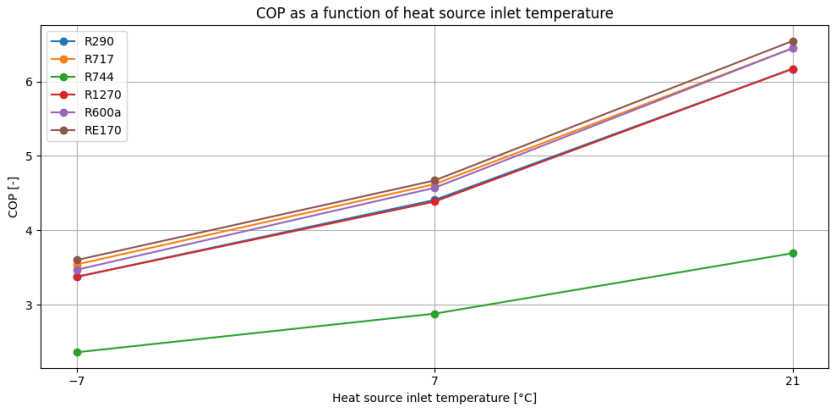


**Figure 5.17:** Effect of heat source inlet temperature on VCHP cycle performance in the concrete drying case using an air-to-water HP.

Figure 5.17 indicates that by raising the temperature of the heat source inlet, the performance of all VCHP cycles increased. As the temperature lift is reduced, the compression work is consequently decreased. The overall improvement in COP across the VCHP cycles is minimal for each heat source inlet temperature, apart from R744, which consequently performs worse compared to the rest of the refrigerants. Importantly, and similar to the SWW case, the COP of the R744 cycle is less sensitive to changes in temperature compared to cycles using other refrigerants.

#### 5.5.1.3 Concrete: Air-to-air

The results presented in this section were obtained by varying the heat sink inlet temperature between -7°C, 7°C, and 21°C, simulating seasonal variations. For the lower temperatures, an additional heater was needed to deliver the specified air temperature of 25°C. Furthermore, the heat source temperature was kept constant at 15°C for the two lower temperatures and 20°C for the scenario with 21°C, as the heat source used in these simulations is the room exhaust air. Due to the use of the additional heater the results are that of the COSP, which in the scenario with a heat sink inlet temperature of 21°C is equal to the COP.

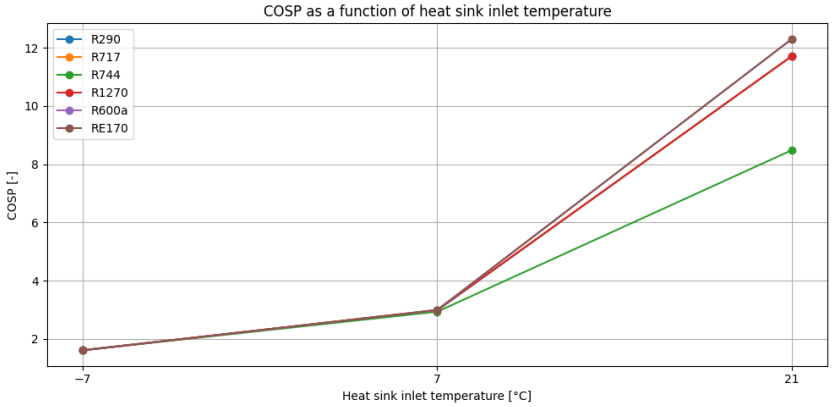


**Figure 5.18:** Effect of heat sink inlet temperature on VCHP cycle performance in the concrete drying case using an air-to-air HP.

Figure 5.18 shows that increasing the heat sink inlet temperature enhances the performance for all of the VCHP cycles and the reverse when the heat source inlet temperature is decreased. The reason for the quite drastic decrease in COSP is due to the added supplementary heating load that is necessary in the -7°C scenario. Similarly for the SWW and CAW cases, a decrease in compression work is noted due to the reduction in temperature lift. While the overall improvement in COSP for the VCHP cycles is minimal at each heat source inlet temperature, the R744 cycle still performs worse compared to the other refrigerants. Notably, the COSP of the R744 cycle in the CAA case is similarly sensitive to temperature changes than the cycles using other refrigerants.

### 5.5.2 Economic sensitivity analyses

In the following section, the results of the economic sensitivity analyses are presented. These analyses examined the impact of price developments on the reference utilities, namely electricity and DH. Additionally, an investigation was conducted to assess the accuracy of the TCI estimate. The TCI estimation sensitivity analysis studied the VCHP cycle with the refrigerant that had the best and worst economic performance, R717 and R744 for the SWW and CAA cases as well as RE170 and R744 for the CAW case.

However, prior to delving into these aspects, a brief exploration was undertaken to evaluate how alterations in operating conditions affect the economic performance of the VCHP cycles, as observed in the thermodynamic sensitivity analyses.

#### 5.5.2.1 Sludge: Water-to-water

The results of the first economic sensitivity analysis are a consequence of the thermodynamic sensitivity analyses, where the inlet heat source temperature in the sludge drying case was varied. The results are presented in Figures 5.19 and 5.20, where the decreased compression work, resulting in a decrease in the electricity consumption of the various VCHPs, is observed to affect the NPV and PBP. Similar to the discussion

in the thermodynamic sensitivity analysis of the SWW case, the VCHP cycle using R744 was not studied at the two highest temperatures due to the limitation of not studying fully critical cycles.

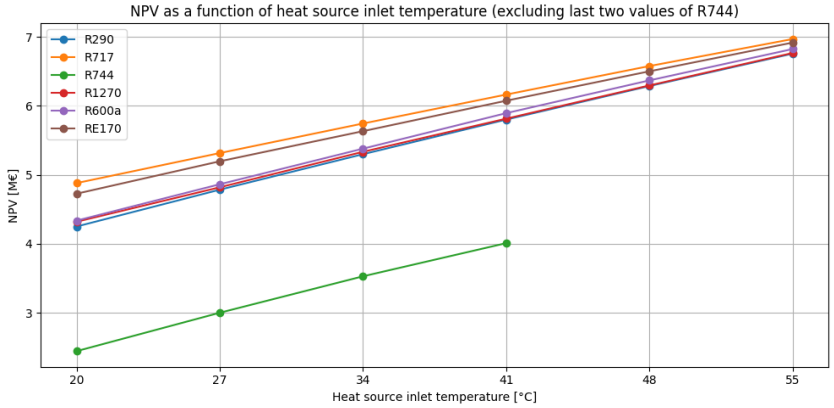


**Figure 5.19:** Effect of heat source inlet temperature on the NPV of VCHP cycles in the sludge drying case using a water-to-water HP.

In Figure 5.19, it can be seen that the NPV of all cycles increases. Notably, the change is greater for the cycles starting at a lower value, and the final values do not differ significantly. The NPV change when the heat source inlet temperature goes from 20°C to 55°C is approximately 2 M€ for all cycles except R744.

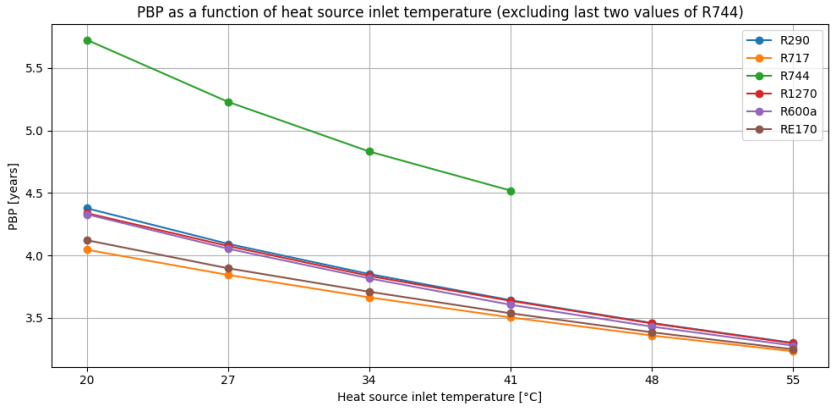


**Figure 5.20:** Effect of heat source inlet temperature on the PBP of VCHP cycles in the sludge drying case using a water-to-water HP.

The PBP results shown in Figure 5.20 exhibit a similar trend to the NPV results, where the change in PBP is greater for the VCHP cycles starting with a higher PBP, and the final values do not differ significantly. The impact of changing the heat source inlet temperatures on the LCOH was studied, the results being similar to both the NPV and PBP results, as depicted in Figure 5.21.

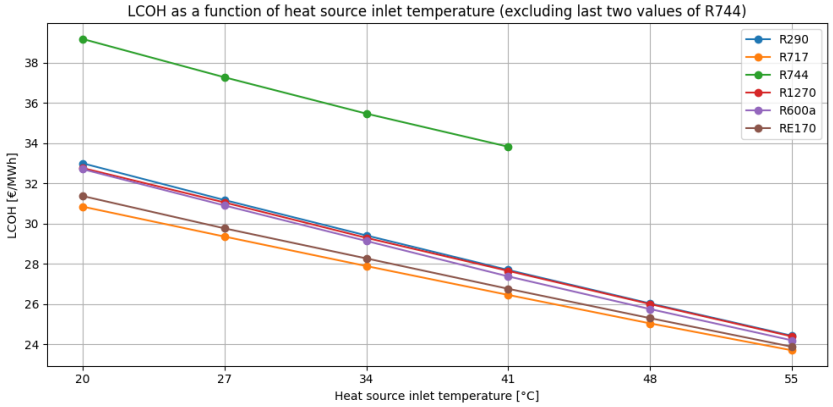


**Figure 5.21:** Effect of heat source inlet temperature on the LCOH of VCHP cycles in the sludge drying case using a water-to-water HP.

It can be seen in that the LCOH decreases when the heat source inlet temperature is increased. This effect correlates to the earlier discussion of the decrease in temperature lift, consequently decreasing the compression work. Since, the LCOH relates to all cost for heat produced by the VCHPs it is reasonable to have a lower cost per MWh, when less electricity is needed to achieve the same amount of delivered heat. The higher LCOH associated with the R744 VCHP cycle is a consequence of the lower cycle performance shown earlier.

Moreover, the impact on the NPV for the VCHP cycles using R717 and R744 is investigated for the SWW case. The results are presented in Table 5.6, where the baseline represents the NPV of the VCHPs when the HPs replace the usage of an electric boiler or DH, while keeping both electricity and DH prices constant throughout the HPs lifetimes. The results presented in the table show the relative change in percentage if the price of electricity and/or DH is kept constant, or increased annually by 2 or 4%. These results were obtained using the variables in Table 4.6.

**Table 5.6:** Change in NPV of VCHPs using R717 and R744 for the sludge drying using a water-to-water HP.

| **CF** | **WF** | **Baseline** | El↑2% DH | El↑4% DH | El DH↑2% | El DH↑4% | El↑2% DH↑4% | El↑4% DH↑2% |
|---|---|---|---|---|---|---|---|---|
| DH | R717 | 4.88 M€ | -14.4 | -32.3 | 51.1 | 114.8 | 100.4 | 18.8 |
| | R744 | 2.45 M€ | -46.6 | -104.7 | 102.0 | 229.1 | 182.5 | -2.7 |
| El | R717 | 5.88 M€ | -12.0 | -26.9 | - | - | -12.0 | -26.9 |
| | R744 | 3.44 M€ | -33.1 | -74.4 | - | - | -33.1 | -74.4 |

The results presented in Table 5.6 indicate that the NPV is more sensitive to price changes of reference utilities in the case where DH is replaced, SWW-DH, compared to the scenario where the VCHP replaces the usage of an electric boiler, as in the SWW-El case. This sensitivity can be clearly observed, given that the magnitude of the NPV changes relative to the baseline when the reference utility is varied. It

can be observed that the same change in either electricity price or DH price leads to a larger NPV change for the SWW-DH case compared to the same scenario for the SWW-El case. Additionally, the relative change is more pronounced for the VCHP using R744 compared to the one using R717. This discrepancy is attributed to the higher compressor work in the R744 cycle, making it more sensitive to changes, especially in electricity price.

Furthermore, the impact of utility price changes does not result in negative or zero NPVs for the VCHP cycle using R717, indicating that this solution shows promising economic performance even if the electricity price were to increase annually by 2 or 4% throughout its lifetime. Conversely, the results for the VCHP cycle using R744 indicate that the solution is more sensitive to electricity price changes. In the case of an annual increase of 4% in electricity price and a constant DH price, this system would have a negative NPV.

The combination of price developments most likely to occur is uncertain; however, according to Holmberg and Tangerås (2023), the price of thermal energy is expected to increase more than the price of electricity [139]. Thus, the scenario results with an annual increase of 2% for electricity and 4% for DH might be the most likely among the presented scenarios.

The first sensitivity analysis on utility cost impact, shown in Figure 5.22, is that of the VCHP using R717 in the sludge drying case. In the analysis, the TCI was varied while keeping reference utility costs constant. Apart from varying the TCI, the electricity price that gave an NPV-value equal to zero was found for each value of the varied TCI.

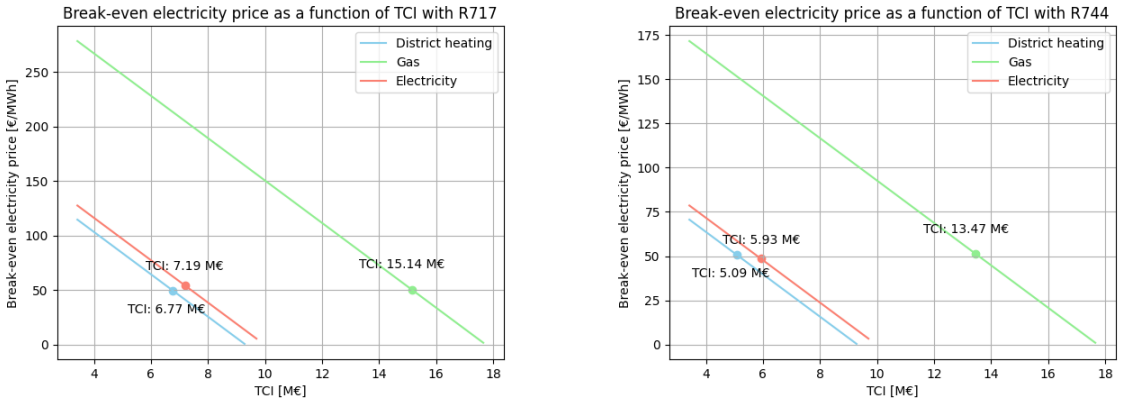


**Figure 5.22:** Break-even electricity price yielding NPV=0 as a function of TCI for the sludge drying case using a water-to-water HP with R717 (left) and R744 (right) as refrigerants.

In Figure 5.22 the break-even electricity price corresponding to an NPV=0 as a function of TCI for SWW case is shown. The calculations assume constant prices of electricity, DH, and gas over the HP's lifetime. Along each line in the figure, the NPV is zero. For instance, with a TCI of 6 M€, the electricity price yielding NPV = 0 is approximately 70 €/MWh if the VCHP using R717 replaces the use of DH.

The dots and their annotated values indicate the break-even TCIs for each VCHP cycle when any of the reference utilities are replaced, while keeping the electricity price constant throughout the HP's lifetime. For example, if a VCHP using R717 were to replace the usage of an electric boiler, the TCI could be 7.19 M€ and still have NPV $\geq 0$. The same value for the VCHP using R744 is 5.93 M€, indicated by the dot on the red break-even line.

The estimated TCI value presented earlier was 3.42 M€. If the true value lies somewhere between this and 7.19 M€ when DH is replaced with a R717 VCHP, the economic performance would still be positive. Indicating that even if the estimated TCI would be an underestimate, there is a margin of error. The margin of error is lower for the cycle using R744 but is still substantial.

#### 5.5.2.2 Concrete: Air-to-water

The NPV and PBP results are presented in Figures 5.23 and 5.24, where the decreased compression work, resulting in a decrease in the electricity consumption of the various VCHPs, is observed to affect the NPV and PBP.

The outcome of increasing the heat source temperature in the CAW case is presented in Figure 5.23. The trend is the same as in the SWW case, where a higher source temperature results in better economic performance, due to the better thermodynamic performance.

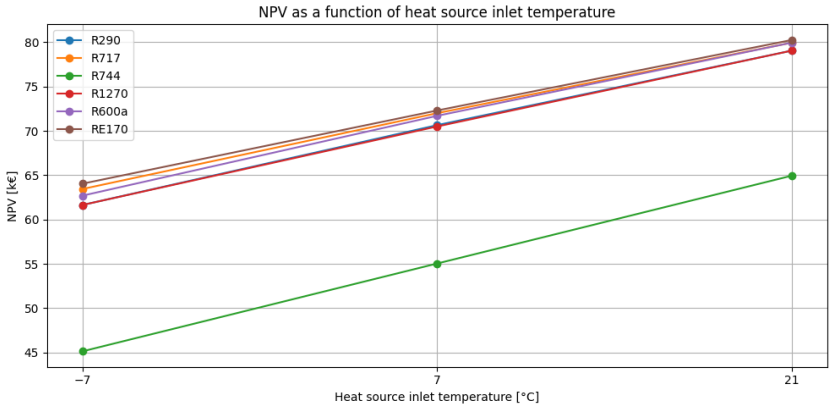


**Figure 5.23:** Effect of heat source inlet temperature on the NPV of VCHP cycles in the concrete drying case using an air-to-water HP.

In Figure 5.23, it can be seen that the NPV of all cycles increases. Notably, the difference between NPV for the VCHP cycles is minimal, except for the cycle using R744, which shows the lowest NPV by a clear margin. The economic performance is supported by the PBP results in Figure 5.24.

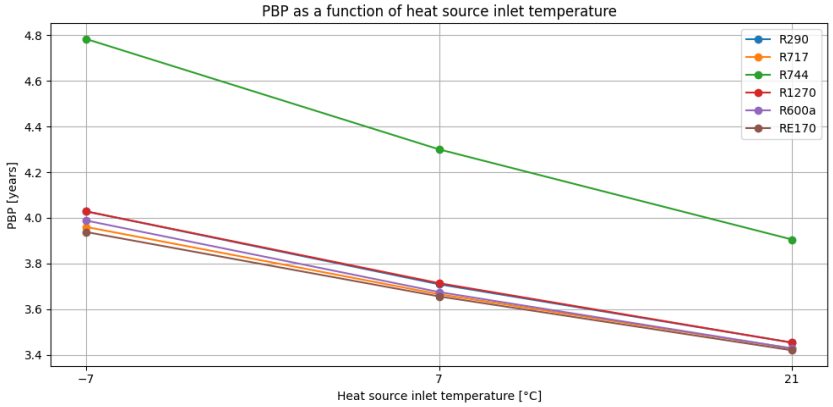


**Figure 5.24:** Effect of heat source inlet temperature on the PBP of VCHP cycles in the concrete drying case using an air-to-water HP.

Here, the R744 cycle has approximately 0.8 years longer PBP in the -7°C scenario, but at the highest heat source temperature, the difference is around 0.4 years. Thus, the cycle using R744 has a better improvement by the increase of the heat source temperature. The same trend appears in the LCOH results in Figure 5.25. Where the difference among the cycles, apart from the one using R744, is only marginal, with a lower LCOH observed at a higher heat source temperature.

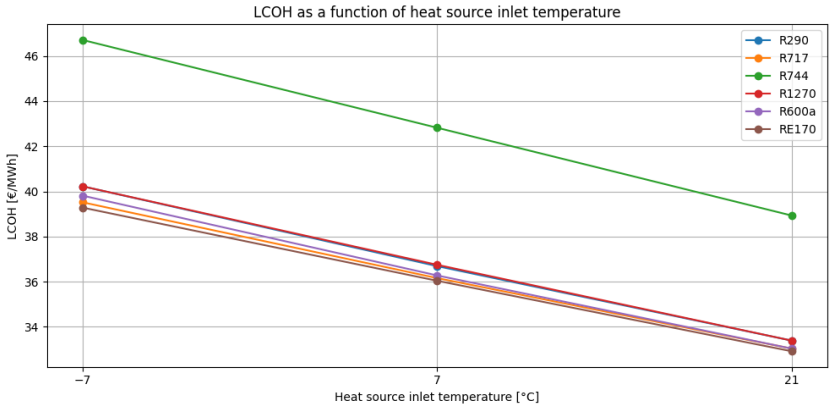


**Figure 5.25:** Effect of heat source inlet temperature on the LCOH of VCHP cycles in the concrete drying case using an air-to-water HP.

Moreover, the impact on the NPV for the VCHP cycles using RE170 and R744 is investigated for the CAW case. The results are presented in Table 5.7, where the baseline represents the NPV of the VCHPs when the HPs replace the usage of an electric boiler or DH, while keeping both electricity and DH prices constant

throughout the HPs lifetimes. The results presented in the table show the relative change in percentage if the price of electricity and/or DH is kept constant, or increased annually by 2 or 4%. These results were obtained using the variables in Table 4.7.

**Table 5.7:** Change in NPV of VCHPs using RE-170 and R744 for the concrete drying case using an air-to-water HP.

| **CF** | **WF** | **Baseline** | El↑2% DH | El↑4% DH | El DH↑2% | El DH↑4% | El↑2% DH↑4% | El↑4% DH↑2% |
|---|---|---|---|---|---|---|---|---|
| DH | RE170 | 72.3 k€ | -6.9 | -15.5 | 40.3 | 91.1 | 84.6 | 25.2 |
| | R744 | 55.0 k€ | -14.7 | -33.0 | 53.5 | 120.2 | 105.5 | 20.5 |
| El | RE170 | 37.9 k€ | -13.1 | -29.5 | - | - | -13.1 | -29.5 |
| | R744 | 20.7 k€ | -39.1 | -87.8 | - | - | -39.1 | -87.8 |

The results presented in Table 5.7 indicate that the NPV is more sensitive to price changes of reference utilities in the case where electric fans are replaced, CAW-El, compared to the scenario where the VCHP replaces the usage of water heated fans, as in the CAW-DH case. This sensitivity can be clearly observed, given that the magnitude of the NPV changes relative to the baseline when the reference utility is varied. It can be observed that the same percentage change in either electricity price or DH price leads to a larger NPV change for the CAW-El case compared to the same scenario for the CAW-DH case. Additionally, the relative change is more pronounced for the VCHP using R744 compared to the one using RE170. This discrepancy is attributed to the higher compressor work in the R744 cycle, making it more sensitive to changes, especially in electricity price.

Furthermore, the impact of utility price changes does result in negative NPVs for the VCHP cycle using RE170, indicating that this solution does not show full economic resilience even if the electricity price were to increase annually by 2 or 4% throughout its lifetime. The same is true for the cycle using R744.

Referring back to the discussion of the results in the SWW case regarding the uncertainty about which combination of price developments is most likely, the scenario with an annual increase of 2% for electricity and 4% for DH might be the most probable among the presented scenarios.

Additionally, the impact of estimated TCI value have been investigated. This sensitivity analysis studied the VCHP cycle with the refrigerant that had the best and worst economic performance, RE170 and R744.

The sensitivity analysis on utility cost impact, shown in Figure 5.26. In the analysis, the TCI was varied while keeping reference utility costs constant.

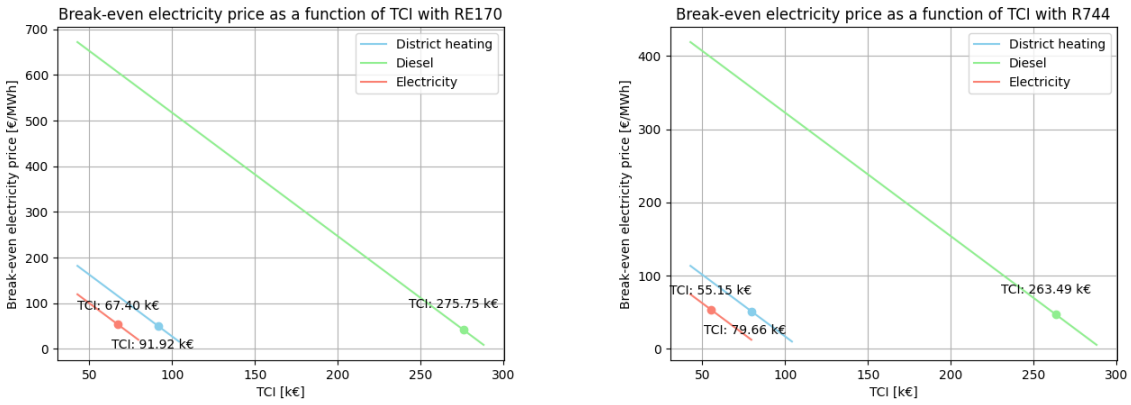


**Figure 5.26:** Break-even electricity price yielding NPV=0 as a function of TCI for the concrete drying case using a air-to-water HP with RE170 (left) and R744 (right) as refrigerants.

In Figure 5.26 the break-even electricity price corresponding to an NPV=0 as a function of TCI for SWW case is shown. The calculations assume constant prices of electricity, DH, and diesel over the HP's lifetime. Along each line in the figure, the NPV is zero. The dots and their annotated values indicate the break-even TCIs for each VCHP cycle when any of the reference utilities are replaced, while keeping the electricity price constant throughout the HP's lifetime. For example, if a VCHP using RE170 were to replace the use of a DH driven water heating fan, the TCI could be 91.92 k€ and still have NPV $\geq$ 0. The same value for the VCHP using R744 is 79.66 k€, indicated by the dot on the red break-even line.

The estimated TCI values for RE170 and R744 presented earlier was 42.89 k€ for both cases. If the true value lies somewhere between this and 91.92 k€ or 79.66 k€, respectively, the economic performance would still be positive for both VCHP cycles, indicating that even if the estimated TCI were an underestimate, there is a margin of error.

#### 5.5.2.3 Concrete: Air-to-air

The NPV and PBP results are presented in Figures 5.27 and 5.28, where the decreased compression work, resulting in a decrease in the electricity consumption of the various VCHPs, is observed to affect the NPV and PBP. Additionally, the decreased need for additional heating as the heat sink temperature is raised affects the outcome.

The outcome of increasing the heat source temperature in the CAA case is presented in Figure 5.27. The NPV of all cycles ended up being almost the same, differing just slightly. Thus, the lines in the figure lie on top of each other.

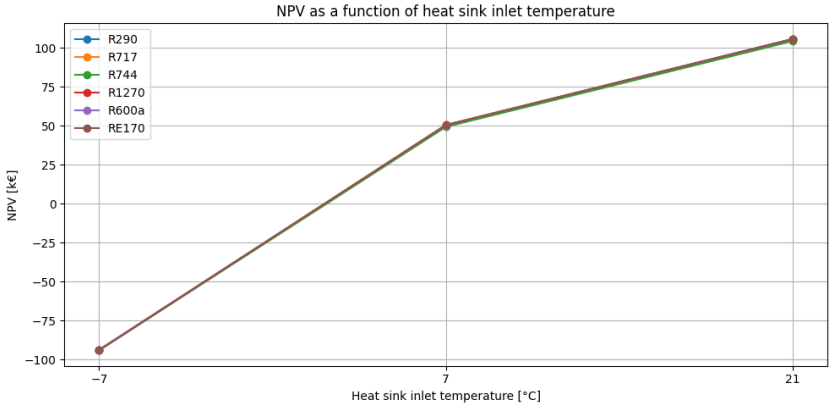


**Figure 5.27:** Effect of heat sink inlet temperature on the NPV of VCHP cycles in the concrete drying case using an air-to-air HP.

The most interesting result in Figure 5.27 is that all cycles had a negative NPV for the scenario with a heat sink inlet temperature of -7°C. Indicating that this design is not favorable in cold outside conditions. On the opposite end of the scenarios, a high heat sink inlet temperature results in a favorable outlook. This can also be seen when studying the PBP results in Figure 5.28.

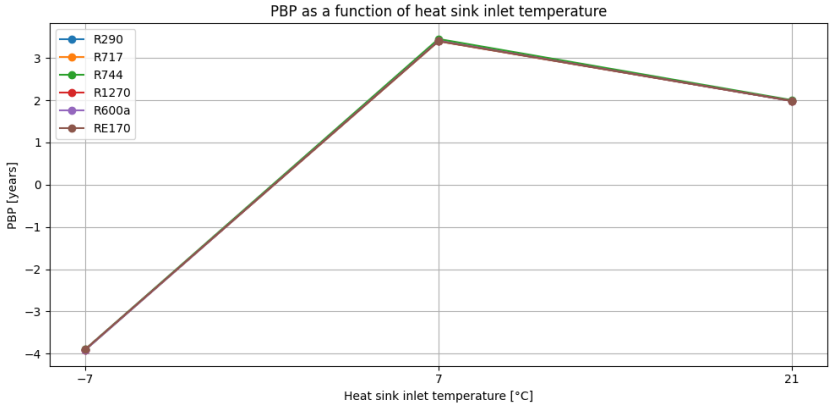


**Figure 5.28:** Effect of heat sink inlet temperature on the PBP of VCHP cycles in the concrete drying case using an air-to-air HP.

In the figure, all PBPs are negative in the -7°C scenario, implying that the investments won't be recovered. The PBP is three years at 7°C and two years at 21°C. The results related to the LCOH is presented in Figure 5.29.

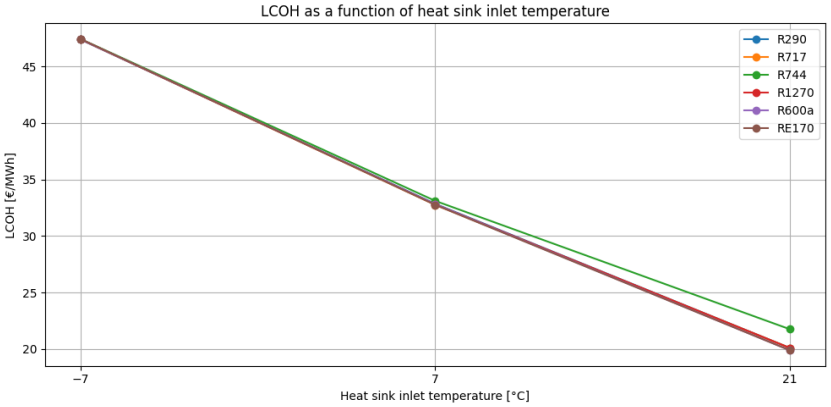


**Figure 5.29:** Effect of heat sink inlet temperature on the LCOH of VCHP cycles in the concrete drying case using an air-to-air HP.

From the figure it is evident that in the scenario of -7°C as heat sink inlet temperature the LCOH is very high, which is due to the non-existing cost saving over the VCHPs lifetime, as indicated by the negative NPV. The LCOH in the scenerio having heat sink inlet temperature of 21°C is approximately the same as in the CAW case, and roughly the double of the CAW values at 7°C.

The impact on the NPV for the VCHP cycles using R717 and R744 is investigated for the CAA case. The results are presented in Table 5.8, where the baseline represents the NPV of the VCHPs when the HPs replace the usage of an electric fan or DH, while keeping both electricity and DH prices constant throughout the HPs lifetimes. The results presented in the table show the relative change in percentage if the price of electricity and/or DH is kept constant, or increased annually by 2 or 4%. These results were obtained using the variables in Table 4.8.

**Table 5.8:** Change in NPV of VCHPs using R717 and R744 for the concrete drying case using an air-to-air HP.

| **CF** | **WF** | **Baseline** | El↑2% DH | El↑4% DH | El DH↑2% | El DH↑4% | El↑2% DH↑4% | El↑4% DH↑2% |
|---|---|---|---|---|---|---|---|---|
| DH | R717 | 50.6 k€ | -20.6 | -46.4 | 52.8 | 118.5 | 97.9 | 6.3 |
| | R744 | 49.4 k€ | -21.6 | -48.5 | 54.0 | 121.4 | 99.8 | 5.5 |
| El | R717 | 31.5 k€ | -33.1 | -74.4 | - | - | -33.1 | -74.4 |
| | R744 | 30.3 k€ | -35.2 | -79.0 | - | - | -35.2 | -79.0 |

The results presented in Table 5.8 indicate that the NPV is sensitive to price changes of both reference utilities. In the case where electric fans are replaced, CAA-El, the cycle using R717 is only slightly better when the electricity price is changed. The percentage change is smaller when VCHP replaces the usage of water heated fans, as in the CAA-DH case. This sensitivity can be clearly observed, given that the magnitude of the NPV changes relative to the baseline when the reference utility is varied. It can be observed that the same percentage change in either electricity

price or DH price leads to a larger NPV change for the CAA-El case compared to the same scenario for the CAW-DH case. Additionally, the relative change is more pronounced for the VCHP using R744 compared to the one using R717.

Furthermore, the impact of utility price changes does not result in negative or zero NPVs for the VCHP cycle using R717, indicating that this solution shows economic resilience even if the electricity price were to increase annually by 2 or 4% throughout its lifetime. The same is true for the cycle using R744, but in the scenario of an annual increase of electricity price by 4% the NPV is close to zero.

Even if future price developments are uncertain the scenario with an annual increase of 2% for electricity and 4% for DH might be the most probable among the presented scenarios, following the same reasoning as in the SWW case.

Additionally, the impact of estimated TCI value have been investigated. This sensitivity analysis studied the VCHP cycle with the refrigerant that had the best and worst economic performance, R717 and R744. The sensitivity analysis on utility cost impact, shown in Figure 5.30.

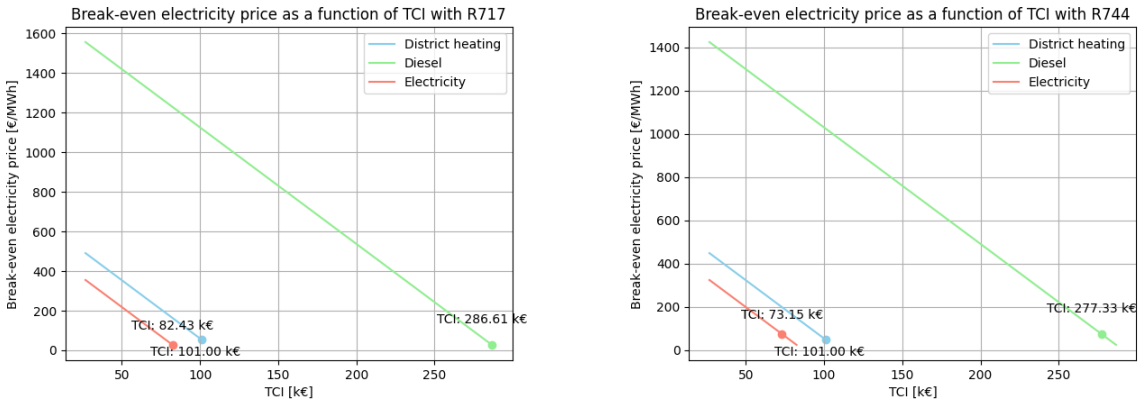


**Figure 5.30:** Break-even electricity price yielding NPV=0 as a function of TCI for the concrete drying case using a air-to-air HP with R717 (left) and (right) as refrigerants.

In Figure 5.26 the break-even electricity price corresponding to an NPV=0 as a function of TCI for SWW case is shown. The calculations assume constant prices of electricity, DH, and diesel over the HP's lifetime. Along each line in the figure, the NPV is zero. The dots and their annotated values indicate the break-even TCIs for each VCHP cycle when any of the reference utilities are replaced, while keeping the electricity price constant throughout the HP's lifetime. The two cycles have the same break-even TCIs when comparing all reference utilities. For example, if a VCHP using either R717 were to replace the use of a heating fan driven by electricity, the TCI could be 82.43 k€ and still have NPV $\geq$ 0.

The estimated TCI values for R717 and R744 presented earlier were both 26.75 k€. If the true value lies somewhere between this and 82.43 k€ and 73.15 k€ respectively, when an electric heating fan is being replaced, the economic performance would

still be positive for both VCHP cycles. Analogously as for the previous cases, this indicates that even if the estimated TCI were an underestimate, there is a margin of error. However, it is important to mention that the solution using an air-to-air HP results in negative NPV at lower temperatures. This discussion is based on the scenario using a heat sink inlet temperature of 7°C.

## 5.6 Comparative economic evaluation

In this final results section, the cost per ton of dried sludge and the cost per square meter of a hypothetical construction site are presented. The VCHP cycles used in the comparisons are those associated with the lowest LCOHs in each case study: the R717 VCHP in the sludge drying case, and the RE170 and R717 cycles in the CAW and CAA cases, respectively. The section begins with the findings from the sludge study, followed by the two concrete cases.

In Table 5.9, the cost per ton of dried sludge is presented together with the variable operation cost of the reference utilities used in this thesis.

**Table 5.9:** Estimated drying cost per metric ton of sludge using an R717 heat pump and reference utilities. For the reference utilities, only variable operation expenditures are considered.

| **Technology** | **Drying cost [€/ton dried sludge]** |
|---|---|
| R717 HP | 17.7 |
| Electric boiler | 29.4 |
| District heating | 27.4 |
| Gas boiler | 52.2 |

For the heat pump-related drying cost, the LCOH for the R717 VCHP at 20°C was used. It is evident that the system using the heat pump is at least 10 € cheaper per ton of dried sludge compared to the reference utilities. The cost of 17.7 € per ton of dried sludge would be an additional cost that, for example, a WWTP would need to pay, or if the dried sludge is being sold as a fuel, this would be the break-even price. This number should not be considered the whole truth, since it does not consider the cost of the belt-dryer itself, instead this is the heat related cost in a sludge drying system.

Moving on to the air-to-water heat pump system in the concrete case study, Table 5.10 presents the cost per square meter of the construction site. Two scenarios of 47 or 116 kWh/m$^2$ are based on the work by N. Karlsson et al. [46].

**Table 5.10:** Estimated drying cost per square meter using an RE170 heat pump in the concrete air-to-water case and reference utilities. For the reference utilities, only variable operation expenditures are considered. The drying costs are estimated assuming a demand of (a) 47 or (b) 116 kWh/m$^2$.

| **Technology** | **Drying cost (a) [€/m$^2$]** | **Drying cost (b) [€/m$^2$]** |
|---|---|---|
| RE170 HP | 1.7 | 4.2 |
| Electric heating fan | 2.4 | 5.9 |
| District heating | 2.8 | 6.8 |
| Diesel generator | 8.0 | 19.8 |

From the table, it is clear that employing a heat pump would result in lower running costs in both scenarios. In these calculations, no regard has been taken into who would pay this cost, but it should instead be seen as an indicator that can be used to minimize the cost of climate control when only considering running costs.

In the air-to-air heat pump system in the concrete case study, Table 5.11 presents the cost per square meter of the construction site. The same two scenarios as in the previously presented results of the air-to-water study are used.

**Table 5.11:** Estimated drying cost per square meter using an R717 heat pump in the concrete air-to-air case and reference utilities. For the reference utilities, only variable operation expenditures are considered. The drying costs are estimated assuming a demand of (a) 47 or (b) 116 kWh/m$^2$.

| **Technology** | **Drying cost (a) [€/m$^2$]** | **Drying cost (b) [€/m$^2$]** |
|---|---|---|
| R717 HP | 1.5 | 3.8 |
| Electric heating fan | 2.4 | 5.9 |
| District heating | 2.8 | 6.8 |
| Diesel generator | 8.0 | 19.8 |

Here, it is evident that using an R717 VCHP would result in even lower running costs for climate control compared to the air-to-water case. This is due to the lower LCOH of this system, given the assumptions made in this thesis. Once again, the numbers should be seen as indicators and not the whole truth, since there are many assumptions related to the calculations.

# 6

# Discussion and Conclusion

In this project, two case studies focusing on heat pump (HP) integrated drying were performed: one involving the drying of municipal sewage sludge, and the other involving drying of concrete during construction. The HPs studied were vapor compression heat pumps (VCHPs) using refrigerants with low (<4) 100-year time horizon global warming potential ($GWP_{100}$) not subjected to current phase-out schemes. In the two case studies, a combination of the simulation tool Aspen Plus and a Python script were used as a method for selecting operational conditions to satisfy a specified minimum temperature difference approach. Additionally, to account for anticipated regulations on per– and polyfluoroalkyl substance (PFAS) chemicals, none of the investigated refrigerants that were investigated are classified as PFAS. In the concrete case study, air-to-air and air-to-water VCHPs using the refrigerants R290, R717, R744, R1270, R600a, and RE170 were investigated. In the sludge case study, water-to-water VCHPs using the same refrigerants were investigated. Moreover, the thermodynamic evaluation only included simple VCHP cycles without efficiency improvement measures, such as intercooling or multistage compression, which could potentially enhance the thermodynamic efficiency of all cycles.

An additional simplification was that the condenser was simulated as one unit instead of a gas cooler, condenser, and subcooler. The same procedure was done for the evaporator, where evaporator and superheater were considered as one unit in the Aspen simulations. This obviously impacts the results, but the approach was considered to be satisfactory within the scope of this thesis project. The same is true for the assumption of zero pressure and heat losses in the cycle simulations, both will affect the thermodynamic performance in reality.

The studied VCHPs had a coefficient of performance (COP) or coefficient of system performance (COSP) around three in all cases investigated, indicating that compared to using for example direct electricity as heat source, a three-folded increase in thermodynamic efficiency can be achieved. In both the sludge case study and the concrete air-to-water case study, the cycles using R744 had lower COP than the other cycles. This refrigerant was thus deemed to be the least promising alternative with respect to thermodynamic performance. On the other hand, R744 is the refrigerant that can be considered the most safe to use considering both toxicity and flammability, which could make it an interesting option regardless of lower performance.

In the sludge case study, the VCHP cycles show promising thermodynamic and economic potential compared to using an electric boiler, district heating, or a gas boiler to provide a sludge belt-dryer with thermal energy. When investigating the effect of future price developments, where the price of electricity and/or district heating (DH) was kept constant, or increased annually by 2 or 4% it was found that the VCHP cycle using R717 had positive net present value (NPV) in all scenarios. The VCHP using R744 had negative NPV only in the scenario where the cost of district heating was constant and the electricity price had an annual increase of 4% during the HP's lifetime, given that the HP replaces the use of DH. This indicates that the VCHP cycle using R744 would not be economically viable if this rather unlikely future scenario were to occur. The cycle using R744 appears to be more sensitive to these changes, mainly due to its lower thermodynamic performance. Notably, even though the economic performance is lower for the cycle using R744, the results indicate that this cycle has economic and environmental benefits, with a positive NPV and lower annual greenhouse gas emissions than the reference utilities in the more likely scenarios of increased price of both district heating and electricity.

In the concrete case study, using air-to-water VCHPs, the outcome related to the price development investigation was similar to that of the cycles in the sludge case. The cycles highlighted were those using RE170 and R744, which had the highest and lowest NPVs, respectively. The NPV for both cycles remained positive for the same price development scenarios as in the sludge case study, indicating resilience to future price changes. The same is true for the second proposed concrete drying system using an air-to-air VCHP, where the cycle using R717 had the highest NPV and the cycle using R744 the lowest.

The break-even electricity price concerning the total capital investment (TCI) for both the most and least efficient cycles among the three proposed HP solutions was also investigated. It was found that all cycles could have TCIs several times higher than estimated while still yielding an NPV $\geq 0$, indicating that the TCIs can be relatively high while still providing economic benefits compared to using the included reference utilities. This illustrates that the TCI can be recuperated at current and higher electricity prices, and with relatively short payback periods (PBP), the theoretical integration would result in cost savings both in large-scale drying, such as that of sludge drying, and in smaller-scale applications, such as for the climate control of construction sites.

Based on all sensitivity analyses, it can be concluded that having a high heat source or sink temperatures (above 7°C in both concrete solutions) results in a system resilient to price developments based on the price development scenarios investigated. This is indicated by the outcomes being NPVs $> 0$ in all scenarios.

Another investigated economic perspective is when comparing the cost per metric ton dried sludge and cost per square meter climate controlled construction site using the VCHP with lowest levelized cost of heat (LCOH) compared to the reference utilities. The costs investigated does not take into account the cost of e.g., the belt-dryer in the sludge case study nor the fans in the concrete case study. Instead the numbers

should be seen as a measure of how much the heating related cost would change if replacing the reference utilities. In the sludge case study the costs would be roughly 10 € lower per ton dried sludge when using an R717 VCHP than district heating. The cost reduction in the two concrete cases was around 0.7 € per square meter when replacing electric fans. Thus, it is safe to say that by using heat pumps the energy related costs in both case studies would be reduced.

Moreover, it was found that the proposed design of the air-to-air HP, using ambient air as the heat sink and room exhaust as the heat source, was not feasible when the ambient temperature was low (-7°C). Having a low ambient temperature as the heat sink resulted in negative NPVs for this solution, regardless of which refrigerant was used. The HP was designed with specified target temperature and volume flow. The results could differ if the volume flow of air was adjusted; i.e., if the volume flow was lower and the HP would be able to reach the target temperature without the additional heating. This observation is solely based on theoretical reasoning and no such simulation was performed.

The major challenge in the concrete case using air-to-air HPs is to find a HP design that is able to handle low ambient temperature conditions, while maintaining a good thermodynamic performance. Thus, apart from the air-to-air HP using ambient air as the heat sink and room exhaust as the heat source, an additional design proposal was briefly evaluated. This variation of the simulation was conducted for the concrete air-to-air HP wherein the buildings exhaust air, serving as the heat source was circulated in a loop and thus utilized as the heat sink as well. This simulation was performed when the ambient temperature was -7°C, under the assumption that electric heating fans initiated the climate control and the HP intervened at feasible indoor temperatures. It was found that every investigated key performance indicator (KPI) improved when looping the exhaust air and using it as an heat sink compared to when the colder ambient air was used as the heat sink. It indicates that this design might be a better option, seen to both thermodynamic and economic performance, and should be further investigated if the HP is to be operated at lower outdoor temperatures. However, this design is associated with other challenges for example the need of ensuring the air quality when recirculating the air, by for example having filters and some fresh air being used.

The air-to-water VCHP proposal utilized ambient air as the heat source and showed positive NPVs at lower temperatures, yet still low ones compared to during nominal conditions ($\sim$ 7°C). These different outcomes indicate that in colder climates, it may not be feasible to use cold ambient air as the heat sink but rather it should act as the heat source. It is worth mentioning that only a limited set of ambient temperatures were considered; therefore, the discussion is based on the investigated scenarios.

It also worth noting that, as mentioned in Section 2.2.4, establishing a tight building envelope (TBE) is of paramount importance when it comes to optimizing the energy usage on a construction site with freshly poured concrete. The running costs of climate control devices can increase exponentially, even if there is seemingly insubstantial leakage to the outside environments during the colder months. Even though that

both HPs, purely seen from the investigated KPIs, in the concrete case studies performs well during nominal conditions ($\sim 7°C$), it does not automatically imply that the HP will perform well on a construction site per se.

One reason for this can be the fact that HPs, especially air-to-air HPs, lack the instantaneous heating capabilities of electric heating fans. Even more so compared to diesel generators, which are often used when drying targets are not met and have a much larger carbon footprint as discussed in Section 5.4. If a window is accidentally left open during the coldest winter months, it could take several hours for the HP to recover the heat loss and return to the target temperature and thus prolong the overall drying time. In contrast, the same recovery with reference utilities could take significantly less time. The same principles apply to the proposed air-to-water HP, but to a lesser extent since heating fans are utilized. Yet, as the proposed air-to-water HP is driven by water circulating in a loop, the load and instantaneous heat delivery is deemed to not be equal to the reference utilities. The heat pump alone may perform well both thermodynamically and economically, but target temperatures and appropriate drying conditions may not be reached without an established TBE.

The proposed concrete VCHPs can also be seen as relatively portable. It was noted that the reference technology used for the proposed air-to-water VCHP can be moved with a forklift to suitable areas in the construction site which provides flexibility for temporary climate control needs or projects on a smaller scale. The proposed air-to-air VCHP resembles a household HP, offering convenience for more stationary installations for projects on a larger scale.

As previously mentioned, six refrigerants have been selected as potential candidates and used in VCHP cycle simulations. Some of these refrigerants are currently used in commercial heat pumps. As fluorinated refrigerants are being phased out and restricted, it is expected that at least some of the studied refrigerants will replace them. Given that, for example, R717 and R744 are used in commercially available heat pumps, it is likely that the TCI would be lower for these solutions compared to a cycle using RE170, which has very few commercially available heat pumps. The effect on the TCI is based on the fact that since some of the technologies are more mature, the ones that are new or not currently used will have higher development costs due to fewer predecessors. Moreover, depending on the specific application and intended location of the heat pumps, different safety measures might be needed, such as forced ventilation in case of leakage. This may increase the TCI, but as indicated by the break-even analysis, there are substantial error margins. Therefore, this is not seen as a major challenge but is worth mentioning.

Another aspect of interest in the sludge drying case study is the implication of the placement of the belt dryer, whether it is located at the wastewater treatment plant or near a power plant where the dried sludge is used as fuel. In this study, this aspect was not considered, but it could affect the available heat source temperatures. For example, if the dryer is located at the wastewater treatment plant, it is likely that the available heat has a relatively low temperature. However, if it is located near a power plant, the likelihood of potential heat source streams with higher temperatures

is greater. Additionally, depending on where the sludge is dried, the removed water in need of treatment would have to be transported different distances, which can be an issue depending on the existing sewage capacity. Furthermore, the weight and volume of the sludge would be lower if the sludge is dried before transporting it to the power plant, which could be beneficial.

Moreover, in this project, the TCI was estimated using cost correlations based on delivered heat, implying that all VCHPs with the same heating capacity appear to have the same costs. Another approach to better understand how the choice of refrigerant would affect the TCI would be to adopt more of a bottom-up approach, where the cost of each component could be estimated. This would allow consideration of, for example, different types of heat exchangers and materials. Additionally, it is expected that the compressor will be the most expensive component, and depending on the working conditions and refrigerant, the available compressors might be more or less expensive. Thus, the TCI is most likely to vary more than it appears in this project. However, as mentioned before, the margin of error in this estimation is substantial for all solutions, so it is expected that the economic potential is still promising even if the TCI would differ in reality.

To summarize the different outcomes: the VCHP cycles in both case studies should be further studied with respect to improvement measures to gain a broader understanding. However, based on the simple cycle setup used in this work, the cycle using R717 shows the best thermodynamic and economic performance and could be the most feasible alternative in the sludge case study. Even if additional investments are needed to meet safety requirements when using R717, it would be a viable solution given the generous margin of error on the TCI for this proposal. On the other hand, in the concrete case study, the air-to-air HP showed very good COPs at high temperatures, and the coefficient of system performance was around 3, but with negative NPVs at low temperature (-7°C). This can be circumvented by planning the time of construction based on regional climate to match the construction phase to the periods when the proposed air-to-air HP has beneficial thermoeconomic performance. When this cannot be done, the air-to-water HP appears to be a more robust alternative in regions where the outdoor air is cold during the construction phase, especially the cycle using RE170, which has the best techno-economic performance in the air-to-water simulations. All studied VCHP cycles—using water-to-water in the sludge case and air-to-water and air-to-air in the concrete case—show positive economic performance. A COP of around three or higher indicates that there is great potential for improving the thermodynamic efficiency of the two drying processes.

## 6.1 Future work

This project was conducted as a case study of specific HP technologies, placed in a Swedish context. Further studies should investigate using other HP technologies, for example absorption HPs, to obtain a broader understanding of potential HP integration. Moreover, due to time limits, the study did not focus on optimizing component costs and instead used rougher capital expenditures and operational

expenditures estimates, to evaluate the system. Future studies could delve deeper into the analysis of HP related TCIs and impact of heat exchanger area, to better grasp the economic outlook.

Another aspect that was not investigated is what the optimal share of sludge utilized as incineration fuel would be. Further work is needed to identify of there is a system optimum as well as providing better understanding the legislative context for both incineration and land spreading. Future work could also investigate whether dried sludge could be seen as a commercial fuel to be sold to a power producer, thus creating an income that could contribute to financing the drying system. In this project the cash flow related to the dried sludge was neglected due to time limitations.

Additionally, future work could focus on possible implementation of smart control systems for the HPs utilized during the climate control in the construction phase, with an emphasis on flexibility in scheduling operation times. As an example, the HP could be run during periods of lowest electricity prices, such as during the night rather than during any possible peaks. This potential strategy not only optimizes the costs of electricity but also avoids creating a workplace that is uncomfortably warm for the personnel on the construction site.

A large focus should be put in investigating the safety of employing HPs on active workplaces such as an construction site with potentially dangerous refrigerants like ammonia due to its toxicity, if a leak were to occur. Future research should focus on leak-proof designs, monitoring of the refrigerant and a durable design capable of being operated in the context of a construction site. With that being said, current HP manufacturers are keeping a high standard when it comes to the safety aspects of the refrigerants. The focus of this research could be to evaluate the associated costs with these kind of improvements. Risk assessment and mitigation strategies if accidents were to occur are vital to ensure no harm is done to either the workers or the surrounding environment.

Furthermore, a second proposal for a sludge drying HP-integrated system was considered, similar to a HP tumble dryer, where the air is looped. In this system, the humid air from the sludge dryer is dehumidified as its latent heat is transferred in the evaporator, then heated in the condenser, and directed back to the wet sludge. This system might be of interest for future investigation, but due to time constraints, it was excluded from this thesis work.

As previously mentioned in the discussion regarding the placement of the sludge dryer and its implications, it would be of interest to investigate both the environmental and economic differences between transporting dried sludge to a power plant and transporting wet sludge to be dried at the power plant to determine which of these alternatives is better.

In this study, fully critical R744 VCHPs were not examined. However, at least one commercial supplier offers this type of HP. It is likely that this kind of heat pump will become more common, and the COP of this design would be interesting to study further.

The methodology of combining Aspen Plus with a Python script to visually handle the minimum temperature approach was tedious but satisfactory. Therefore, it would be of great interest to develop a more automated procedure for data transfer from Aspen to, for example, the Python script used. This would promote a more user-friendly and faster process.

Finally, the VCHP cycle studies only considered simple cycles. It would be of great interest to investigate the techno-economic performance of more complex cycles in the context of drying applications, such as in construction sites and sludge drying.

# Bibliography


[1] Osmanski S. *How Do Carbon Emissions Affect the Environment?* [accessed: 16-01-2023]. Green Matters, 2020. URL: https://www.greenmatters.com/p/how-do-carbon-emissions-affect-environment.

[2] IEA. *Achieving net-zero emissions by 2050 – World Energy Outlook 2020 – Analysis - IEA*. [accessed: 16-01-2024]. Paris: International Energy Agency, 2000. URL: https://www.iea.org/reports/world-energy-outlook-2020/achieving-net-zero-emissions-by-2050.

[3] UNFCCC. *The Paris Agreement*. [accessed: 01-02-2024]. Bonn: United Nations Framework Convention on Climate Change, n.d. URL: https://unfccc.int/process-and-meetings/the-paris-agreement.

[4] UN. *For a livable climate: Net-zero commitments must be backed by credible action*. [accessed: 01-02-2024]. New York: United Nations, n.d. URL: https://www.un.org/en/climatechange/net-zero-coalition.

[5] UNEP. *Emissions Gap Report 2023*. [accessed: 01-02-2024]. Nairobi: UN Environment Programme, 2023. URL: https://www.unep.org/resources/emissions-gap-report-2023.

[6] IEA. *Net Zero Roadmap: A Global Pathway to Keep the 1.5 °C Goal in Reach*. [accessed: 02-02-2024]. Paris: International Energy Agency, 2023. URL: https://www.iea.org/reports/net-zero-roadmap-a-global-pathway-to-keep-the-15-0c-goal-in-reach.

[7] IEA. *Understanding GEC Model scenarios – Global Energy and Climate Model – Analysis - IEA*. [accessed: 01-02-2024]. Paris: International Energy Agency, 2023. URL: https://www.iea.org/reports/global-energy-and-climate-model/understanding-gec-model-scenarios.

[8] IEA. *Industrial energy consumption by fuel in the Net Zero Scenario, 2000-2030*. [accessed: 02-02-2024]. Paris: International Energy Agency. URL: https://www.iea.org/data-and-statistics/charts/industrial-energy-consumption-by-fuel-in-the-net-zero-scenario-2000-2030.

[9] European Commission. *Net-Zero Industry Act*. [accessed: 01-02-2024]. Brussels: European Commission, 2023. URL: https://commission.europa.eu/strategy-and-policy/priorities-2019-2024/european-green-deal/green-deal-industrial-plan/net-zero-industry-act_en.

[10] U.S. Department of Energy. *A BestPractices SteamTechnical Brief Industrial Heat Pumps for Steam and Fuel Savings Energy Efficiency and Renewable*

*Energy*. [accessed: 01-02-2024]. 2003. ISBN: 1020031735. URL: www.eere.energy.gov.

[11] IEA. *Renewables*. [accessed: 01-02-2024]. Paris: International Energy Agency, 2023. URL: https://www.iea.org/energy-system/renewables.

[12] IEA Heat Pump Centre. *Application of Industrial Heat Pumps: IEA Industrial Energy-related Systems and Technologies Annex 13 IEA Heat Pump Programme Annex 35 (Final Report Part 1)*. [accessed: 08-022024]. Borås, 2014. ISBN: 978-91-88001-92-4.

[13] Pacanowsky A. *Types of Industrial Process Heating and Applications - Powerblanket*. Feb. 2022. URL: https://www.powerblanket.com/blog/types-of-industrial-process-heating-and-applications/.

[14] The Edistors of Encyclopaedia Britannica. *sludge*. [accessed: 26-02-2024]. Encyclopedia Britannica, 2017. URL: https://www.britannica.com/topic/sludge.

[15] Chen G., Yue P. L., and Mujumdar A. S. "SLUDGE DEWATERING AND DRYING". In: *Drying Technology* 20 (4-5 2002), pp. 883–916. ISSN: 07373937. DOI: 10.1081/DRT-120003768. URL: https://www.tandfonline.com/doi/abs/10.1081/DRT-120003768.

[16] Swedish Enviornmental Protection Agency. *Avlopp*. [accessed: 15-05-2024]. n.d. URL: https://www.naturvardsverket.se/amnesomraden/avlopp/.

[17] Videbris K-E. *Miljörapport Gryaab, Ryaverket 2022*. Göteborg: Gryaab, 2023. URL: https://www.gryaab.se/wp-content/uploads/2023/04/Miljorapport-Ryaverket-2022-med-bilagor.pdf.

[18] Hydropress HUBER AB. *HUBER Slamtork BT*. [accessed: [accessed: 31-01-2024]]. Lindome: Hydropress HUBER AB, c2024. URL: https://www.hubersverige.se/fileadmin/huber-se/documents/pdf/pro_bt-slamtork_se.pdf.

[19] Sun J. et al. "A Review of Super-High-Temperature Heat Pumps over 100 °C". In: *Energies 2023, Vol. 16, Page 4591* 16 (12 June 2023), p. 4591. ISSN: 1996-1073. DOI: 10.3390/EN16124591. URL: https://www.mdpi.com/1996-1073/16/12/4591/htm%20https://www.mdpi.com/1996-1073/16/12/4591.

[20] Fernández L. *Global industrial energy consumption 2050*. [accessed: 16-01-2024]. Statista, Oct. 2023. URL: https://www.statista.com/statistics/263471/industrial-energy-consumption-worldwide/.

[21] Kemp I. C. *Fundamentals of Energy Analysis of Dryers*. Ed. by Tsotsas E. and Mujumdar A. S. Vol. 4. John Wiley & Sons, Ltd, Jan. 2012, pp. 1–45. ISBN: 9783527315598. DOI: 10.1002/9783527631681.CH1. URL: https://onlinelibrary.wiley.com/doi/10.1002/9783527631681.ch1.

[22] Myhr A. and Villner M. *Discharges to water and sewage sludge production in 2020 Municipal wastewater treatment plants, pulp and paper industry and some other industries*. [accessed: 12-02-2024]. Havs- och Vattenmyndigheten and Statistikmyndigheten Scb, 2020.

[23] EurEau. *March 2021 Draft external version Briefing Note Waste water treatment-sludge management*. [accessed: 13-02-2024]. Brussels: European Federation of National Associations of Water Services, 2021. URL: https://w

ww.eureau.org/resources/briefing-notes/5629-briefing-note-on-sludge-management/file.

[24] Judd S. *Incineration of sludge*. [accessed: 18-01-2024]. Buckinghamshire: Sludge Processing, 2020. URL: https://www.sludgeprocessing.com/oxidative-thermochemical-treatment/incineration-sludge/.

[25] Fijalkowski K. et al. "The presence of contaminations in sewage sludge – The current situation". In: *Journal of Environmental Management* 203 (Dec. 2017), pp. 1126–1136. ISSN: 0301-4797. DOI: 10.1016/J.JENVMAN.2017.05.068.

[26] Gao N. et al. "Thermochemical conversion of sewage sludge: A critical review". In: *Progress in Energy and Combustion Science* 79 (July 2020), p. 100843. ISSN: 0360-1285. DOI: 10.1016/J.PECS.2020.100843.

[27] IEA HPT TCP (Heat Pumping Technologies Technology Collaboration Programme). *Heat Pumps for Drying - Annex 59*. [accessed: 30-01-2024]. Paris, n.d. URL: https://heatpumpingtechnologies.org/annex59/.

[28] Yuan G. and Chu K. H. "Heat pump drying of industrial wastewater sludge". In: *Water Practice and Technology* 15 (2 June 2020). [accessed: 08-02-2024], pp. 404–415. ISSN: 1751231X. DOI: 10.2166/WPT.2020.029. URL: http://iwaponline.com/wpt/article-pdf/15/2/404/764295/wpt0150404.pdf.

[29] Shincci Global. *Waste Heat Belt-type Sludge Dryer Parameters*. [accessed: 08-02-2024]. n.d. URL: https://shincci-global.com/products/sludge%20dryer/new-waste-heat-dryer.

[30] Naturskyddsföreningen. *Avfallstrappan*. [accessed: 27-02-2024]. Naturskyddsföreningen, 2021. URL: https://www.naturskyddsforeningen.se/faktablad/avfallstrappan/.

[31] Swedish Enviornmental Protection Agency. *Avfallshierarkin visar stegen vi behöver ta*. [accessed: 27-02-2024]. Swedish Enviornmental Protection Agency, n.d. URL: https://www.naturvardsverket.se/amnesomraden/avfall/pagaende-arbeten/avfallshierarkin-visar-stegen-vi-behover-ta/.

[32] Åkerblom A. et al. *Wastewater treatment in Sweden 2020*. Stockholm: Swedish Enviornmental Protection Agency, 2022. ISBN: 978-91-620-8896-5. URL: https://www.naturvardsverket.se/4acbd4/globalassets/media/publikationer-pdf/8800/978-91-620-8896-5.pdf.

[33] Finnson A. *Aktivt uppströmsarbete med Revaq-certifiering - Svenskt Vatten*. [accessed: 22-04-2024]. 2023. URL: https://www.svensktvatten.se/vattentjanster/avlopp-och-miljo/kretslopp-och-uppstromsarbete/revaq-certifiering/.

[34] Johannesdottir S. et al. *Slamhygienisering-kartläggning och utvärdering av tekniker*. 2023. ISBN: 0850600200. URL: https://vattenbokhandeln.svensktvatten.se/wp-content/uploads/2024/02/svu-rapport-2023-12.pdf.

[35] Strömberg B. and Herstad Svärd S. *Anläggnings- och förbränningsteknik 1234: Bränslehandboken 2012*. Stockholm, 2012.

[36] Swedish Enviornmental Protection Agency. *Avloppsslam på jordbruksmark*. [accessed: 27-03-2024]. Swedish Enviornmental Protection Agency, 2023. URL: https://www.naturvardsverket.se/data-och-statistik/avfall/avloppsslam-pa-jordbruksmark/.

[37] Jordbruksverket. “Användning av avloppsslam på jordbruksmark”. In: (2021). URL: https://jordbruksverket.se/download/18.666a627517078da0aba4a5a4/1646227175268/Informationsblad-slam-tga.pdf.

[38] Starberg K., Haglund J-E, and Hultgren J. *Slamförbränning*. Stockholm: Svenskt Vatten AB. ISBN: 9189182251. URL: https://vav.griffel.net/filer/VA-Forsk_99-11.pdf.

[39] Sludge Processing. *Sludge treatment – properties of drying sludge*. [accessed: 27-02-2024]. Buckinghamshire: Sludge Processing, 2022. URL: https://www.sludgeprocessing.com/sludge-drying/properties-of-drying-sludge/.

[40] Judd S. *What is sludge?* [accessed: 26-02-2024]. Buckinghamshire: Sludge Processing, 2021. URL: https://www.sludgeprocessing.com/sludge-basics/what-is-sludge-characteristics/.

[41] Inayat A. et al. “Review of the Integration of Drying and Thermal Treatment Processes for Energy Efficient Reduction of Contaminants and Beneficial Reuse of Wastewater Treatment Plant Biosolids”. In: *Energies 2023, Vol. 16, Page 1964* 16 (4 Feb. 2023), p. 1964. ISSN: 1996-1073. DOI: 10.3390/EN16041964. URL: https://www.mdpi.com/1996-1073/16/4/1964/htm%20https://www.mdpi.com/1996-1073/16/4/1964.

[42] Gerdin A. *Energieffektiv uttorkning och klimathållning under byggprocessen-Förutsättningar för innovationsupphandling eller tekniktävling LÅGAN Rapport Januari 2023*. CIT Renergy, Jan. 2023. URL: www.laganbygg.se.

[43] *The Importance of Concrete in Construction - Hanson Malaysia*. June 2020. URL: https://www.hanson.my/en/importance-concrete-construction.

[44] Spangler J. *How Long Does Concrete Take to Dry? Expert Tips*. [accessed: 19-01-2023]. Oregon, US, June 2023. URL: https://www.wagnermeters.com/concrete-moisture-test/concrete-info/how-to-speed-up-concrete-drying-time/.

[45] *How Long Does It Take for Concrete to Dry? (2024 Guide)*. July 2020. URL: https://todayshomeowner.com/concrete/finishes-and-considerations/.

[46] Karlsson N., Larsson C., and Burke S. *Energianvändning vid klimathållning och avfuktning under byggproduktion-Förstudie*. LÅGAN, Dec. 2019. URL: www.laganbygg.se.

[47] Augustyn A. *Concrete | Definition, Composition, Uses, Types, & Facts | Britannica*. Jan. 2024. URL: https://www.britannica.com/technology/concrete-building-material.

[48] *Concrete Basics: Essential Ingredients For A Concrete Mixture | CSC*. URL: https://concretesupplyco.com/concrete-basics/.

[49] Gagg C. R. “Cement and concrete as an engineering material: An historic appraisal and case study analysis”. In: *Engineering Failure Analysis* 40 (May 2014), pp. 114–140. ISSN: 1350-6307. DOI: 10.1016/J.ENGFAILANAL.2014.02.004.

[50] Malaga K. *Vad du behöver veta inför ett eventuellt stopp | RISE*. URL: https://www.ri.se/sv/berattelser/vad-du-behover-veta-infor-ett-eventuellt-stopp.

[51] Van Damme H. "Concrete material science: Past, present, and future innovations". In: *Cement and Concrete Research* 112 (Oct. 2018), pp. 5–24. ISSN: 0008-8846. DOI: 10.1016/J.CEMCONRES.2018.05.002.

[52] Hanein T. et al. "Decarbonisation of calcium carbonate at atmospheric temperatures and pressures, with simultaneous CO 2 capture, through production of sodium carbonate". In: *Energy & Environmental Science* 14.12 (Dec. 2021), pp. 6595–6604. ISSN: 17545706. DOI: 10.1039/D1EE02637B. URL: https://pubs.rsc.org/en/content/articlehtml/2021/ee/d1ee02637b%20https://pubs.rsc.org/en/content/articlelanding/2021/ee/d1ee02637b.

[53] Petersson J. *Thermal Plasma in a Rotary Kiln for Cement Production An Investigation of the Heat Transfer Mechanisms Master's thesis in Sustainable Energy Systems*. Gothenburg, 2022. URL: https://odr.chalmers.se/server/api/core/bitstreams/ff16668a-1c6c-4921-9163-eb8eb372673c/content.

[54] *Cementbranschen - Fossilfritt Sverige*. 2023. URL: https://fossilfrittsverige.se/roadmap/cementbranschen/.

[55] Skinner B. and Lalit R. *Concrete: 8% of global emissions and rising. Which innovations can achieve net zero by 2050? - Energy Post*. Jan. 2023. URL: https://energypost.eu/concrete-8-of-global-emissions-and-rising-which-innovations-can-achieve-net-zero-by-2050/.

[56] Hamidreza Gohari Darabkhani, Hirbod Varasteh, and Bahamin Bazooyar. "Main technologies in CO2 capture". In: *Carbon Capture Technologies for Gas-Turbine-Based Power Plants* (Jan. 2023), pp. 19–38. DOI: 10.1016/B978-0-12-818868-2.00002-3.

[57] *CCUS*. 2020. URL: https://cembureau.eu/policy-focus/climate-energy/ccus/.

[58] Ali Raza Kalair et al. "Waste to energy conversion for a sustainable future". In: *Heliyon* 7.10 (Oct. 2021). ISSN: 2405-8440. DOI: 10.1016/J.HELIYON.2021.E08155.

[59] B. V. Rangan. "Engineering properties of geopolymer concrete". In: *Geopolymers: Structures, Processing, Properties and Industrial Applications* (Jan. 2009), pp. 211–226. DOI: 10.1533/9781845696382.2.211.

[60] Nicholas B. Winter. *Understanding Cement: The Fast Star User-friendly Insight into Cement Production, Cement Hydration and Cement and Concrete Chemistry*. WHD Microanalysis Consultants Ltd, 2012, p. 206. ISBN: 0957104529. URL: https://books.google.com/books/about/Understanding_Cement.html?hl=sv&id=b8qznQEACAAJ.

[61] Peter C. Taylor. *Curing concrete*. CRC Press, Jan. 2013, pp. 1–184. ISBN: 9780203866139. DOI: 10.1201/B15519/CURING-CONCRETE-PETER-TAYLOR. URL: https://www.taylorfrancis.com/books/mono/10.1201/b15519/curing-concrete-peter-taylor.

[62] Y. Pawar and Shrikant Kate. "Curing of Concrete: A Review". In: (2020).

[63] D. J. Hannant, S. B. Venkata Siva, and P. S. Rama Sreekanth. "5.15 Cement-Based Composites". In: *Comprehensive Composite Materials II* (Jan. 2018), pp. 379–420. DOI: 10.1016/B978-0-12-803581-8.03903-5.

[64] Olivier Lamaignere. *What is cement hydration? - Maturix - concrete monitoring*. Mar. 2021. URL: https://maturix.com/knowledge-center/what-is-cement-hydration/.

[65] Olivier Lamaignere. *What is cement hydration? - Maturix - concrete monitoring*. Mar. 2021. URL: https://maturix.com/knowledge-center/what-is-cement-hydration/.

[66] Jennifer A Lewis. *Concrete: Scientific Principles*. URL: http://matse1.matse.illinois.edu/concrete/prin.html.

[67] "Guide to Curing". In: *Dayton Superior* (Nov. 2008). URL: www.daytonsuperior.com.

[68] Mishra G. *Curing of Cement Concrete - Time and Duration - The Constructor*. URL: https://theconstructor.org/concrete/concrete-curing-time-duration/11119/.

[69] *Humidity, Evaporation, and Boiling | Physics*. URL: https://courses.lumenlearning.com/suny-physics/chapter/13-6-humidity-evaporation-and-boiling/.

[70] Branz N.l. "Is that concrete floor dry yet? " In: *Build Magazine* (Feb. 2006).

[71] Wilson A. *How to Remove Mould from Carpet | ProLux Cleaning Blog*. Jan. 2023. URL: https://www.proluxcleaning.co.uk/how-to-remove-mould-from-carpet.

[72] Nesbitt A. *Is your wooden floor lifting? Here's why | DiscountFlooringDepot.co.ukDiscount Flooring Depot Blog*. Oct. 2016. URL: https://www.discountflooringdepot.co.uk/blog/2016/10/wooden-floor-lifting-heres/.

[73] *Laminate Floor Water Damage - Morris County, NJ*. Mar. 2023. URL: https://www.servicemasterrestore.com/servicemaster-restoration-by-timeless/why-us/blog/2023/march/signs-of-laminate-floor-water-damage-in-morris-county-nj/.

[74] *The Efflorescence of Concrete: Dangers and Solutions - B-Protek*. July 2021. URL: https://www.bprotek.com/the-efflorescence-of-concrete-dangers-and-solutions/.

[75] Peter Brander. *Verktyg för optimering av byggtorkning*. Lund, 2009.

[76] *Altiflex | Interimaflukninger*. URL: https://www.altiflex.dk/sv/interimaflukninger.

[77] Polygon Group. *Nyhetsbrev september 2016 - Polygon Group*. Sept. 2016. URL: https://www.polygongroup.com/sv-SE/Nyheter/nyhetsbrev-september-2016/.

[78] ACI Committee 207., Stephen Brent. Tatro, and American Concrete Institute. "Report on thermal and volume change effects on cracking of mass concrete". In: (2007), p. 28.

[79] Rådet för byggkompetens. *Fuktmätningsmanual - Betong & Golvavjämning*. Feb. 2023. URL: https://www.rbk.nu/ladda-ned/fuktmatningsmanual__36.

[80] Raksystems. *Så går en RBK fuktmätning i betong till - Raksystems Sverige*. Oct. 2021. URL: https://raksystems.se/sa-gar-en-rbk-fuktmatning-i-betong-till/.

[81] Chemicalen. "13 Different Types of Dryers in the Chemical Industry". In: (2022). [accessed: 26-02-2024]. URL: https://chemicalen.com/types-of-dryers-in-chemical-industry/.

[82] El-Björn. *Commercial Heating Fans - TF 30HW EBS*. URL: https://www.elbjorn.co.uk/product/tf-30hw-ebs-heaters/.

[83] El-Björn. *AD 450E 230V - Kondensavfuktare*. URL: https://www.elbjorn.com/sv-se/klimat/byggavfuktare/eb14562/.

[84] IEA. *The Future of Heat Pumps*. Paris: International Energy Agency, 2022. URL: https://www.iea.org/reports/the-future-of-heat-pumps/how-a-heat-pump-works.

[85] DryFiciency. "Closed loop". In: (c2021). [accessed: 29-02-2024]. URL: https://dryficiency.eu/industrial-heat-pumps/closed-loop/.

[86] DryFiciency. "Open loop". In: (c2021). [accessed: 29-02-2024]. URL: https://dryficiency.eu/industrial-heat-pumps/open-loop/.

[87] Mohamed A. "Modelling the performance of horizontal heat exchanger of ground-coupled heat pump systems with Egyptian conditions". PhD thesis. Feb. 2013. DOI: 10.13140/RG.2.1.3230.7688.

[88] Benjamin Zühlsdorf, Jonas Kjær Jensen, and Brian Elmegaard. "Heat pump working fluid selection—economic and thermodynamic comparison of criteria and boundary conditions". In: *International Journal of Refrigeration* 98 (Feb. 2019), pp. 500–513. ISSN: 0140-7007. DOI: 10.1016/J.IJREFRIG.2018.11.034.

[89] Rosenberg J. R. and Sotsil Silva-Sotelo. "Energy Evaluation of the Use of an Absorption Heat Pump in Water Distillation Process". In: *Distillation - Innovative Applications and Modeling* (June 2017). DOI: 10.5772/67094. URL: https://www.researchgate.net/publication/318073790_Energy_Evaluation_of_the_Use_of_an_Absorption_Heat_Pump_in_Water_Distillation_Process.

[90] Kim G. et al. "Performance analysis of type 1 and type 2 hybrid absorption heat pump using novel working pairs". In: *Energy* 241 (Feb. 2022), p. 122872. ISSN: 0360-5442. DOI: 10.1016/J.ENERGY.2021.122872.

[91] Qing C., Gao P., and Zhang C. L. "Thermodynamic analysis on feasible operating region of two-stage hybrid absorption-compression heat pump cycles". In: *International Journal of Refrigeration* 121 (Jan. 2021), pp. 43–50. ISSN: 0140-7007. DOI: 10.1016/J.IJREFRIG.2020.09.017.

[92] Ahrens M. U., Hafner A., and Eikevik T. M. "Development of ammonia-water hybrid absorption-compression heat pumps." In: *Proceedings of the 25th IIR International Congress of Refrigeration: Montréal , Canada, August 24-30, 2019*. 2019-August (2019), pp. 4942–4949. ISSN: 01511637. DOI: 10.18462/IIR.ICR.2019.1869. URL: https://iifiir.org/fr/fridoc/developpement-de-pompes-a-chaleur-hybrides-a-absorption-compression-35141.

[93] Makhnatch P. and Khodabandeh R. "The Role of Environmental Metrics (GWP, TEWI, LCCP) in the Selection Of Low GWP Refrigerant". In: *Energy Procedia* 61 (Jan. 2014), pp. 2460–2463. ISSN: 1876-6102. DOI: 10.1016/J.EGYPRO.2014.12.023.

[94] DCCEEW. *Ozone depleting substances*. [accessed: 30-04-2024]. Canberra, 2021. URL: https://www.dcceew.gov.au/environment/protection/ozone/ozone-science/ozone-depleting-substances.

[95] American Society of Mechanical Engineers. "Perkins Vapor-Compression Cycle for Refrigeration A HISTORIC MECHANICAL ENGINEERING LANDMARK The Vapor Compression Cycle for Mechanical Cooling". In: (2020). URL: http://www.scienceve.com/10-greatest-inventions-changed-.

[96] Elkins J. W. "Chlorofluorocarbons (CFCs)". In: *The Chapman & Hall Encyclopedia of Environmental Science* (1999). URL: https://gml.noaa.gov/hats/publictn/elkins/cfcs.html.

[97] Hossaini R. et al. "The increasing threat to stratospheric ozone from dichloromethane". In: *Nature Communications* 8 (June 2017). ISSN: 20411723. DOI: 10.1038/NCOMMS15962. URL: /pmc/articles/PMC5490265/%20/pmc/articles/PMC5490265/?report=abstract%20https://www.ncbi.nlm.nih.gov/pmc/articles/PMC5490265/.

[98] UNEP. "About Montreal Protocol". In: (n.d.). [accessed: 09-02-2024]. URL: https://www.unep.org/ozonaction/who-we-are/about-montreal-protocol.

[99] Council of the European Union European Parliament. *REGULATION (EU) No 517/2014 OF THE EUROPEAN PARLIAMENT AND OF THE COUNCIL*. 2014. URL: https://eur-lex.europa.eu/legal-content/EN/TXT/?uri=celex%3A32014R0517.

[100] European Parliament Council of the European Union. *EUROPAPARLAMENTETS OCH RÅDETS FÖRORDNING (EU) 2024/573*. Strasbourg, 2024. URL: https://eur-lex.europa.eu/legal-content/SV/TXT/HTML/?uri=OJ:L_202400573.

[101] Nair V. "HFO refrigerants: A review of present status and future prospects." In: *International Journal of Refrigeration* 122 (Feb. 2021). [accessed: 09-02-2024], pp. 156–170. ISSN: 0140-7007. DOI: 10.1016/J.IJREFRIG.2020.10.039.

[102] NaturalRefrigerants.com. *European Chemical Agency Publishes Proposal to Restrict PFAS Chemicals, Including Some F-Gases and TFA*. 2023. URL: https://r744.com/european-chemical-agency-publishes-proposal-to-restrict-pfas-chemicals-including-some-f-gases-and-tfa/.

[103] Varmt & Kallt. *PFAS förbud publicerad*. [accessed: 26-04-2024]. URL: https://varmtochkallt.se/nyhet/pfas-forbud-publicerad/.

[104] Varmt & Kallt. *Köldmedier*. [accessed: 26-04-2024]. URL: https://varmtochkallt.se/koldmedier/.

[105] ASHRAE and UNEP. *Update on New Refrigerants Designations and Safety Classifications*. [accessed: 14-03-2024]. URL: https://wedocs.unep.org/bitstream/handle/20.500.11822/29025/NEWRefr.pdf?sequence=1&isAllowed=y.

[106] Benjamin Zühlsdorf, Jonas Kjær Jensen, and Brian Elmegaard. "Heat pump working fluid selection–economic and thermodynamic comparison of criteria and boundary conditions". In: *International Journal of Refrigeration* 98 (Feb. 2019), pp. 500–513. ISSN: 0140-7007. DOI: 10.1016/J.IJREFRIG.2018.11.034.

[107] Carel Industries S.p.A. *Natural refrigerants from a theoretical point of view*. [accessed: 08-03-2024]. Padova, n.d. URL: https://natref.carel.com/what-are-natural-refrigerants.

[108] Wu D. et al. "The performance comparison of high temperature heat pump among R718 and other refrigerants". In: *Renewable Energy* 154 (July 2020), pp. 715–722. ISSN: 0960-1481. DOI: 10.1016/J.RENENE.2020.03.034.

[109] de la Calle-Arroyo C., López-Fidalgo J., and Rodríguez-Aragón L. J. "Optimal designs for Antoine Equation". In: *Chemometrics and Intelligent Laboratory Systems* 214 (July 2021), p. 104334. ISSN: 0169-7439. DOI: 10.1016/J.CHEMOLAB.2021.104334.

[110] Dimian A. C., Bildea C S., and Kiss A. A. "Pinch Point Analysis". In: *Computer Aided Chemical Engineering* 35 (Jan. 2014), pp. 525–564. ISSN: 1570-7946. DOI: 10.1016/B978-0-444-62700-1.00013-9.

[111] Kemp I. C. "Key concepts of pinch analysis". In: *Pinch Analysis and Process Integration*. Butterworth-Heinemann, Jan. 2007. Chap. 2, pp. 15–40. ISBN: 978-0-7506-8260-2. DOI: 10.1016/B978-075068260-2.50007-9.

[112] Linnhoff March. *Introduction to Pinch Technology*. 1998. URL: www.linnhoffmarch.com.

[113] Delahunt J. *What Are Superheat and Subcooling? - Understand Your HVAC*. [accessed: 23-04-2024]. 2021. URL: https://www.buildingengines.com/blog/knowledge-superheat-and-subcooling/.

[114] Ardita I. N., Wirajati I. G.A.B., and Sudirman. "The effect of changing superheat degrees on energy consumption in a split air conditioning". In: *Journal of Physics: Conference Series* 1450 (1 Mar. 2020). ISSN: 17426596. DOI: 10.1088/1742-6596/1450/1/012091. URL: https://www.researchgate.net/publication/339907325_The_effect_of_changing_superheat_degrees_on_energy_consumption_in_a_split_air_conditioning.

[115] Amperayani H. K. *Internal Heat Exchanger Application in Heat Pumps Evaluation and testing of different internal heat exchangers for efficiency improvement Master's thesis in Sustainable Energy Systems*. [accessed: 23-04-2024]. 2021. URL: https://odr.chalmers.se/server/api/core/bitstreams/8cc78245-6e32-4633-b3fc-94e04bd4ba01/content.

[116] Atlas Copco UAE. *Comparing Air Compressor Intercooler and Aftercooler*. [accessed: 23-04-2024]. URL: https://www.atlascopco.com/en-ae/compressors/air-compressor-blog/air-compressor-intercooler-and-aftercooler.

[117] Arpagaus C. et al. "Multi-Temperature Heat Pumps - A Literature Review". In: *International Refrigeration and Air Conditioning Conference* (). URL: http://docs.lib.purdue.edu/iracc/1569.

[118] Tarrad A. "Thermodynamic Evaluation for Intermediate Temperature Optimization in Low Temperature Heat Source Cascade Heat Pump Technology". In: *Asian Journal of Engineering and Technology* (2017).

[119] Scrivener G. *Compressors and compression ratios*. [accessed: 17-04-2024]. Plumbing & HVAC. URL: https://plumbingandhvac.ca/compressors-and-compression-ratios/.

[120] Stewart M. “Reciprocating compressors”. In: *Surface Production Operations* (Jan. 2019), pp. 655–778. DOI: 10.1016/B978-0-12-809895-0.00009-0. URL: https://linkinghub.elsevier.com/retrieve/pii/B9780128098950000090.

[121] Adamson K. M. et al. “High-temperature and transcritical heat pump cycles and advancements: A review”. In: *Renewable and Sustainable Energy Reviews* 167 (Oct. 2022), p. 112798. ISSN: 1364-0321. DOI: 10.1016/J.RSER.2022.112798.

[122] Tavangar A. *Mathematics of Finance*. eCampus Ontario, 2024.

[123] Kiran D.R. “Machinery replacement analysis”. In: *Principles of Economics and Management for Manufacturing Engineering* (Jan. 2022), pp. 259–267. DOI: 10.1016/B978-0-323-99862-8.00002-9.

[124] Gallo Amy. *A Refresher on Payback Method*. 2016. URL: https://hbr.org/2016/04/a-refresher-on-payback-method.

[125] Wang Y. and He W. “Temporospatial techno-economic analysis of heat pumps for decarbonising heating in Great Britain”. In: *Energy and Buildings* 250 (Nov. 2021), p. 111198. ISSN: 0378-7788. DOI: 10.1016/J.ENBUILD.2021.111198.

[126] Witte F. *fwitte/fluprodia: fluprodia version 3.0*. Version v3.0. Apr. 2024. DOI: 10.5281/zenodo.11075008. URL: https://doi.org/10.5281/zenodo.11075008.

[127] Bell I. et al. “Pure and Pseudo-pure Fluid Thermophysical Property Evaluation and the Open-Source Thermophysical Property Library CoolProp”. In: *Industrial & Engineering Chemistry Research* 53.6 (2014), pp. 2498–2508.

[128] E. W. Lemmon et al. *NIST Standard Reference Database 23: Reference Fluid Thermodynamic and Transport Properties-REFPROP, Version 10.0, National Institute of Standards and Technology*. 2018. DOI: https://doi.org/10.18434/T4/1502528. URL: https://www.nist.gov/srd/refprop.

[129] Marina A. et al. “An estimation of the European industrial heat pump market potential”. In: *Renewable and Sustainable Energy Reviews* 139 (Apr. 2021), p. 110545. ISSN: 1364-0321. DOI: 10.1016/J.RSER.2020.110545.

[130] Climate-Data.org. *KLIMAT GÖTEBORG (SVERIGE)*. 2022. URL: https://sv.climate-data.org/europa/sverige/vaestra-goetalands-laen/goeteborg-197/.

[131] El-Björn AB. *Mobil värmepump HeatBox Hydro 90 kW*. [accessed: 10-05-2024]. c2024. URL: https://www.elbjorn.com/sv-se/klimat/mobil-varmepump/eb16000-mobil-varmepump/.

[132] Entalpy AS. *Miljøvennlig byggvarme - Energisparende varmepumpe*. [accessed: 10-05-2024]. c2024. URL: https://entalpy.no/produkter#modeller.

[133] Nord Pool. *Day-ahead prices*. [accessed: 18-04-2024]. URL: https://data.nordpoolgroup.com/auction/day-ahead/prices?deliveryDate=2023-03-13%C2%A4cy=SEK&aggregation=Monthly&deliveryAreas=SE3.

[134] Göteborg Energi. *Fjärrvärmepriser företag*. [accessed: 18-04-2024]. URL: https://www.goteborgenergi.se/foretag/fjarrvarme/fjarrvarmepriser.

[135] SCB. *Priser på naturgas för icke-hushåll. Halvår 2014H2 - 2023H2*. [accessed: 18-04-2024]. Stockholm: Statistiska centralbyrån. URL: https://www.statis

tikdatabasen.scb.se/pxweb/sv/ssd/START__EN__EN0302/SSDHalvarGasIckehus/.

[136] Torstensson S. *Dieselskatt*. [accessed: 14-05-2024]. URL: https://www.ekonomifakta.se/sakomraden/elfakta/styrmedel/dieselskatt_1208801.html.

[137] Webster I. *€100 in 2018 → 2024 | Euro Inflation Calculator*. [accessed: 18-04-2024]. URL: https://www.in2013dollars.com/europe/inflation/2018?amount=100.

[138] Webster I. *€100 in 2014 → 2024 | Euro Inflation Calculator*. [accessed: 01-05-2024]. URL: https://www.in2013dollars.com/europe/inflation/2014?amount=100.

[139] Holmberg P. and Tangerås T. P. *The Swedish electricity market – today and in the future*. Sveriges Riksbank, 2023. URL: https://www.riksbank.se/globalassets/media/rapporter/pov/artiklar/engelska/2023/230512/2023_1-the-swedish-electricity-market--today-and-in-the-future.pdf.

[140] Pieper H. et al. "Allocation of investment costs for large-scale heat pumps supplying district heating". In: *Energy Procedia* 147 (Aug. 2018), pp. 358–367. ISSN: 1876-6102. DOI: 10.1016/J.EGYPRO.2018.07.104.

[141] S. Wolf et al. *Analyse des Potenzials von Industriewärmepumpen in Deutschland : Forschungsbericht : Endbericht*. Tech. rep. Stuttgart: Universität Stuttgart, Institut für Energiewirtschaft und Rationelle Energieanwendung, Dec. 2014.

[142] IEA. *Levelised cost of heating for air-to-air and air-to-water heat pumps and gas boilers for selected countries, and sensitivity to fuel prices, H1 2021 - H1 2022*. Paris: International Energy Agency, 2022. URL: https://www.iea.org/data-and-statistics/charts/levelised-cost-of-heating-for-air-to-air-and-air-to-water-heat-pumps-and-gas-boilers-for-selected-countries-and-sensitivity-to-fuel-prices-h1-2021-h1-2022.

# A

# Appendix A

## A.1 Approximation of district heating price

In this appendix, the approximation of the specific cost of district heating is presented using Göteborg Energi's price model [134]

The first part, energy, was estimated using the sludge dryer's annual energy requirement, $E_{annual}$, calculated using Eq. A.1.

$$E_{annual} = Dryer_{energy-demand} \cdot h \qquad [MWh] \tag{A.1}$$

Here, $\text{Dryer}_{\text{energy-demand}}$ represents the dryer's energy demand calculated with Eq. 3.17 in section 3.3.5.1, and $h$ denotes the operating hours.

The energy component, $EC$, of the DH price was determined using Eq. A.2.

$$EC = E_{annual} \cdot C_{energy} \qquad [SEK] \tag{A.2}$$

In this equation, $C_{\text{energy}}$ is the annual average of the monthly prices found on Göteborg Energi's website [134].

The power component, $PC$, consisting of both a fixed and variable part, was determined using Eq. A.3.

$$PC = C_{power,fixed} + C_{power,variable} \cdot E_{annual} \qquad [SEK] \tag{A.3}$$

Here, $C_{\text{power,fixed}}$ represents the fixed annual price determined using a three-day average of energy consumed, and $C_{\text{power,variable}}$ is the variable price multiplied by the total energy consumption, since the dryer is assumed to have a constant load throughout its operating time.

The third and final component of the DH price, efficiency–related cost, can either be positive or negative depending on the return temperature [134]. If the return temperature from the dryer system is higher than the district heating system's

average return temperature, it is associated with a cost. The cost of the efficiency component, $EfC$, was determined using Equation A.4.

$$EfC = C_{efficiency} \cdot \Delta T_{return} \qquad [SEK] \tag{A.4}$$

In this equation, $C_{\text{efficiency}}$ represents the cost/saving of having a higher/lower return temperature than the district heating system's average return temperature, and $\Delta T_{\text{return}}$ is the temperature difference between the two mentioned return temperatures.

The total price of DH is the sum of the three components, $EC$, $PC$, and $EfC$. To get an average specific cost, the total annual price was divided by the total energy consumption of the dryer, using Eq. A.5.

$$C_{DH} = \frac{EC + PC + EfC}{Dryer_{energy-demand} \cdot h} \cdot Conv \qquad [\frac{€}{MWh}] \tag{A.5}$$

In this equation, $Conv$, is the conversion rate from SEK to €.

For the estimation of the specific price of DH data and assumptions are presented in Table A.1.

**Table A.1:** Data used for cost estimation of district heating.

| DH price component | Value | Unit |
|---|---|---|
| SWW case - consumption > 2500 kW | | |
| $C_{\text{power,fixed}}$ | 252760[a] | SEK/year |
| $C_{\text{power,variable}}$ | 822[a] | SEK/kW,year |
| $\Delta T_{\text{return}}$ | 48-37 | °C |
| CAA/CAW case - consumption < 100 kW | | |
| $C_{\text{power,fixed}}$ | 10360[a] | SEK/year |
| $C_{\text{power,variable}}$ | 1089[a] | SEK/kW,year |
| $\Delta T_{\text{return}}$ | 40-37 | °C |
| Shared assumptions: | | |
| $C_{\text{energy}}$ | 325[b] | SEK/MWh |
| $C_{\text{efficiency}}$ | 7[a] | SEK/MWh,°C |
| $Conv$ | 11.6216[c] | SEK/€ |

[a] Value from Göteborg Energi in 2024 [134].
[b] Value derived from Göteborg Energi in 2024 [134].
[c] Conversion rate on 18th of April 2024 09:43 (GMT+2).

The $C_{energy}$ was calculated as an annual average based on each monthly cost. Additionally, the two $\Delta T_{\text{return}}$ expressions being the difference between heat source outlet temperature and an average DH return temperature (37°C)[134].

# B

# Appendix B

## B.1 Python script code

In this appendix, the code used to generate the T-s diagrams and perform the pinch point analysis is presented:

```
locals().clear()
from fluprodia import FluidPropertyDiagram
import numpy as np
import matplotlib.pyplot as plt
import CoolProp.CoolProp as CP

################################
# Input data in Celsius and Bar
################################

Ref = "R717"  # Refrigerant name

P_evap=3.83
T_evap=-3.01
T_evapSS=T_evap+5

P_cond=20.35
T_cond=142.61

T_throttle=45.04
Q_throttle=0

isentropic_efficiency=0.875

# Pinch analysis lines - CONDENSER
# Given points
T1cond = 40  # in Celsius
T2cond = 45  # in Celsius
deltaTmincond = 5

# Pinch analysis lines - EVAPORATOR
# Given points
T1evap = 2  # in Celsius
T2evap = 7  # in Celsius
```

```
deltaTmin_evap = deltaTmincond


###################################
# Refrigerant properties/parameters
###################################

# Create a FluidPropertyDiagram object for Ref
diagram = FluidPropertyDiagram(Ref)
diagram.set_unit_system(T="C", p="bar", s="kJ/kgK")

# Define the temperature range for isolines
iso_T = np.arange(-75, 151, 25)
diagram.set_isolines(T=iso_T)
diagram.calc_isolines()

# Create a figure and axis for the plot
fig, ax = plt.subplots(1, figsize=(16, 10))

# Plot isolines
mydata = {
    "T": {"style": {"color": "g"}, "values": iso_T, "label_position
    ": 0.8},
    "v": {"values": np.array([])},
}
# R290 - Propane
# diagram.draw_isolines(fig, ax, 'Ts', isoline_data=mydata, x_min
    =1, x_max=2.6, y_min=-10, y_max=150)
# R717 - Ammonia
diagram.draw_isolines(fig, ax, "Ts", isoline_data=mydata, x_min=1,
    x_max=7, y_min=-20, y_max=200)
# R744 - CO2
# diagram.draw_isolines(fig, ax, 'Ts', isoline_data=mydata, x_min
    =0.8, x_max=2.25, y_min=-10, y_max=150)
# R1270 - Propylene
# diagram.draw_isolines(fig, ax, 'Ts', isoline_data=mydata, x_min
    =0.75, x_max=3, y_min=0, y_max=140)
# R600a - Isobutane
# diagram.draw_isolines(fig, ax, 'Ts', isoline_data=mydata, x_min
    =1, x_max=3, y_min=-1, y_max=200)
# RE170 - DME
# diagram.draw_isolines(fig, ax, 'Ts', isoline_data=mydata, x_min
    =0, x_max=2.2, y_min=-10, y_max=140)

###############
# EVAPORATOR
###############

#########################################################################
# Code used to determine the initial entropy of the evaporator,
    s_evap

# Calculate enthalpy [kJ/kg] using CoolProp for saturated liquid
    state (quality = 0)
h_throttle = CP.PropsSI('H', 'T', T_throttle + 273.15, 'P', P_cond
    * 1e5, Ref) / 1000
```

```
# Calculate the entropy [kJ/kg*K] using CoolProp for the given
    enthalpy and pressure
s_evap = CP.PropsSI('S', 'P', P_evap * 1e5, 'H', h_throttle * 1000,
     Ref) / 1000

######################################################################

# Define data for the evaporator isolines using the updated
    Initial_s
dataEVAP = {
    'isoline_property': 'p',
    'isoline_value': P_evap,
    'starting_point_property': 's',
    'starting_point_value': s_evap,
    'ending_point_property': 'T',
    'ending_point_value': T_evapSS
}

# Calculate datapoints for the evaporator isoline
datapointsEVAP = diagram.calc_individual_isoline(**dataEVAP)

# Plot the evaporator isoline and mark the endpoints with numbers
_ = ax.plot(datapointsEVAP['s'], datapointsEVAP['T'], color='g')
_ = ax.plot(datapointsEVAP['s'][0], datapointsEVAP['T'][0], 'bo',
    markersize=5)
_ = ax.plot(datapointsEVAP['s'][-1], datapointsEVAP['T'][-1], 'bo',
     markersize=5)
ax.text(datapointsEVAP['s'][0], datapointsEVAP['T'][0], 'EVAPORATOR
     Start', fontsize=12, ha='right', va='bottom')
ax.text(datapointsEVAP['s'][-1], datapointsEVAP['T'][-1], '
    COMPRESSOR Start', fontsize=12, ha='right', va='bottom')


###############
# COMPRESSOR
###############

# Define the entropy values for the compressor

# Entropy superheated evaporator
# Calculate entropy using CoolProp for superheated vapor
s_evapSS = CP.PropsSI('S', 'T', T_evapSS + 273.15, 'P', P_evap * 1
    e5, Ref) / 1000   # s1

# Enthalpy superheated evaporator
h_evapSS = CP.PropsSI('H', 'T', T_evapSS + 273.15, 'P', P_evap * 1
    e5, Ref)

# Ideal enthalpy condenser inlet
h_cond_s = CP.PropsSI('H', 'T', T_cond + 273.15, 'P', P_cond * 1e5,
     Ref)

# Real enthalpy condenser inlet
h_cond = h_cond_s - isentropic_efficiency * (h_cond_s - h_evapSS)
```

```
# Entropy condenser inlet
s_cond = CP.PropsSI('S', 'T', T_cond + 273.15, 'P', P_cond * 1e5,
    Ref) / 1000 #s2

# Calculate the slope of the line (change in entropy / change in
    temperature) for compressor line
slope = (s_cond - s_evapSS) / ((T_cond + 273.15) - (T_evapSS+
    273.15))

# Generate temperature values between T_evapSS and T_cond
temperature_values = np.linspace(T_evapSS + 273.15, T_cond +
    273.15, 100)

# Calculate corresponding entropy values using the slope calculated
    earlier
entropy_values = s_evapSS + slope * (temperature_values - (T_evapSS
    + 273.15))

# Plot the line connecting the points for the compressor
ax.plot(entropy_values, temperature_values - 273.15, linestyle='-',
    color='g', label='Line T1 to T2')

###############
# CONDENSER
###############

s_throttle = CP.PropsSI('S', 'T', T_throttle + 273.15, 'P', P_cond
    * 1e5, Ref) / 1000   # s1

# Define data for the condenser isolines
dataCOND = {
    'isoline_property': 'p',
    'isoline_value': P_cond,
    'starting_point_property': 's',
    'starting_point_value': s_cond,
    'ending_point_property': 's',
    'ending_point_value': s_throttle
}

# Calculate datapoints for the condenser isoline
datapointsCOND = diagram.calc_individual_isoline(**dataCOND)

# Plot the condenser isoline and mark the endpoints with numbers
_ = ax.plot(datapointsCOND['s'], datapointsCOND['T'], color='g')
_ = ax.plot(datapointsCOND['s'][0], datapointsCOND['T'][0], 'bo',
    markersize=5)
_ = ax.plot(datapointsCOND['s'][-1], datapointsCOND['T'][-1], 'bo',
    markersize=5)
ax.text(datapointsCOND['s'][0], datapointsCOND['T'][0], 'CONDENSER
    Start', fontsize=12, ha='right', va='bottom')


###############
# THROTTLE
###############
```

```
# Define data for the throttle isolines
dataTHROTTLE = {
    'isoline_property': 'h',
    'isoline_value': h_throttle * 1000,
    'starting_point_property': 'p',
    'starting_point_value': P_cond,
    'ending_point_property': 'p',
    'ending_point_value': P_evap
}

# Calculate datapoints for the throttle isoline
datapointsTHROTTLE = diagram.calc_individual_isoline(**dataTHROTTLE
    )

# Plot the throttle isoline and mark the endpoints with numbers
_ = ax.plot(datapointsTHROTTLE['s'], datapointsTHROTTLE['T'], color
    ='g')
_ = ax.plot(datapointsTHROTTLE['s'][0], datapointsTHROTTLE['T'][0],
    'bo', markersize=5)
_ = ax.plot(datapointsTHROTTLE['s'][-1], datapointsTHROTTLE['T'
    ][-1], 'bo', markersize=5)
ax.text(datapointsTHROTTLE['s'][0], datapointsTHROTTLE['T'][0], '
    THROTTLE Start', fontsize=12, ha='right', va='bottom')

# s_throttle = CP.PropsSI('S', 'T', T_throttle + 273.15, 'P',
    P_cond * 1e5, 'Ammonia') / 1000   # s1

# Adjust layout and save the figure
plt.tight_layout()



######################################################################
# Pinch analysis lines - CONDENSER
######################################################################



S1cond = s_throttle   # in kJ/kgK
S2cond = s_cond # in kJ/kgK
T_pinchcond = CP.PropsSI('T', 'S', s_throttle * 1000, 'P', P_cond *
    1e5, Ref) -273.15
s_pinchcond = CP.PropsSI('S', 'T', T_pinchcond + 273.15 + 0.5, 'P',
    P_cond * 1e5, Ref) / 1000  # FEL HÄĐR

# Calculate the entropy and temperature changes
delta_Scond = S2cond - S1cond
delta_Tcond = T2cond - T1cond

# Generate temperature values between T1cond and T2cond
temperature_values_cond = np.linspace(T1cond + 273.15, T2cond +
    273.15, 100)

# Calculate corresponding entropy values using the change in
    entropy and temperature
entropy_values_cond = S1cond + (delta_Scond / delta_Tcond) * (
```

```
    temperature_values_cond - (T1cond + 273.15))

# Plot the blue line connecting the points T1 and T2 for the
    condenser
condenser_line, = ax.plot(
    entropy_values_cond,
    temperature_values_cond - 273.15,
    linestyle="-",
    color="b",
    label="Condenser - Sink water",  # Label for the condenser line
)


# Initialize an array to store the temperature differences
temperature_differences = []

# Loop over each value in entropy_values_cond
for s_cond_value in entropy_values_cond:
    # Find the corresponding temperature value on the blue line
    idx_closest_to_s_cond = np.argmin(np.abs(entropy_values_cond -
    s_cond_value))
    T_blue_line = temperature_values_cond[idx_closest_to_s_cond]

    # Calculate the temperature value on the condenser line
    idx_closest_to_s_condenser = np.argmin(np.abs(datapointsCOND['s
    '] - s_cond_value))
    T_condenser_line = datapointsCOND['T'][
    idx_closest_to_s_condenser]

    # Calculate the temperature difference between the lines
    temperature_difference = T_condenser_line - T_blue_line

    # Append the temperature difference to the array
    temperature_differences.append(temperature_difference)

# Find the minimum temperature difference and its corresponding
    index
min_temperature_difference = min(temperature_differences)
idx_min_temperature_difference = temperature_differences.index(
    min_temperature_difference)



# Get the corresponding entropy and temperature values where the
    minimum difference occurs
s_min_temperature_difference = entropy_values_cond[
    idx_min_temperature_difference]
T_min_temperature_difference = temperature_values_cond[
    idx_min_temperature_difference]

# Plot the minimum temperature difference point
ax.plot(s_min_temperature_difference, T_min_temperature_difference
    - 273.15, marker='o', color='black', markersize=10)

# Annotate the point
ax.annotate(f'Min Temp Difference', xy=(
```

```
    s_min_temperature_difference, T_min_temperature_difference -
    273.15), xytext=(-20, 10), textcoords='offset points', fontsize
    =12, color='black')


# Get the index of the closest entropy value on the condenser line
    to s_min_temperature_difference
idx_closest_to_s_min_temperature_difference = np.argmin(np.abs(
    datapointsCOND['s'] - s_min_temperature_difference))

# Get the corresponding temperature value on the condenser line
T_condenser_line_at_min_temperature_difference = datapointsCOND['T'
    ][idx_closest_to_s_min_temperature_difference]

# Plot the line from (s_min_temperature_difference,
    T_min_temperature_difference) to (s_min_temperature_difference,
    T_condenser_line_at_min_temperature_difference)
ax.plot([s_min_temperature_difference, s_min_temperature_difference
    ],
         [T_min_temperature_difference - 273.15,
    T_condenser_line_at_min_temperature_difference],
         linestyle='--', color='black')

# Plot the minimum temperature difference point
ax.plot(s_min_temperature_difference,
    T_condenser_line_at_min_temperature_difference,
         marker='o', color='black', markersize=10)

actual_temperature_differencecond=
    T_condenser_line_at_min_temperature_difference - (
    T_min_temperature_difference - 273.15)



if actual_temperature_differencecond > deltaTmincond:
     print("Condenser pinch check ok!")
     print(f"Condenser temperature difference: {
    actual_temperature_differencecond:.2f}ÂřC")
else:
     print("Condenser pinch violation detected, adjust values!")
     print(f"Condenser temperature difference: {
    actual_temperature_differencecond:.2f}ÂřC, deltaTmin is !")


######################################################################
# Pinch analysis lines - EVAPORATOR
######################################################################


S1evap = s_evap   # in kJ/kgK
S2evap = s_evapSS # in kJ/kgK
T_pinchevap = CP.PropsSI('T', 'S', s_evap * 1000, 'P', P_evap * 1e5
    , Ref) -273.15
s_pinchevap = CP.PropsSI('S', 'T', T_pinchevap + 273.15 + 0.1, 'P',
     P_evap * 1e5, Ref) / 1000
```

```
# Calculate the entropy and temperature changes
delta_Sevap = S2evap - S1evap
delta_Tevap = T2evap - T1evap

# Generate temperature values between T1evap and T2evap
temperature_values_evap = np.linspace(T1evap + 273.15, T2evap +
    273.15, 100)

# Calculate corresponding entropy values using the change in
    entropy and temperature
entropy_values_evap = S1evap + (delta_Sevap / delta_Tevap) * (
    temperature_values_evap - (T1evap + 273.15))

# Plot the red line connecting the points T1 and T2 for the
    evaporator
evaporator_line, = ax.plot(
    entropy_values_evap,
    temperature_values_evap - 273.15,
    linestyle="-",
    color="r",
    label="Evaporator - Source air",  # Label for the evaporator
    line
)
# Initialize an array to store the temperature differences
temperature_differences = []

# Loop over each value in entropy_values_evap
for s_evap_value in entropy_values_evap:
    # Find the corresponding temperature value on the blue line
    idx_closest_to_s_evap = np.argmin(np.abs(entropy_values_evap -
    s_evap_value))
    T_blue_line = temperature_values_evap[idx_closest_to_s_evap]

    # Calculate the temperature value on the evaporator line
    idx_closest_to_s_evaporator = np.argmin(np.abs(datapointsEVAP['
    s'] - s_evap_value))
    T_evaporator_line = datapointsEVAP['T'][
    idx_closest_to_s_evaporator]

    # Calculate the temperature difference between the lines
    temperature_difference = abs(T_evaporator_line - T_blue_line)

    # Append the temperature difference to the array
    temperature_differences.append(temperature_difference)

# Find the minimum temperature difference and its corresponding
    index
min_temperature_difference = min(temperature_differences)
idx_min_temperature_difference = temperature_differences.index(
    min_temperature_difference)

# Get the corresponding entropy and temperature values where the
    minimum difference occurs
s_min_temperature_difference = entropy_values_evap[
    idx_min_temperature_difference]
T_min_temperature_difference = temperature_values_evap[
```

```
    idx_min_temperature_difference]

# Plot the minimum temperature difference point
ax.plot(s_min_temperature_difference, T_min_temperature_difference
    - 273.15, marker='o', color='black', markersize=10)

# Annotate the point
ax.annotate(f'Min Temp Difference', xy=(
    s_min_temperature_difference, T_min_temperature_difference -
    273.15), xytext=(-20, 10), textcoords='offset points', fontsize
    =12, color='black')

# Get the index of the closest entropy value on the evaporator line
     to s_min_temperature_difference
idx_closest_to_s_min_temperature_difference = np.argmin(np.abs(
    datapointsEVAP['s'] - s_min_temperature_difference))

# Get the corresponding temperature value on the evaporator line
T_evaporator_line_at_min_temperature_difference = datapointsEVAP['T
    '][idx_closest_to_s_min_temperature_difference]

# Plot the line from (s_min_temperature_difference,
    T_min_temperature_difference) to (s_min_temperature_difference,
    T_evaporator_line_at_min_temperature_difference)
ax.plot([s_min_temperature_difference, s_min_temperature_difference
    ],
         [T_min_temperature_difference - 273.15,
    T_evaporator_line_at_min_temperature_difference],
         linestyle='--', color='black')

# Plot the minimum temperature difference point
ax.plot(s_min_temperature_difference,
    T_evaporator_line_at_min_temperature_difference,
         marker='o', color='black', markersize=10)

actual_temperature_difference_evap = abs(
    T_evaporator_line_at_min_temperature_difference - (
    T_min_temperature_difference - 273.15))



if actual_temperature_difference_evap > deltaTmin_evap:
     print("Evaporator pinch check ok!")
     print(f"Evaporator temperature difference: {
    actual_temperature_difference_evap:.2f}ÂřC")
else:
     print("Evaporator pinch violation detected, adjust values!")
     print(f"Evaporator temperature difference: {
    actual_temperature_difference_evap:.2f}ÂřC, deltaTmin is !")

plt.xlabel('Entropy [kJ/kgK]')
plt.ylabel('Temperature [ÂřC]')
plt.title("Case BWA: R717 - Ammonia")

ax.legend(handles=[condenser_line, evaporator_line], loc="upper
    right")
```

```
plt.show()
```

**Listing B.1:** T-s diagram and PPA script for case SWA: R717 - Ammonia

# C

# Appendix C

## C.1 Sensitivity analysis results

In this appendix, additional results from the sensitivity analyses of all cases are presented. The results are the NPV and PBP in the three cases, where the reference utility in the sludge drying case are electricity or gas, and in the concrete drying cases diesel or electricity. The results using DH as reference utility are found in the report.

## C.2 Sludge: Water-to-water

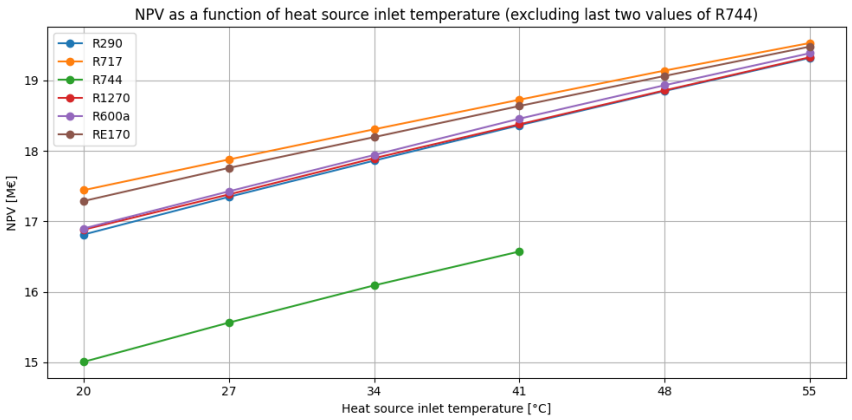


**Figure C.1:** Effect of heat source inlet temperature on NPV in the sludge drying case using a water-to-water HP, with gas as reference.

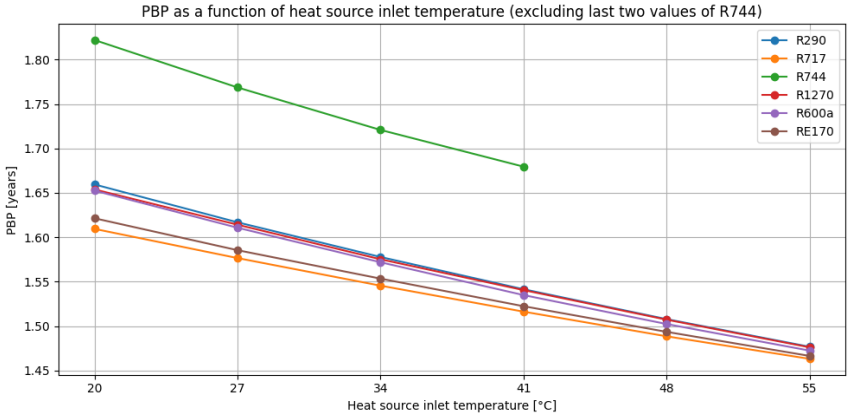


**Figure C.2:** Effect of heat source inlet temperature on the PBP in the sludge drying case using a water-to-water HP, with gas as reference.

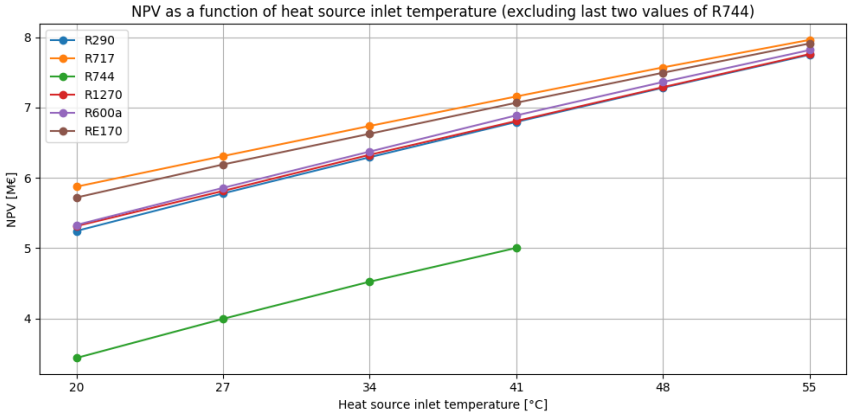


**Figure C.3:** Effect of heat source inlet temperature on the NPV in the sludge drying case using a water-to-water HP, with electricity as reference.

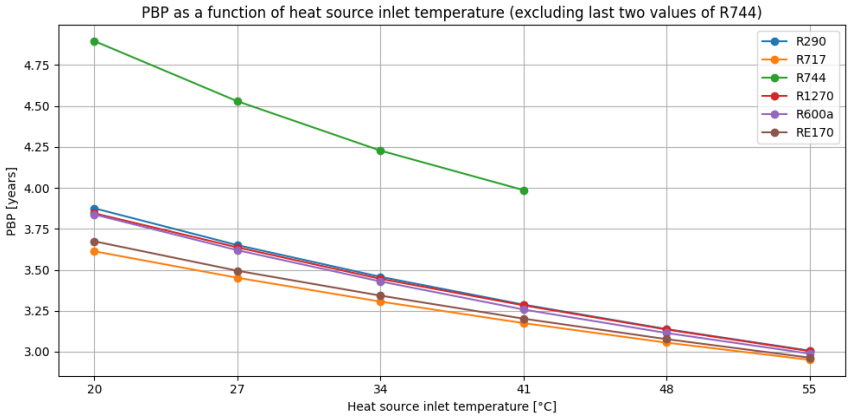


**Figure C.4:** Effect of heat source inlet temperature on the PBP in the sludge drying case using a water-to-water HP, with electricity as reference.

## C.3 Concrete: Air-to-water

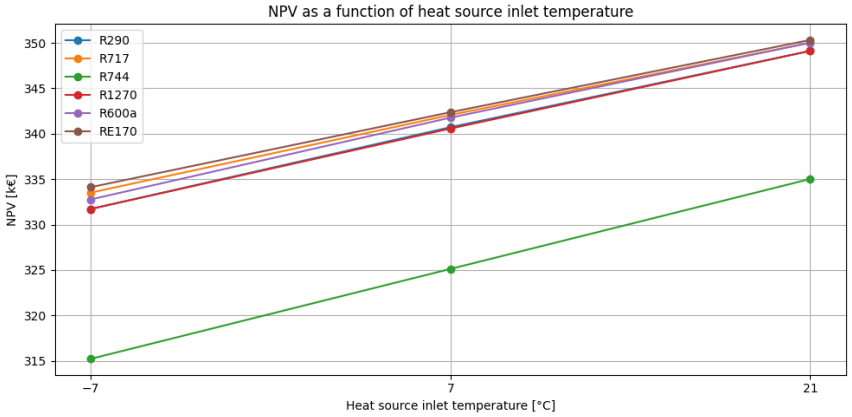


**Figure C.5:** Effect of heat source inlet temperature on the NPV in the concrete drying case using an air-to-water HP, with diesel as reference.

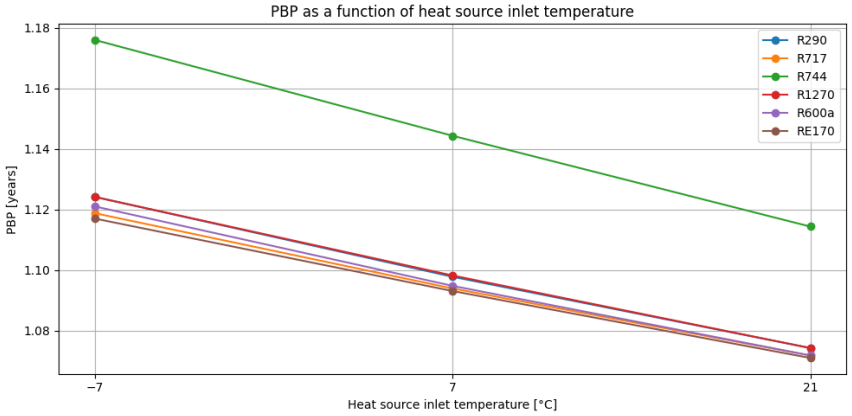


**Figure C.6:** Effect of heat source inlet temperature on the PBP in the concrete drying case using an air-to-water HP, with diesel as reference.

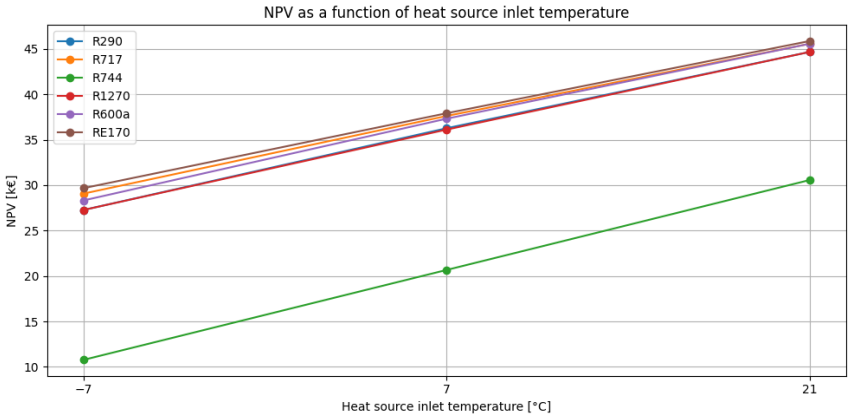


**Figure C.7:** Effect of heat source inlet temperature on the NPV in the concrete drying case using an air-to-water HP, with electricity as reference.

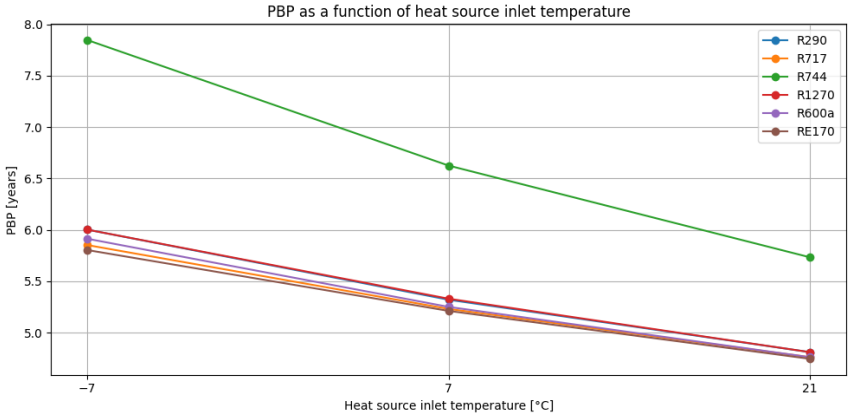


**Figure C.8:** Effect of heat source inlet temperature on the PBP in the concrete drying case using an air-to-water HP, with electricity as reference.

## C.4 Concrete: Air-to-air

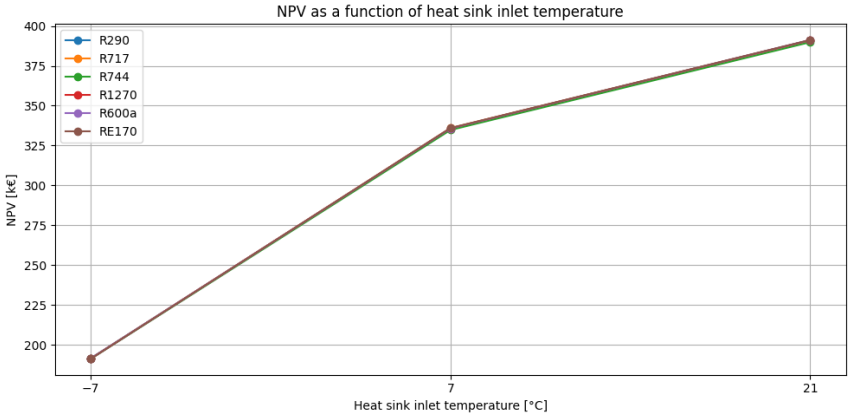


**Figure C.9:** Effect of heat source inlet temperature on the NPV in the concrete drying case using an air-to-air HP, with diesel as reference.

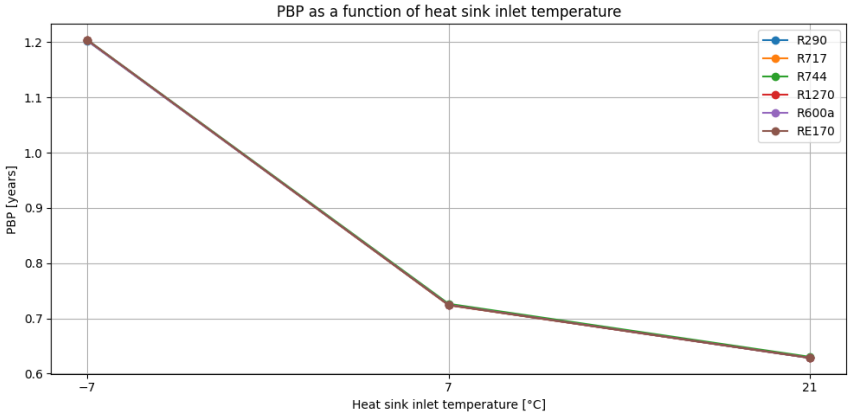


**Figure C.10:** Effect of heat source inlet temperature on the PBP in the concrete drying case using an air-to-air HP, with diesel as reference.

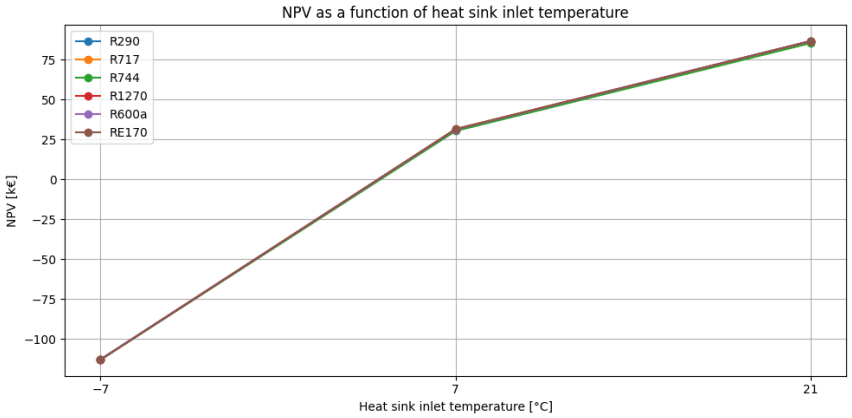


**Figure C.11:** Effect of heat source inlet temperature on the NPV in the concrete drying case using an air-to-air HP, with electricity as reference.

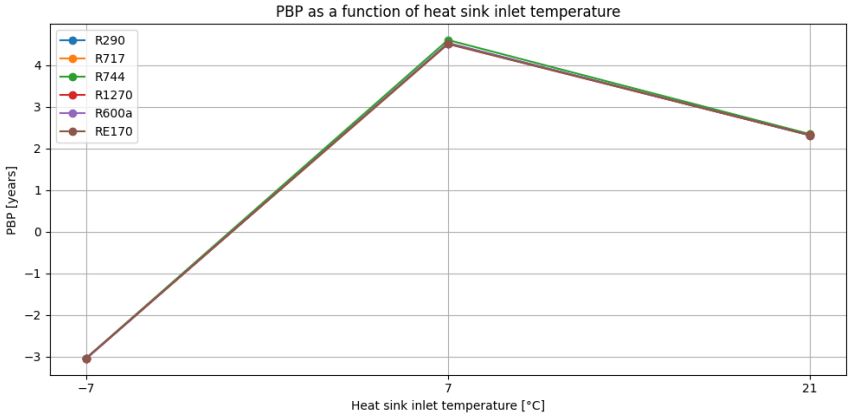


**Figure C.12:** Effect of heat source inlet temperature on the PBP in the concrete drying case using an air-to-air HP, with electricity as reference.

# D

# Appendix D

## D.1 Total capital cost estimations

In this appendix, the cost functions used to estimate the different VCHP cycles are presented. To estimate the TCI for the studied VCHP cycles in the SWW case, a cost function based on the heat source and HP capacity was used, which is valid for heat pump capacities between 0.3 and 10 MW. Thus, in the SWW case, the TCI was estimated using Eq. D.1, where the constants 0.64114 and 0.29677 are from the work of Pieper et al. [140].

$$TCI_{\mathrm{SWW}} = 0.64114 \cdot \dot{Q}_{\mathrm{SWW,sink}} + 0.29677 \quad [€] \tag{D.1}$$

For the CAW case, a different cost function had to be used due to the HP capacity being outside the valid interval of Eq. D.1. Therefore, the TCI for the CAW case was estimated using Eq. D.2, where the constants 4127.33 and 0.47 are from the work of Wolf et al. [141].

$$TCI_{\mathrm{CAW}} = 4127.33 \cdot (\dot{Q}_{\mathrm{CAW,sink}})^{0.47} \quad [€] \tag{D.2}$$

However, since the cost function in Eq. D.2 was determined for air-to-water HPs [141], it was assumed that an air-to-air HP was 1.6 times less expensive, based on data from the IEA comparing LCOH for air-to-air and air-to-water HPs, showing the CAPEX share for both air-to-air and air-to-water in Sweden [142].

$$TCI_{\mathrm{CAA}} = \frac{TCI_{\mathrm{CAW}}}{1.6} \quad [€] \tag{D.3}$$

To account for the fact that the cost function in Eq. D.1 is from 2018, an index markup of 1.2298 was applied to adjust for inflation [137]. In contrast, the index markup in the CAW case was 1.2781, as the cost function in Eq. D.2 is from 2014 [138].

# E

# Appendix E

## E.1 Mechanical vapour reheat study

Apart from the previously presented sludge drying system with an integrated VCHP cycle, a preliminary investigation of the potential of integration of a MVR was performed. The idea was to investigate if it would be possible to make use of the temperature increase in the raw biogas, resulting from compression of the raw biogas before it is transfered to upgrading processes. The reference raw biogas production plant is Ryaverket in Gothenburg, using their annual production levels as well as their existing transportation pipelines to the upgrading plant owned by Göteborg Energi [17].

However, after an initial interview with the process engineer B. Limani (personal communication 2024-04-18), this investigation was discontinued. The major concerns being the relatively low amount of available heat leading to an exceedingly small COP-value but also the presence of corrosive components in the raw biogas. This heat could potentially be utilized in a useful way but it will most likely not be handled with a HP and is thus not of interest for this thesis.

# F

# Appendix F

## F.1 System variation - Concrete: Air-to-air

It was investigated how the KPIs of the CAA HP-system, using R290 as a refrigerant, would be affected for the scenario of -7°C, if the heat source outlet, i.e. the warm exhaust air were to be recirculated in the system and used as the heat sink. Analogously to the modeling of case CAA, the updated input values for the system varied case CAA are shown in Table F.1.

**Table F.1:** Input values used in the evaluation of the system variate concrete case using an air-to-air R290 HP.

| **Case CAA - System variation** | **Value** | **Unit** |
|---|---|---|
| **HP target values:** | | |
| $\dot{Q}_{\text{CAA,var}}$ | 86 | [kW] |
| $\dot{Q}_{\text{SH,var}}$ | 53.8 | [kW] |
| $T_{CAA,var_{H_{Source,1}}}$ | 4.58 | [°C] |
| $T_{CAA,var_{H_{Sink,1}}} = T_{CAA,var_{H_{Source,1}}}$ | 4.58 | [°C] |
| $T_{CAA,var_{H_{Sink,2}}}$ | 16.22 | [°C] |
| $T_{\text{SH,in}} = T_{CAA,var_{H_{Sink,2}}}$ | 16.22 | [°C] |
| $T_{\text{SH,out}}$ | 25 | [°C] |
| **Process input values:** | | |
| $RH_{\text{air}}$ | 60 | [%] |
| $X_{\text{air}}$ | $\sum X_{sub,i}$=1 | [-] |
| $X_{\text{H}_2\text{O}}$ | 0.0063 | [$\text{kg}_{H_2O}/\text{kg}_{air}$] |
| $X_{\text{O}_2}$ | 0.23145 | [$\text{kg}_{O_2}/\text{kg}_{air}$] |
| $X_{\text{N}_2}$ | 0.76225 | [$\text{kg}_{N_2}/\text{kg}_{air}$] |
| $\dot{V}_{\text{CAA,var,air}}$ | 18500 | [$\text{m}^3/h$] |
| $\dot{m}_{\text{CAA,var,air}}$ | 6.02 | [kg/s] |

The volumetric air flow, $\dot{V}_{\text{CAA,var,air}}$ of 18,500 $\text{m}^3$/h, is the same for the original CAA case shown in Table 4.8. From the volumetric mass flow, the mass air flow $\dot{m}_{\text{CAA,var,air}}$, was calculated by utilizing $X_{\text{O}_2}$, $X_{\text{H}_2\text{O}}$, $X_{\text{N}_2}$ in Table F.1, which are the mass fractions of oxygen, water vapor, and nitrogen in the air. The mass fractions was determined as functions of the relative humidity $RH_{\text{air}}$ and the temperature $T_{CAA,var_{H_{Source,1}}}$ by utilizing eq. (3.1) through (3.5). Additionally, the heating capacity, $\dot{Q}_{\text{CAA,var}}$ and target inlet temperature

$T_{\text{SH,var,in}}$ was assumed to remain the same as in the original CAA case, specifically 86 kW and 25 °C respectively. It was concluded using the air conditions stated in Table F.1, that the additional electric heater $\dot{Q}_{\text{SH}}$, was to be sized at 30.2 kW to ensure the 25°C target inlet temperature.

The results of the system varied CAA case are show in Table F.2.

**Table F.2:** KPIs for the concrete air-to-air R290 HP operating with recirculated heat source air as heat sink

| **COSP** [-] | **NPV** [k€] | | | **PBP** [years] | | | **LCOH** [$\frac{€}{kWh}$] |
|---|---|---|---|---|---|---|---|
| | **DH** | **Diesel** | **El.** | **DH** | **Diesel** | **El.** | |
| 2.28 | 16.8 | 302.2 | -2.2 | 6.0 | 0.8 | 10.7 | 32.0 |

It is noted that the COSP increased with approximately 43% compared to the original CAA case, while the LCOH decreased marginally with approximately 3%. The NPV increased by 118%, 60.7% and 98% when replacing DH, Diesel and electricity, respectively, with the varied CAA VCHP-system. The NPV is only negative when replacing electricity as a utility with the varied VCHP system.

The PBP improved from being purely negative to 6 years when replacing DH, decreased with 33% when replacing Diesel and improved from being purely negative to 10.7 years when replacing electricity.

In conclusion, the results indicate that a system capable of incorporating exhaust air as a potential heat sink is advantageous.

**DEPARTMENT OF SPACE, EARTH AND ENVIRONMENT**
**CHALMERS UNIVERSITY OF TECHNOLOGY**
Gothenburg, Sweden
www.chalmers.se


CHALMERS
UNIVERSITY OF TECHNOLOGY